Polymer-Gold Composite Particles: Synthesis, Characterization, Application, and Beyond

by

Mingmeng Zhang

A Dissertation Presented in Partial Fulfillment
of the Requirements for the Degree
Doctor of Philosophy

Approved June 2015 by the
Graduate Supervisory Committee:

Lenore Dai, Co-Chair
Patrick Phelan, Co-Chair
Todd Otanicar
Jerry Lin
Ximin He

ARIZONA STATE UNIVERSITY

August 2015

ABSTRACT

Polymer-gold composite particles are of tremendous research interests. Contributed by their unique structures, these particles demonstrate superior properties for optical, catalytic and electrical applications. Moreover, the incorporation of "smart" polymers into polymer-gold composite particles enables the composite particles synergistically respond to environment-stimuli like temperature, pH and light with promising applications in multiple areas.

A novel Pickering emulsion polymerization route is found for synthesis of core-shell structured polymer-gold composite particles. It is found that the surface coverage of gold nanoparticles (AuNP) on a polystyrene core is influenced by gold nanoparticle concentration and hydrophobicity. More importantly, the absorption wavelength of polystyrene-gold composite particles is tunable by adjusting AuNP interparticle distance. Further, core-shell structured polystyrene-gold composite particles demonstrate excellent catalyst recyclability.

Asymmetric polystyrene-gold composite particles are successfully synthesized via seeded emulsion polymerization, where AuNPs serve as seeds, allowing the growth of styrene monomers/oligomers on them. These particles also demonstrate excellent catalyst recyclability. Further, monomers of "smart" polymers, poly (N-isopropylacrylamide) (PNIPAm), are successfully copolymerized into asymmetric composite particles, enabling these particles' thermo-responsiveness with significant size variation around lower critical solution temperature (LCST) of 31 ℃. The significant size variation gives rise to switchable scattering intensity property, demonstrating potential applications in intensity-based optical sensing.

Multipetal and dumbbell structured gold-polystyrene composite particles are also successfully synthesized via seeded emulsion polymerization. It is intriguing to observe that by controlling reaction time and AuNP size, tetrapetal-structured, tripetal-structured and dumbbell-structured gold-polystyrene are obtained. Further, "smart" PNIPAm polymers are successfully copolymerized into dumbbell-shaped particles, showing significant size variation around LCST. Self-modulated catalytic activity around LCST is achieved for these particles. It is hypothesized that above LCST, the significant shrinkage of particles limits diffusion of reaction molecules to the surface of AuNPs, giving a reduced catalytic activity.

Finally, carbon black (CB) particles are successfully employed for synthesis of core-shell PNIPAm/polystyrene-CB particles. The thermo-responsive absorption characteristics of PNIPAm/polystyrene-CB particles enable them potentially suitable to serve as "smart" nanofluids with self-controlled temperature. Compared to AuNPs, CB particles provide desirable performance here, because they show no plasmon resonance in visible wavelength range, whereas AuNPs' absorption in the visible wavelength range is undesirable.

ACKNOWLEDGEMENTS

I have the great pleasure to express my acknowledgements to people who supported and helped me during my progress towards completing my doctoral dissertation. First of all, I would like to thank Professor Lenore L. Dai with my sincere gratitude. I am very grateful for the tremendous efforts she provided on guiding and supporting my research throughout the four years, as well as her kindness and patience beyond research. I've inspired and improved by her positive work ethic with diligence, motivation, thoughtfulness and kindness. It would not be possible to finish this dissertation without her valuable guidance and support. I would also express my deep appreciation to Professor Patrick E. Phelan. I'm thankful for his efforts and kindness to support and guide my research. He always provides insightful suggestions on my research projects, and responds to my request and questions immediately. I would also like to express my sincere appreciation to Professor Todd P. Otanicar and thank for his leadership on this research project collaboration. I feel very grateful for his specific guidance on optical-related research. I sincerely thank my dissertation committee members, Professor Jerry Lin and Professor Ximin He, for the efforts and kindness to serve on my committee and valuable suggestions on my undergoing projects and future work.

I would like to express my thanks to my group members contributing to my research. Dr. Sriya Sanyal kindly helped me during my first research year and tried her efforts to assist me to transit the Pickering emulsion polymerization research into gold nanoparticles related systems. Andrey Gunawan kindly helped me on study of nanofluids natural convection heat transfer. Wei Lv assisted me on investigation of optical properties of metal particles. Thao Ngo assisted me on the catalytic experiment utilizing

polystyrene-gold composite particles and contributed to my first publication. Noelle Rabiah assisted me on synthesis and characterization of asymmetric composite particles, and contributed to my first and second publications. I also express my thanks to other colleagues and friends at Arizona State University, particularly Bohan Shan, Prithwish Chatterjee, Haobo Chan, Jin Zou, Elizabeth Nofen, Yuwen Dong, Mingzhi Dai, who supported me and made my four year research life more enjoyable and memorable.

I would also thank the support from LeRoy Eyring Center for solid state science for usage of TEM and SEM instruments, and Biodesign institute for usage of UV-Vis instrument. I'm thankful for Jun Wu's assistance on TEM techniques.

Most importantly, I would like to express my gratitude to my mother, Li Xu, my aunt Ping Xu and uncle Hong Wang for their unconditioned moral support throughout my life. I sincerely wish them a healthy, joyful and fruitful life.

TABLE OF CONTENTS

Page

LIST OF FIGURES xii

CHAPTER

1 INTRODUCTION 1

2 BACKGROUND AND MOTIVATION 6

2.1 Pickering Emulsion Polymerization 6

2.1.1 Mechanism of Pickering Emulsion Polymerization 7

2.1.2 “Smart” Composite Particles Synthesized via Pickering Emulsion Polymerization. 10

2.1.3 Solid Particles as Pickering Emulsion Stabilizers. 12

2.2 Seeded Emulsion Polymerization 18

2.2.1 Solid Particles as Seeds for Seeded Emulsion Polymerization 21

2.3 Gold Nanoparticles with their Optical and Catalytic Properties. 23

2.3.1 Surface Plasmon Resonance 23

2.3.2 Catalytic Properties. 25

2.4 Motivations 32

2.4.1 Core-shell Polystyrene-Gold Composite Particles via Pickering Emulsion Polymerization. 32

2.4.2 “Smart” PNIPAm-Gold Composite Particles with Tunable Optical Properties via Pickering Emulsion Polymerization. 35

2.4.3 Gold-Polymer Composite Particles with Complex Structure and their Modulatable Catalytic Activities 38

CHAPTER Page

2.4.4 “Smart” Nanofluids with Self-controlled Temperature. 40

3 METHODOLOGY 45

3.1 Materials 45

3.2 Particle Synthesis 45

3.3 Catalytic Study of Gold Composite Particles 46

3.4 Characterization Techniques 46

4 RESULTS AND DISCUSSION 48

4.1 Core-Shell and Asymmetric Polystyrene-Gold Composite Particles via One-step Pickering Emulsion Polymerization. 48

4.1.1 Core-Shell Polystyrene-Gold Composite Particles 48

4.1.2 Asymmetric Polystyrene-Gold Composite Particles and Their Formation Mechanism 55

4.1.3 Catalytic Study of Polystyrene-Gold Composite Particles 60

4.2 Thermo-responsiveness and Optical Properties of Asymmetric Polystyrene/PNIPAm-Gold Composite Particles. 64

4.2.1 Bimodal Size Distribution of Polystyrene/PNIPAm-Gold Composite Particles 64

4.2.2 Thermo-responsiveness of Polystyrene/PNIPAm-Gold Composite Particles 66

4.2.3 Tunable Optical Properties of Asymmetric Polystyrene/PNIPAm-Gold Composite Particles 72

4.3 Multipetal-shaped and Dumbbell-shaped Gold-Polymer Composite Particles with

CHAPTER Page

Modulatable Catalytic Activity. 78

4.3.1 Multipetal-Shaped and Dumbell-Shaped Gold-Polystyrene Composite Particles. 78

4.3.2 Effect of Reaction Time on Particle Morphology 80

4.3.3 Effect of AuNP size on Particle Morphology 82

4.3.4 Formation Mechanism of Multipetal-shaped and Dumbbell-shaped Gold-Polystyrene Composite Particles. 83

4.3.5 Thermo-responsiveness of Dumbbell-Structured Gold-PNIPAm/polystyrene Composite Particles 86

4.3.6 Modulatable Catalytic Activity of Dumbbell-shaped Gold-PNIPAm/polystyrene Composite Particles 91

4.3.7 Conclusion 98

4.4 “Smart” Core-Shell Structured CB-PNIPAm/polystyrene Composite Particles .. 99

4.4.1 Synthesis of Core-shell Structured CB-PNIPAm/polystyrene Composite Particles 99

4.4.2 Thermo-responsiveness of Core-Shell Structured CB-PNIPAm/polystyrene Composite Particles 101

4.4.3 Study of Optical Properties of Core-Shell Structured CB-PNIPAm/polystyrene Composite Particles 103

4.4.4 Conclusion 108

5 SUMMARY AND FUTURE WORK 109

5.1 Summary 111

CHAPTER Page

5.2 Future Work 112

5.2.1 “Smart” Core-Shell PNIPAm/polystyrene-Gold Composite Particles 112

5.2.2 Self-controlled Natural Convection of Nanofluids Composed of Asymmetric PNIPAm/polystyrene-Gold Composite Particles 114

REFERENCES 117

LIST OF FIGURES

Figure Page

2.1 SEM image (a) and Cross-sectioned TEM Image (b) of Core-Shell Polystyrene-Silica Composite Particles 9

2.2 Possible Mechanisms of Pickering Emulsion Polymerization.....9

2.3 Schematic Illustration of the Thermo-responsiveness of PNIPAm Polymer. 10

2.4 Schematic Illustration of Controlled Drug Release upon Temperature Stimulation of Polystyrene/PNIPAm Silica Core-Shell Composite Particles. 12

2.5 Theoretical Relationship between Detachment Energy and Particle Radius. 14

2.6 Effect of Particle Size on Stability of Alumina-stabilized Emulsions. 14

2.7 Theoretical Relationship between Desorption Energy and Contact Angle at a Planar Oil−Water Interface. 16

2.8 Silica Nanoparticle-stabilized Water-in-Toluene Emulsions with a List of Contact angles 16

2.9 Carboxylate-modified Methacrylate Copolymer Latex Particles Synthesized via Seeded Emulsion Polymerization 20

2.10 Relationship between Latex Particle Size and Weight Seed 20

2.11 (a) Illustration of Formation Pathway of Silica-Polystyrene Composite Particles with Daisy Shape and Multipod Shape. (b) TEM and SEM Images of Silica-Polystyrene Composite Particles with Daisy Shape and Multipod Shape.....22

2.12 Illustration of SPR Oscillations Triggered by an Oscillating E-field. 24

2.13 Illustration of Summary of Reaction Mechanism for Nucleophilic Addition to Carbon-carbon Triple Bonds Catalyzed by Gold Nanomaterials 27

Figure Page

2.14 Illustration of Rearrangement Reaction of o-alkynyl Substituted Furans Intophenols Catalyzed by Gold Nanomaterials 28

2.15 Schematic Illustration of Polymer-supported AuNPs. a) Polymer (PVP)-capped AuNPs b) Functionalized Resin-supported AuNPs. AuNPs are Anchored within the Resin Pores c) AuNPs Embedded inside the Polymer Substrate and d) AuNPs Supported on the Surface of Polymer Particle Substrate. 31

2.16 Schematic Illustration of Tunable Surface Plasmon Resonance Properties of Core-Shell Structured Polymer-Gold Composite Particles. 33

2.17 Schematic Illustration of Dual Use Solar Thermal Collector/Night-Sky Radiator....36

2.18 Illustration of Composite Particles with Dumbbell and Multipetal Shapes.....39

2.19 (Left) Deformation and Bending of Absorber Plate at Edge Due to its Constrained Thermal Expansion during Stagnation; (Middle) Permanent Deflection of Absorber Plate due to Constrained Thermal Expansion of Solar Collector Absorber Plate;(Right) Degradation of Propylene-Glycol/Water Solution after Increased Time-Exposure to High Temperatures.....41

2.20 Schematic Illustration of Performance of "Smart" Nanofluids of Pnipam-Gold Core-Shell Particles.....42

2.21 Relationship between Stagnation Temperature and Absorption of Heat Transfer Fluids.....42

2.22 Numerical Results of Absorption Efficiency for Pnipam-Gold Core-Shell Particles below LCST (Blue) and above LCST (Green) 44

4.1 (a) SEM Images of Core-Shell Gold-Polystyrene Composite Particles. (b) TEM

Image of Core-Shell Gold-Polystyrene Composite Particles. (c) Corresponding EDS Spectrum of Particles in (b). Corresponding AuNP Concentration is 0.092 wt%.....49

4.2 Comparison of Synthesized Product Using Different Types of AuNPs. (a) SEM Image of Composite Particles Synthesized By Nsol-Capped (Alkyl Acrylate) AuNP (AuNP Diameter: 20 nm). (b) SEM Image of Composite Particles Synthesized by PVP-Capped AuNPs. (AuNP Diameter: 20 nm) (c) and (d): Corresponding Photos for Solutions before (Left) and after (Right) Emulsion Polymerization with Nsol Capped AuNPs and PVP-Capped AuNPs Respectively. AuNP Concentration for both Type of AuNPs are 0.092 wt%. 51

4.3 (a) Influence of AuNPs Concentration on Reduced Surface Coverage of Core-Shell Gold-Polystyrene Particles. the Scale Bar for Each TEM Image is 100 nm. Corresponding AuNPs Concentration is 0.009 wt%, 0.019 wt%, 0.046 wt%, 0.07 wt%, 0.092 wt%, Respectively. Capping Agent: Nsol (Alkyl Acrylate). Styrene Monomer Concentration is Kept as Constant. (b) Corresponding UV-Vis Spectra of Composite Particles for Figure 4a. 54

4.4 (a) TEM of the Bimodal Size Distribution of Polystyrene-Gold Composite Particles. (b) DLS of the Bimodal Size Distribution of Polystyrene-Gold Composite Particles. Corresponding AuNPs Concentration is 0.046 wt%.....56

4.5 (a) TEM Images of the Asymmetric Gold-Polystyrene Particles. (b) SEM Images of the Asymmetric Gold-Polystyrene Particles. Corresponding AuNPs Concentration is 0.009 wt%. (c) UV-Vis Spectra of Asymmetric Particles (Curve 1) and Pure Gold Nanoparticles (Curve 2). 56

Figure Page

4.6 Schematic Illustration of formation of Core-Shell Structured and Asymmetric Polystyrene-Gold Composite Particles via Pickering Emulsion Polymerization. 57

4.7 Formation Mechanism of Asymmetric Particles: Seeded Growth. a. Proposed Seeded Growth Mechanism. b. TEM Images of Particles Sampled at Reaction Time of 0.5 hour, 1 hour, 4 hours, respectively. 59

4.8 Time Study on UV-Vis Absorbance of Rhodamine B under Redox Reaction Catalyzed by Core-Shell Polystyrene-Gold Composite Particles Catalysts. inset Photos are Taken Before Reaction (Left) and after Reaction (Right) Respectively...61

4.9 Comparison of the Reaction Time for Three Types of AuNPs. Reaction Condition: [Rhb] = 4×10^{-5} mol/L, [$NABH_4$] =5×10^{-2} mol/L, Concentration of the Three Types of AuNPs Particles are Kept at 9.2×10^{-4} wt %.....61

4.10 Catalysts Recyclability Study: Comparison of the Final Conversion of Rhb for Core-Shell Particles, Asymmetric Particles and Pure AuNPs. 63

4.11 TEM Images of Pure AuNPs Recollected after (a) 3rd Reaction Cycle and (b) 5th Reaction Cycle for Particle Recyclability Study. 63

4.12 Scheme of Core-Shell and Asymmetric Polystyrene/PNIPAm-Gold Composite Particles formation via Pickering Emulsion Polymerization. 65

4.13 Bimodal Size Distribution of Polystyrene/PNIPAm-Gold Composite Particles. (a) is the TEM Image of Bimodal-Sized Polystyrene/PNIPAm-Gold Composite Particles. (b) is the Number-Weighted Size Distribution from the DLS Measurement. (c) and (d) are the Filtrated Core-Shell Composite Particles and Filtrated Asymmetric Particles Respectively. (e) and (F) Represent EDS Analysis Focused on the

Asymmetric Particles and Blank Area Respectively in Image (d). 65

4.14 (a) (b) Represent DLS Result of Core-Shell and Asymmetric Polystyrene/PNIPAm-Gold Composite Particles Respectively. (c) Comparison of Shrinking Ratio between Core-Shell and Asymmetric Polystyrene/PNIPAm-Gold Composite Particles with NIPAAm Content of 33 wt% and 50 wt%. the Shrinking Ratio is the Ratio of Particle Diameter at a Given Temperature to Particle Diameter at 40 ℃ 69

4.15 (a) Shrinking Ratio of Asymmetric Polystyrene-NIPAAm-Gold Composite Particles with Different NIPAAm Content. (b) Corresponding Particle Diameter at 25 ℃ and 40 ℃. (c) TEM Images of Asymmetric Particles with 50 wt%, 71 wt%, 83 wt% NIPAAm Content under the Electron Beam, Particles' Temperature increases above their LCST of 31 ℃.....70

4.16 Influence of A Cross-Linker on Thermo-Responsiveness. Comparison of thermo-Responsiveness of Asymmetric Polystyrene/PNIPAm-Gold Composite Particles Synthesized with 5% MBA and without MBA. NIPAAm Content for Both Types of Particles is 83 wt%.....71

4.17 Viscosity Measurement of Asymmetric Polystyrene-NIPAAm-Gold Composite Particles Suspension with NIPAAm Content of 83 wt% (a) and 71 wt% (b) under 20 ℃ and 40 ℃. Particle Concentration for (a) and (b) is Kept at 3 wt%. 71

4.18 Thermal Responsiveness of Extinction and Scattering intensity. (a) Extinction and Scattering intensity at Different Temperatures with NIPAAm Content of 83 wt%. the Laser Wavelength for the Extinction/Scattering intensity Measurement is Kept at 639 nm. (b) Photos of Asymmetric Particle Sample at 20 ℃ and 40 ℃. (c) Effect

of Different NIPAAm Content on Extinction/Scattering intensity increase Ratio. (d) Reusability Study of Asymmetric Polystyrene/NIPAAm-Gold Composite Particles. 75

4.19 (a) Normalized Extinction Spectra of Asymmetric Particles Synthesized under NIPAAm Content of 83 wt% at 20 ℃ and 40 ℃. the Arrow Represents the Variation Trend of Plots from 20 ℃ to 40 ℃. (b) and (c) are Normalized Extinction Spectra of Pure AuNPs and Asymmetric Particles with Different NIPAAm-Styrene Feed Ratio at 20 ℃ and 40 ℃, Respectively. the Arrow in (b) Represents Variation Trend of Plots from 83wt% NIPAAm Content to 0% NIPAAm Content 77

4.20 Multipetal-Structured and Dumbbell-Structured Gold-Polystyrene Composite Particles. (a)(b) Particles with Tetrapetal Structure. (Particles Synthesized with 125 nm AuNPs, 1 hr Reaction Time). (c)(d) Tripetal-Structured Particles. (Particles Synthesized with 80 nm AuNPs, 1 hr Reaction Time). (e)(F) Dumbbell-Structured Particles. (Particles Synthesized with 80 nm AuNPs, 4 hrs Reaction Time).....79

4.21 TEM Images of Gold-Polystyrene Composite Particles Sampling after Different Reaction Time (1hr, 2 hr, 4 hr) (a)(b)(c) are Samples Synthesized with 80 nm AuNP, (d)(e)(f) are Samples Synthesized with 125 nm AuNP 81

4.22 Influence of AuNP Size on Particle Morphology. (a) Comparison of Number of Polystyrene Petals on a Single AuNPs between 80 nm AuNP System and 125 nm AuNP System. The Counting and Calculation of Number of Petals on Each AuNP Center is Based on 10 TEM Images for Each Sample. (b) Multipetal-Shaped Gold-Polystyrene Particle with 125 nm AuNPs, Where 6 Polystyrene Petals attach on a

Figure Page

Single AuNP 83

4.23 Illustration of formation Pathway of (a) Multipetal-Shaped and Dumbbell-Shaped Gold-Polystyrene Composite Particles and (b) Seeded Growth Formation Mechanism of Multipetal-Shaped Gold-Polystyrene Composite Particles 85

4.24 Thermo-Responsiveness of Dumbbell-Shaped Gold-Polymer Composite Particles with Different PNIPAm Content. DLS Results Show Relationship between Particle Size and Temperature for Particles with 83 wt% and 91 wt% PNIPAm Content. Inset TEM Images Show Morphology Comparisons between Dumbbell-Shaped Gold-Polymer Composite Particles without PNIPAm Content (Left) and with 83 wt% PNIPAm Content (Right). 89

4.25 TEM Image of Gold-PNIPAm/Polystyrene Composite Particles with 83 wt% (Left) and 91 wt% (Right) PNIPAm Content, Respectively. Samples are Taken after 1hr and 4 hrs Reaction Time 90

4.26 UV-Vis Results of the Rhb Reduction Reaction Catalyzed By Gold PNIPAm/Polystyrene Particles. (a) UV-Vis Spectra of Sample with 91 wt% PNIPAm during Reaction at 31 ℃. Spectrum is Measured Every 40 Seconds Until Rhb Peak Disappears Completely. (b) (c) (d) Relationships between Reaction Temperature and Reaction Rate for Particles with 83 wt% 91 wt%, and 0 wt% NIPAAm Content Respectively. (e) Comparison of Catalyst Activity Decrease Percentage between 83 wt% and 91 wt% NIPAAm Content Composite Particles ...93

4.27 Illustration of Proposed Reason of Modulatable Catalytic Activity of Gold-PNIPAm/Polystyrene Dumbbell-Shaped Composite Particles.....96

Figure Page

4.28 Relationship of Scattering intensity of Dumbbell-Structured Gold PNIPAm/Polystyrene Composite Particles with Temperature. (a) DLS Result of Scattering intensity increase Ratio for Temperature Range of 25 ℃ – 39 ℃ for Particles with 83 wt% and 91 wt% PNIPAm Content Respectively. (b) (c) (d) are the Normalized Extinction Spectra Measured via UV-Vis Spectrometer for Particles with PNIPAm Content of 0 wt%, 83 wt% and 91 wt% Respectively with Temperature Range of 25 ℃ - 37 ℃. the Extinction intensity Measured from the UV-Vis Spectrometer includes Scattering and Absorbing Intensities.....96

4.29 Relationship of Extinction Intensity of Dumbbell-Shaped Gold-PNIPAm/Polystyrene Composite Particles with Temperature Obtained via UV-Vis Spectrometer. Extinction Intensity Increase Ratio for Temperature Range of 25 ℃ – 39 ℃ for Particles with 83 wt% and 91 wt% PNIPAm Content Respectively. the Extinction Intensity Measured from the UV-Vis Spectrometer includes Scattering and Absorbing Intensities 97

4.30 (a)(b) TEM Images of CB-PNIPAm/Polystyrene Composite Particles. (c)(d) EDX Results of CB-PNIPAm/Polystyrene Composite Particles. the Left and Right EDX Results Represent Results where Electron Beam is Focused on the Blank Space and on the Particle, Respectively.....100

4.31 DLS Analysis of CB-PNIPAm/Polystyrene Composite Particles with 83 wt% PNIPAm Content under Increasing Temperatures. (a)(b)(c)(d) Represent Results of Sample with 1 Hr, 2 hrs, 3 hrs, 4 hrs Reaction Time, Respectively. (e) Comparison of Shrinkage Ratio of the above Four Samples with 83 wt% PNIPAm Content under

Figure Page

Increasing Temperatures 102

4.32 UV-Vis Spectrometer Analysis of CB-PNIPAm/Polystyrene Composite Particles with 83 wt% PNIPAm Content under 20 ℃ and 40 ℃. (a)(b)(c)(d) Represent Results of Sample with 1 Hr, 2 hrs, 3 hrs, 4 hrs Reaction Time, Respectively 105

4.33 Relationship between Scattering Intensity Increase Ratio and Temperatures of CB-PNIPAm/Polystyrene Composite Particles with 83 wt% PNIPAm. the Four Plots Represent Results of Sample with 1 Hr, 2 hrs, 3 hrs, 4 hrs Reaction Time, Respectively. The Laser Wavelength of DLS for Scattering Intensity Measurement is Kept at 639 nm 107

5.1 Formation Pathway of Polystyrene-Gold Core-Shell Composite Particles 113

5.2 Illustration of Glass Cell Setups for Natural Convection Heat Transfer. (a) Cross-Section of the Cell's Three Compartments; (b) Interchangeable Middle Compartments which are Made to Fit Different Electrode Spacing Distance; (c) the Cell Setups are Stabilized in Horizontal and Vertical Orientation, Providing Three Orientations for Measurements 116

Chapter 1

INTRODUCTION

In recent years, gold nanoparticles (AuNPs) have drawn significant research interest due to their desired optical, catalytic, and electric properties. These properties have wide applications in catalysis,[1-5] sensing,[6-7] and surface enhanced Raman scattering (SERS).[8-9] As compared to single component AuNPs, gold composite particles with unique structures are able to surpass the limitations of single component alone. For example, for core-shell composite particles with a dielectric core and AuNPs shell, the particles exhibit unique surface plasmon resonance (SPR) properties corresponding to the dimension ratio of the core and the shell.[10-13] This tunable SPR wavelength feature is attractive for applications in solar energy harvesting, conducting polymer devices, drug delivery, and biosensors.[14-18] For gold composite particles with structures such as asymmetric structure (a single gold nanoparticle is attached on each polystyrene substrate particle), dumbbell structure and multi-petal structure, etc., they are capable of meeting the rising demand of fabricating advanced ordered and hierarchical building blocks, such as photonic band-gap materials, nanopatterns by colloidal lithography, with the potential applications in self-assembly,[19-20] opto-electronics,[21] catalyst supports,[22-23] etc. For instance, if the asymmetric particles are synthesized with anisotropic distribution of electric charges, the particles can self-assemble into an electric-field-oriented pattern under a given electric field. For multi-petal structured particles, their unique structures enable them to serve as building blocks for advanced supra-colloidal materials; in addition, they might serve for building super-hydrophobic and super-hydrophilic surfaces.[24-25] Particles with three-dimensional structure could also serve as potential building blocks for diamond lattice

(fcc dielectric structure), which has three-dimensional photonic bandgap, as predicted 20 years ago.[26]

Pickering emulsions are emulsions stabilized by solid particles. Here we employ a one-step Pickering emulsion polymerization to synthesize core-shell structured polymer−gold composite particles. The one-step Pickering emulsion polymerization route has the following advantages: sophisticated instrumentation is not required, commercialized stabilizing particles can be directly used without further treatment, and the synthesis is completed in one step. In addition, seeded emulsion polymerization is utilized to synthesize gold-polymer composite particles with structures such as the asymmetric (a single gold nanoparticle is attached on each polystyrene substrate particle), dumbbell, and multi-petal structure. AuNPs are able to serve as seeds to interact with aromatic rings provided by styrene, allowing further growth of styrene and other co-monomers.

The synergistic combination of "smart" polymers and inorganic nanomaterials has attracted increasing interest in recent years. In response to temperature[27-32] or pH[33-35], the stimuli-responsive polymers are able to adjust nanomaterial's optical[27-30], catalytic[31-32] and transport properties[33-34]. In particular, poly (N-isopropylacrylamide) (PNIPAm) is a water-based gel and compatible with many biological systems. Its unique thermo-responsiveness enables the gel to undergo a sharp volume phase transition at lower critical solution temperature (LCST).[36] We find that a significant thermo-responsiveness of scattering intensity is achieved for asymmetric polystyrene/PNIPAm-gold composite particles, based on the large temperature-dependent shrinking/swelling of the polystyrene/PNIPAm core. This leads to great potentials in sensing applications,

especially for intensity-based optical sensors. For example, particles with switchable scattering intensity could be utilized in thermal sensors, in which the thermo-responsive scattering intensity serves as signals. In addition, the "smart" PNIPAm polymers are successfully incorporated into dumbbell-shaped gold-polymer composite particles; a self-modulated catalytic activity is demonstrated.

Other than the AuNPs systems, carbon black (CB) particles are incorporated for Pickering emulsion polymerization to synthesize core-shell PNIPAm/polystyrene-CB composite particles. Compared to AuNPs system, carbon black particles do not show absorption characteristics at visible wavelength range, potentially useful for applications where the AuNPs' absorption at visible wavelength range is undesirable. For instance, CB particles have potential to be served as "smart" nanofluids with self-controlled temperature to potentially address stagnation problems occurred in heat transfer fluid systems.

In summary, this thesis includes employing a Pickering emulsion polymerization method and a seeded emulsion polymerization method to synthesize polystyrene-gold composite particles with four structures (core-shell, asymmetric, multipetal and dumbbell structures, respectively), as well as thermal responsive PNIPAm/polystyrene-gold composite particles. The catalytic and optical properties are explored. In addition, CB particles are employed for synthesis of thermos-responsive core-shell PNIPAm/polystyrene-CB composite particles via Pickering emulsion polymerization. The report is structured as follows. Chapter 2 provides the background and motivations on the topics discussed in this thesis. The background is focused on topics of Pickering emulsion polymerization, seeded emulsion polymerization, effect of solid stabilizers on

Pickering emulsions, AuNPs' optical and catalytic properties. The motivation is focused on tunable optical properties and self-modulated catalytic properties of "smart" polymer-gold composite particles. Chapter 3 describes the materials and methodology used in this thesis. In Chapter 4, the results and discussion are laid out in the following order: Section 4.1 illustrates the utilization of one-step Pickering emulsion polymerization to synthesize core-shell structured polystyrene-gold composite particles; it is intriguing to find that asymmetric structured particles are formed simultaneously, due to a seeded growth formation mechanism. The catalytic study shows both the core-shell and asymmetric particles have good recyclability. In Section 4.2, it is shown that thermal-responsive PNIPAm polymers are successfully copolymerized into core-shell structured and asymmetric structured composite particles via seeded emulsion polymerization, without the aid of cross-linker. The asymmetric particles show a significant thermal-responsiveness, leading to switchable scattering intensity of the particles. Section 4.3 discusses the successful synthesis of multipetal-shaped and dumbbell-shaped gold-polystyrene particles. It will be demonstrated that by increasing the diameter of AuNPs from 20 nm to 80 nm and 125 nm, multipetal-structured and dumbbell-structured AuNP-polystyrene composite particles are synthesized via seeded emulsion polymerization. By controlling the reaction time and size of the AuNPs, the structure of the composite particles could be controlled. Furthermore, thermal-responsive PNIPAm polymers are proven to be successfully copolymerized into dumbbell-shaped composite particles, enabling these particles a self-modulated catalytic activity. Section 4.4 shows the utilization of CB particles as stabilizers for the synthesis of PNIPAm/polystyrene-CB composite particles via Pickering emulsion polymerization. These particles show

potential applications to be served as “smart” nanofluids with self-controlled temperature to solve stagnation problems occurred in heat transfer fluid systems. Chapter 5 provides the summary and future work. The first proposed work is synthesis of “smart” core-shell PNIPAm/polystyrene-gold composite particles with tunable absorption properties triggered by temperature variation. Applying a chemical reduction route, the Au shells are expected to be continuous. These particles have potential applications of dual use solar thermal collector/night-sky radiator. Another interesting application of these particles is a thermo-optical switch, which could serve as a nanofluid filter switching between opaque and transparent status. The second proposed work is application of asymmetric PNIPAm/polystyrene-gold composite particles to serve as nanofluids with controllable natural convection heat transfer. These “smart” nanofluids are suitable for applications in which increased heat transfer is needed in the daytime (above LCST of 31°C) for the purpose of releasing energy, while decreased heat transfer is needed in the nighttime (below LCST of 31°C) for the purpose of energy storage.

Chapter 2

BACKGROUND AND MOTIVATION

2.1 Pickering Emulsion Polymerization

Pickering emulsions are emulsions stabilized by solid particles, in contrast to conventional emulsions in which surfactants serve as stabilizer. The discovery and early studies of solid particles as a new type of emulsion stabilizer are achieved by Ramsden[37] in 1903 and Pickering[38] in 1907. Pickering emulsions have been widely used in various fields, including petroleum, cosmetic, pharmaceutical applications etc.[39-41] For instance, in oil recovery applications, solid particles are able to spontaneously self-assemble at the oil-water interface. The stabilization of oil droplets is necessary and beneficial for extraction and separation of oil from water.[39] In cosmetic industry, metal particles such as titanium dioxide (TiO_2) nanoparticles are shown to have the potential as stabilizers for skin-care and sunscreen emulsions, providing an alternative for traditional emulsion product stabilized by surfactants.[40]

Pickering emulsion polymerization provides a direct way of combining soft materials (e.g. polymers) with solid particles to synthesize composite particles with core-shell structure, where monomer droplets undergo polymerization to form the core, and solid particles form the shell layer. Conventionally, the reported synthesis methods of core-shell structured composite particles are mainly based on chemical binding or electrostatic attraction interaction and often require multiple procedures and sophisticated instruments. For example, AuNP-polymer core-shell composite particles involve preforming AuNPs and driving them to coat the substrate particles[10-11, 42] or directly forming the AuNPs at the substrate particles' surface.[43-45] During these processes, modifying the substrate

particle or AuNP's surface is required. Recently, we have developed the one-step Pickering emulsion polymerization route to synthesize polymer-silica core-shell nanocomposite particles[46-47] (Figures 2.1 and 2.2), This method bears the advantage that sophisticated instrumentation is not required. In addition, commercialized stabilizing particles can be directly used without further treatment, and the synthesis is completed in one step.

2.1.1 Mechanisms of Pickering Emulsion Polymerization

For conventional surfactant-stabilized emulsion polymerization, the reaction mechanism has been actively discussed over half a century. Some consensus has been reached that three nucleation mechanisms exist: micellar nucleation,[48-49] homogeneous coagulative nucleation,[48, 50-53] and droplet nucleation.[46] During the micellar nucleation, micelles capture free radicals, subsequently undergo continuous swelling, followed by polymerization of monomers inside the swelling emulsions. The reaction terminates as the monomers are consumed up. Throughout the homogenous nucleation, oligomers are formed via radical polymerization of monomer dispersed in water phase. Then, the nuclei and primary particles are formed by oligomer coagulation. These surfactant-stabilized primary particles grow by monomer swelling or oligomer deposition. For the droplet nucleation, the monomer droplets accept oligomer radical entry, followed by solidification to form particles.

Previously, our group utilizes silica nanoparticles to synthesize polystyrene-silica core-shell composite particles and investigate the reaction mechanism of Pickering emulsion polymerization. Ma et al propose the following possible reaction mechanism of

Pickering emulsion polymerization.[46] As summarized in Figure 2.2, emulsions undergo homogeneous coagulative nucleation and droplet nucleation. At the beginning of the reaction, the decomposed initiators react with monomers dispersed in the water phase to produce oligomer. In homogenous nucleation pathway, the nuclei composed of oligomers become monomer swollen particles, stabilized by silica nanoparticles. These particles grow via monomer swelling and subsequent polymerization inside the core, under the continuous supply of monomers via diffusion from monomer droplets. On the other hand, in the droplet nucleation pathway, the monomer droplets accept oligomers with radicals, followed by polymerization to form solid particles. No significant size growth is noted in the droplet nucleation pathway. Through the investigation of the sample sampling from different reaction time, Ma et al suggest for system using the VA-086 initiator (2,2'-Azobis[2-methyl-N-(2-hydroxyethyl)propionamide]), homogeneous nucleation is dominating, as it is observed that particles grow via monomer swelling and undergo polymerization to form sub-micron sized particles, an indication of homogeneous nucleation. However, for system using KPS (potassium persulfate) initiators, both homogeneous nucleation and droplet nucleation are present.

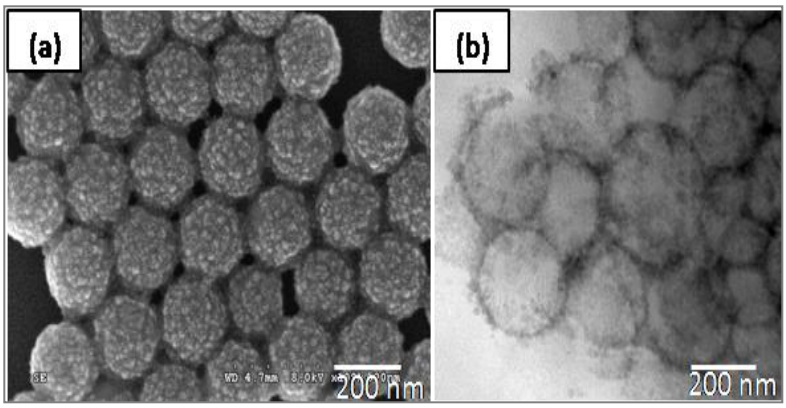

Figure 2.1 SEM image (a) and cross-sectioned TEM image (b) of core-shell polystyrene-silica composite particles. Adapted from Reference 46.

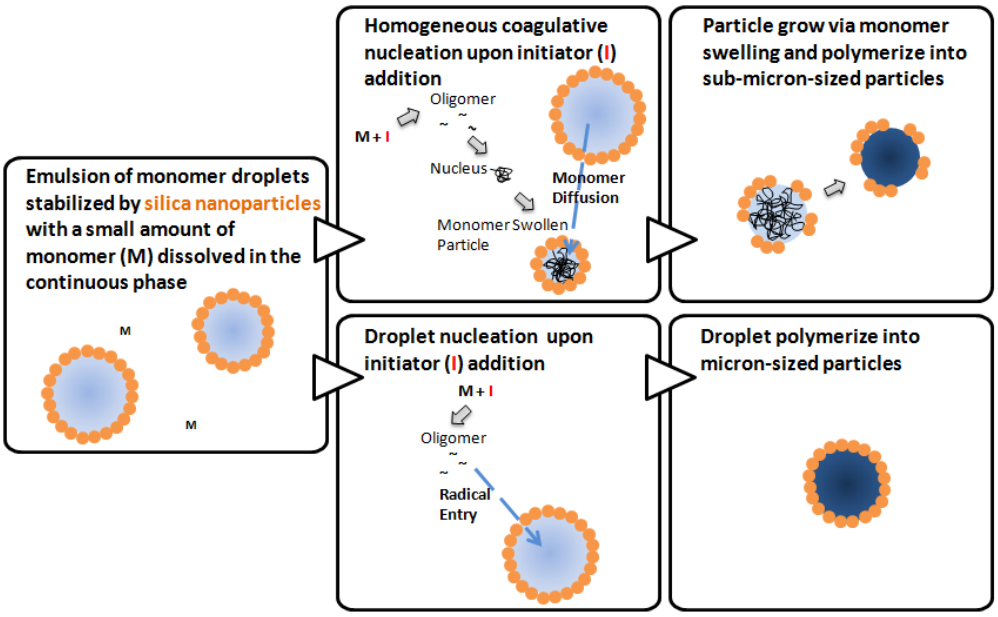

Figure 2.2 Possible mechanisms of Pickering emulsion polymerization. Adapted from Reference 46.

2.1.2 “Smart” Composite Particles Synthesized via Pickering Emulsion Polymerization.

“Smart” materials are defined as materials with the capability of adjusting their properties upon environmental stimuli such as temperature, pH or light etc. Recently, poly (N-isopropylacrylamide) (PNIPAm) polymer has received an intense research interest due to its unique thermo-responsiveness. PNIPAm polymer is a water-based gel and compatible with many biological systems. Its unique thermo-responsiveness enables the gel to undergo a sharp volume phase transition at a lower critical solution temperature (LCST) (see Figure 2.3).[36] In a pure water solution, LCST is determined as 32 ℃. Below LCST, PNIPAm polymer’s hydrogen bonding between polymer polar groups and water molecules are strong, enabling the polymer backbone expands and stretches; above the LCST, PNIPAm polymer’s hydrogen bonding is weakened, dominated by hydrophobic interactions among hydrophobic parts, leading to a collapsed polymer backbone.

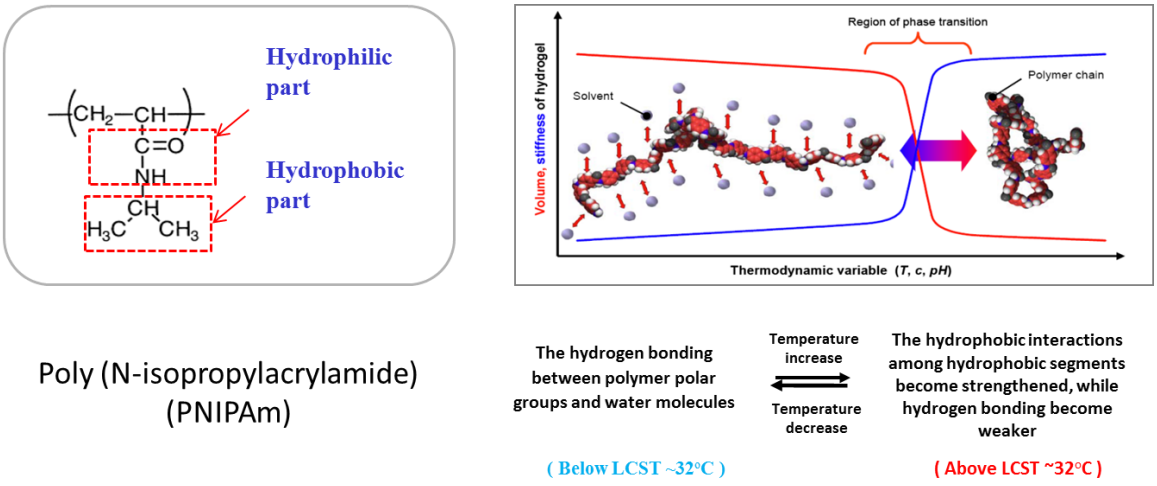

Figure 2.3 Schematic illustration of the thermo-responsiveness of PNIPAm polymer. Adapted from Reference 54.

In our group, Ma et al successfully synthesize "smart" polystyrene/PNIPAm silica core-shell composite particles by incorporating thermo-responsive PNIPAm via Pickering emulsion polymerization, using the similar recipe of synthesizing polystyrene silica core-shell composite particles. A Dynamic Light Scattering (DLS) study shows for 15 wt% NIPAAm content polystyrene/PNIPAm silica core-shell composite particles, an 8 % size decrease is achieved as temperature increases above particle's LCST of 32 °C. The LCST is not shifted, indicating silica nanoparticles and copolymerization of polystyrene do not influence the LCST in this case. This is because silica nanoparticles are located at the surface of the composite particles. A possible hypothesis to explain what appears to be no influence of copolymerization of polystyrene is that a phase separation exists inside the polymeric particles. Duracher et al suggest a polystyrene rich core with PNIPAm rich shell.[55]

Sanyal et al. further the study of "smart" polystyrene/PNIPAm silica core-shell composite particles into drug release application (Figure 2.4).[47] During the reaction synthesis, anticancer agent 17-(Allylamino)-17-demethoxygeldanamycin (17-AAG) is loaded into the polymer core. Fluorescence images show that these composite particles are successfully taken up by human prostate cancer (PC3 and PC3-PSMA) cells. Upon temperature increase, drug release is successfully observed due to the shrinkage of the particles. The ability of controlled drug release by "smart" polystyrene/PNIPAm silica core-shell composite particles is demonstrated.

The thermal transition of "smart" polystyrene/PNIPAm silica core-shell composite particles is also studied by Sanyal et al.[56] It is found that the degree of thermal transition

increases with NIPAAm content increase. In addition, the LCST could be adjusted by addition of cross-linkers, co-monomers, surfactants and co-solvents.

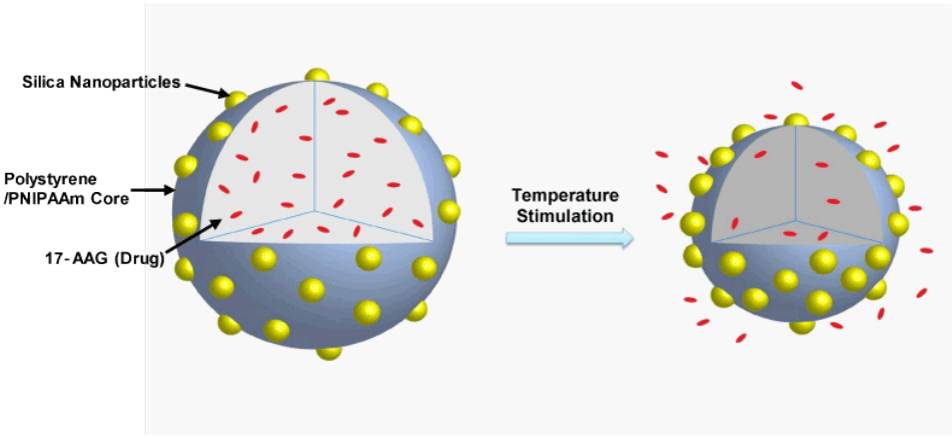

Figure 2.4 Schematic illustration of controlled drug release upon temperature stimulation of polystyrene/PNIPAm silica core-shell composite particles. Adapted from Reference 47.

2.1.3 Solid Particles as Pickering Emulsion Stabilizers

The stabilization of emulsions by solid particles is driven by thermodynamic requirement.[57] Theoretically, the absorption of solid particles onto liquid-liquid interface is a spontaneous process, because this process drives towards the preferable lower free energy condition. Compared with conventional surfactants, the absorption of solid particles onto liquid-liquid interface is a near-irreversible process; on the other hand, the conventional surfactants tend to undergo absorption-desorption process at the liquid-liquid interface, due to weak absorption energy at the liquid-liquid interfaces. The stability of solid particle absorption on the interface is quantified by calculation of desorption energy via the following equation:

$$\Delta G = \pi\alpha^2\gamma_{ow}(1 \pm \cos\theta)^2 \quad (1)$$

where ΔG is the desorption energy, α is the radius of particles, γ_{ow} is the tension at the oil-water interface, θ is the three phase contact angle.

2.1.3.1 Effect of Particle Size

Particle size is an important factor determining the capability of particles absorption on the liquid-liquid interface. Theoretically from Equation 1, the desorption energy increases with particle size. This relationship is illustrated in Figure 2.5. Binks have shown that for particles of intermediate hydrophilicity ranging from micron size to several nanometer size, the desorption energy is significantly larger than thermal energy, indicating irreversible absorption; whereas for particles less than 1 nm, the desorption energy is comparable with thermal energy, leading to the possibility of particles' desorption from the liquid-liquid interface.[58] However, the influence of particle size on emulsion stability is still under debate. Experimental results show that increasing particle size leads to decreased emulsion stability until a critical size is approached. Binks and Lumsdon et al suggested from experimental results that particles with bigger size tend to have less emulsion stability.[59] Tambe et al studied the effect of particle size on emulsion stability by utilizing alumina particles on decane-water system.[60] Shown in Figure 2.6, the larger particles (37 μm) could not stabilize the emulsions, whereas smaller particles (4 μm) are able to stabilize them. It should be mentioned that the theoretical analysis on thermodynamics of particle absorption assumes flat liquid-liquid interfaces with considerably small particle size. For curved liquid-liquid interfaces, studies have shown that the curvature of interface influences the desorption energy and position of particles at the interfaces.[61]

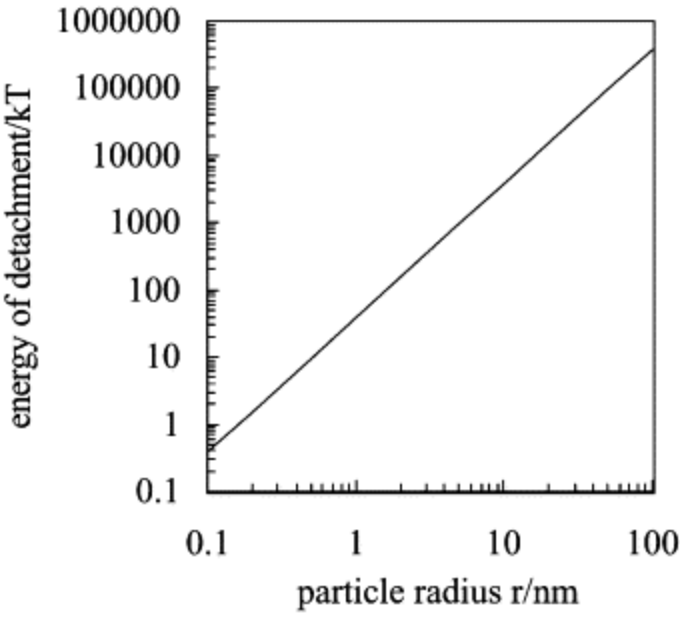

Figure 2.5 Theoretical relationship between detachment energy and particle radius. Particle contact angle is 90 °at planar oil-water interface at 298 K. Adapted from Reference 58.

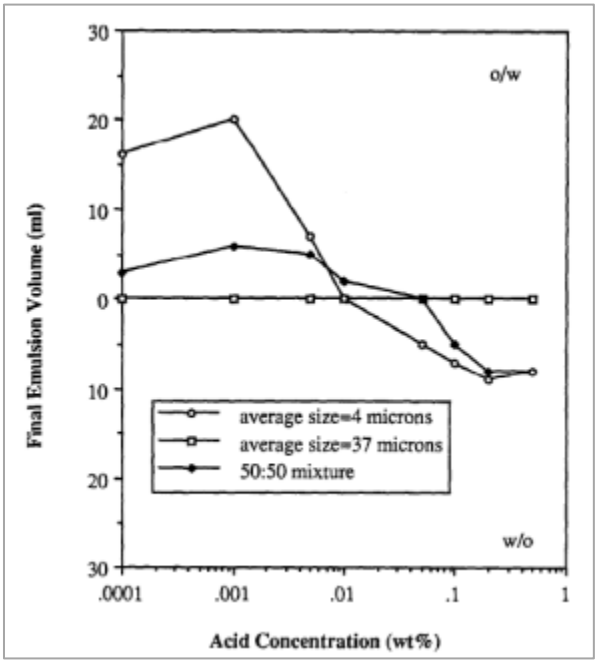

Figure 2.6 Effect of particle size on stability of alumina-stabilized emulsions. Adapted from Reference 60.

2.1.3.2 Effect of Particle Hydrophilicity

The hydrophilicity of particles is an important factor influencing desorption energy. Reflected from three-phase in Equation 1, the contact angle θ, the desorption energy is the highest when $\theta = 90°$, as particles are equally wetted by both liquid phases. Away from 90°, the desorption energy drops sharply. This indicates an intermediate hydrophilicity of the particles will increase the stability of particles' attachment at the liquid-liquid interface. The influence of hydrophilicity is illustrated in Figure 2.7. Experimental work is first conducted by Schulman et al. demonstrating the 90° contact angle for particles with intermediate hydrophilicity provides the most stable emulsions.[62] Yan et al also find that the most stable emulsions are formed with intermediate contact angle.[63] In their work, latex particles, clay particles and fumed silica nanoparticles with different hydrophilicity are used to stabilize toluene-water emulsions. Figure 2.8 are the results from Yan et al for emulsions stabilized by fumed silica nanoparticles with contact angle ranging from 0° to 96°. This demonstrates that particles with contact angle much lower than 90° (0° and 60°) could not stabilize the emulsions.

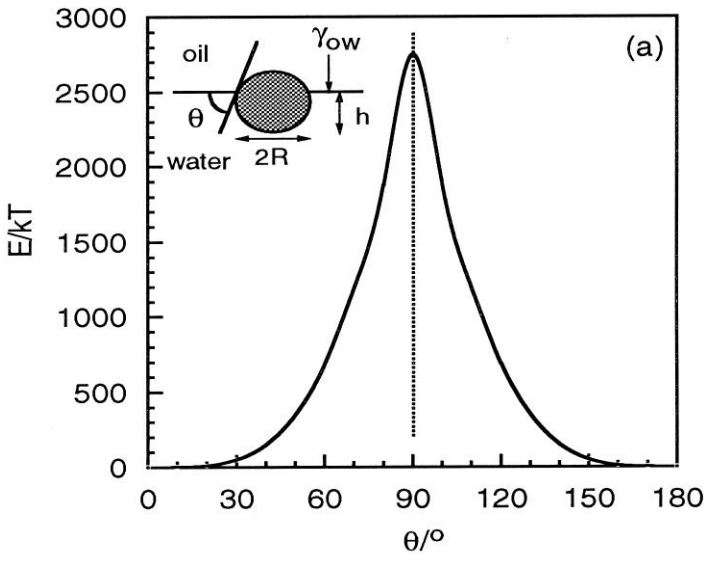

Figure 2.7 Theoretical relationship between desorption energy and contact angle at a planar oil−water interface. Particle radius R = 1 × 10^{-8} m, interfacial tension γ_{ow}= 36 × 10^{-3} N m^{-1} The contact angle θ is measured from the water phase at 298 K. Adapted from Reference 59.

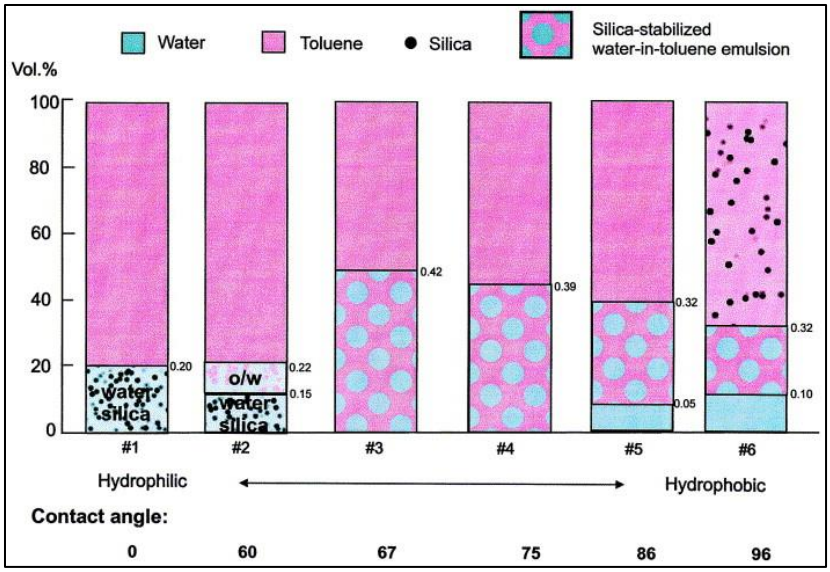

Figure 2.8 Silica nanoparticle-stabilized water-in-toluene emulsions with a list of contact angles. Volume fraction of water is 0.20. Silica concentration is 5 kg m^{-3}. Adapted from Reference 63.

2.1.3.3 Effect of Particle Concentration

Particle concentration is an important factor for emulsion stability. Several publications show that increase of particle concentration will improve emulsion stability.[64-66] As particle concentration increases, the surface coverage of emulsions increases, providing an improved emulsion stability. In addition, increased particle concentration might provide increased viscosity of continuous phase to improve emulsion stability. Binks et al utilize 25 nm silica nanoparticle-PDMS-water system to study the effect of viscosity on emulsion stability. They find the viscosity of continuous phase increases with particle concentration, while the emulsion size remains constant.[64] Thieme et al find that at high particle concentration, excess particles in continuous phase may provide a three-dimensional network surrounding emulsions to increase their stability.[61] Although increased viscosity of continuous phase might improve emulsion stability, it will lead to production and application problems. Therefore, particle concentration requires a careful selection.

Increased particle concentration might also lead to phase inversion under some conditions. For instance, Binks et al report that under high silica particle concentration, the silicon oil-water emulsions switch from oil in water (o/w) to water in oil (w/o) emulsions.[67] This phenomenon is due to a hydrophilicity change as particle concentration increased; in the oil phase, particles form aggregates and more hydrogen bond forms between silanol groups at particle surface, causing decreased hydrophilicity.

2.2 Seeded Emulsion Polymerization

For emulsion polymerization, the size of latex particles is determined by both the short nucleation stage at the beginning of nuclei stabilization stage during latex particle growth in reaction. A potential issue is that the short nucleation is a variable process, determined by radical formation. This variability results in fluctuation of polymerization speed and final particles' size.[68] In order to solve the above-mentioned problem, seed particles are added at the beginning of reaction to minimize variability during nucleation stage. This enables researchers to control polymerization reaction rate and the size of latex particles in an easy way. Furthermore, less reactor build up is necessary for seeded polymerizations. The addition of seed provides more stable lattices, as evidenced by reduced customer complains. Moreover, the formation of bimodal latex with less product viscosity is feasible under careful control of seed concentration applied.

For seeded emulsion polymerization, nucleation stage during the starting few percentage conversion is a very important. As the seeds are formed in nucleation stage, their growth continues to form final latex particles. Nucleation stage influences both the size of final latex particles and polymerization rate, because the number and surface area of seeds determine latex particle growth rate.[69] For semi-batch polymerization reaction and reactions require feeding during reaction process, nucleation stage is very important.

During the nucleation step, initiation takes place as initiators decompose to form radical species, due to external stimuli like increased temperature or addition of reducing agent. Oligomer radicals are formed as initiator radicals interact with monomer species with increasing molecular weight. Increased molecular weight of these oligomers induces their decreased solubility in water. Subsequently, nuclei are formed as these oligomers

precipitate and aggregate with other precipitated oligomers. Several factors determine radical initiation include dissolved oxygen concentration, inhibitors and impurities.[70] In some cases, these factors are difficult to eliminate/control. This results in considerable variability of polymerization reaction rate and the size of latex particles. Seeded emulsion polymerization is an effective way to reduce this problem by providing uniform seeds from which oligomers/polymers are able to grow.

Any type of small particles (organic polymers or inorganic materials) could potentially serve as seeds for seeded emulsion polymerization to form final latex particles. Under the condition that the surface area or number of seeds is sufficient to absorb all dispersing oligomers radical species, final latex particles with uniform size will be obtained. The concentration and size of final latex particles depend on seed particle concentration. Seeds particles need to be small enough and stable in reaction environment; however, it is not necessary to be the same composition with the final latex particles. Reports demonstrate that the properties of the final latex particles are not changed by utilizing seeds containing only 5 wt% reaction polymers. The size distribution of seeds plays a role on the size of final latex particles.[71]

Reports demonstrate seeded emulsion polymerizations are applied to produce waterborne paints, where 200 nm final latex particles are formed (Figure 2.9). Carboxylate-modified methacrylate copolymer latex particles serve as seed particles with reproducible particle size of 70 nm. In order to obtain a uniform latex particle size, pH has to be raised above 6 as the latex was modified by carboxylate groups.[72] As shown in Figure 2.10, the weight of seeds is in linear relationship with final latex particle size, where the size of latex particles decreases with increased seed weight. It is calculated that

for each seed are present in reaction environment, two final latex particles are formed. This indicates some in-situ nucleation takes place. Compared to other emulsion polymerization process, seeded emulsion polymerizations provide more repeatable results and desirable particle size control.

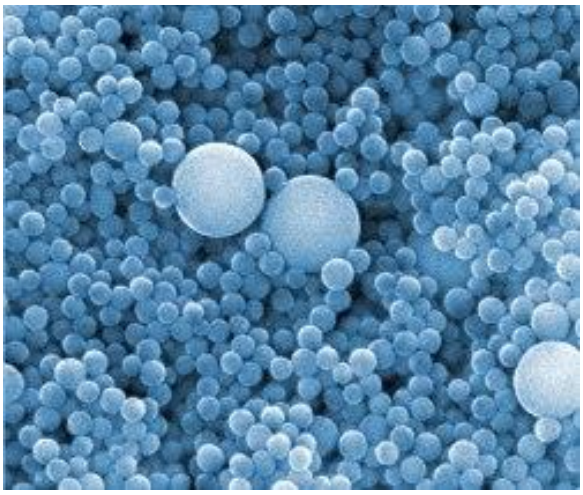

Figure 2.9 Carboxylate-modified methacrylate copolymer latex particles synthesized via seeded emulsion polymerization Adapted from Reference 71.

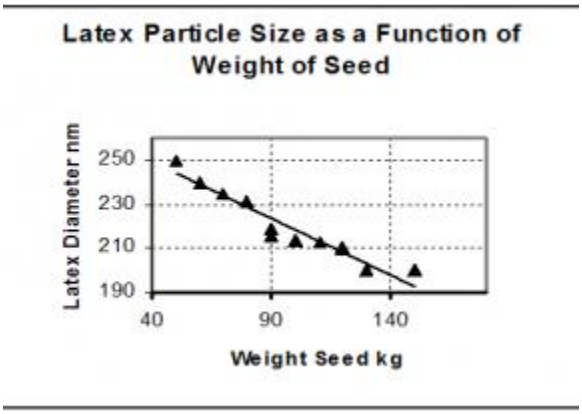

Figure 2.10 Relationship between latex particle size and weight seed. (Figure adapted from http://www.chemical-associates.co.uk/)

2.2.1 Solid Particles as Seeds for Seeded Emulsion Polymerization

Currently, both organic polymer particles and inorganic particles could serve as seeds for seeded emulsion polymerization. For organic polymer particles, seeds are not limited to particles with same composition as final latex particles. Under the condition that the surface area or number of seeds is sufficient to absorb all dispersing oligomers radical species, final particles are usually formed with uniform particle size. For inorganic particles as seeds, in order to allow monomers grow on the seeds, chemical bindings are needed between inorganic particles and monomers. Utilizing inorganic particles as seeds for seeded emulsion polymerization, final particles with unique complex structure could be obtained.

Ravaine's group utilizes silica nanoparticles as seeds for synthesis of silica-polymer composite particles with different structures.[73-74] These silica particles' surfaces are modified with methacrylate group, allowing subsequent emulsion polymerization of styrene to form daisy-shaped and multipod-shaped composite particles (Figure 2.11). Via simple control of the density of polymerizable groups at silica's surface and reaction time, the morphology of these particles can be controlled. These particles show potential applications as building blocks for more complex and hierarchical supra-particular assemblies.

(a)

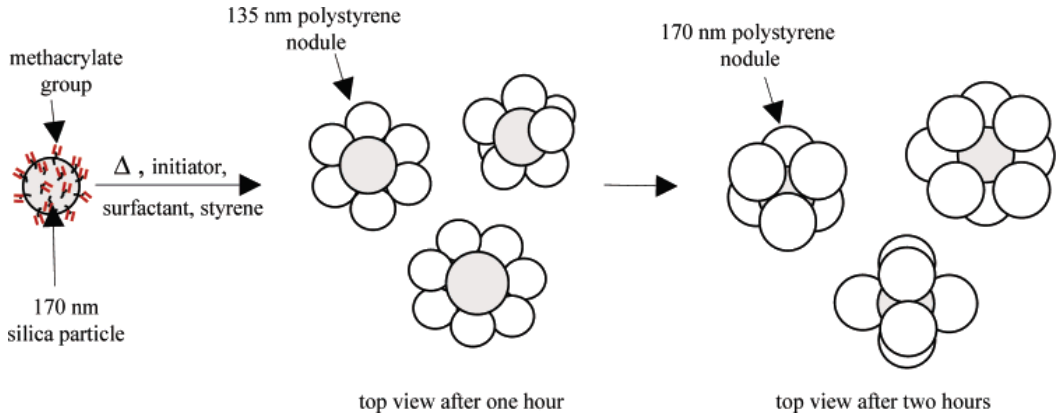

(b)

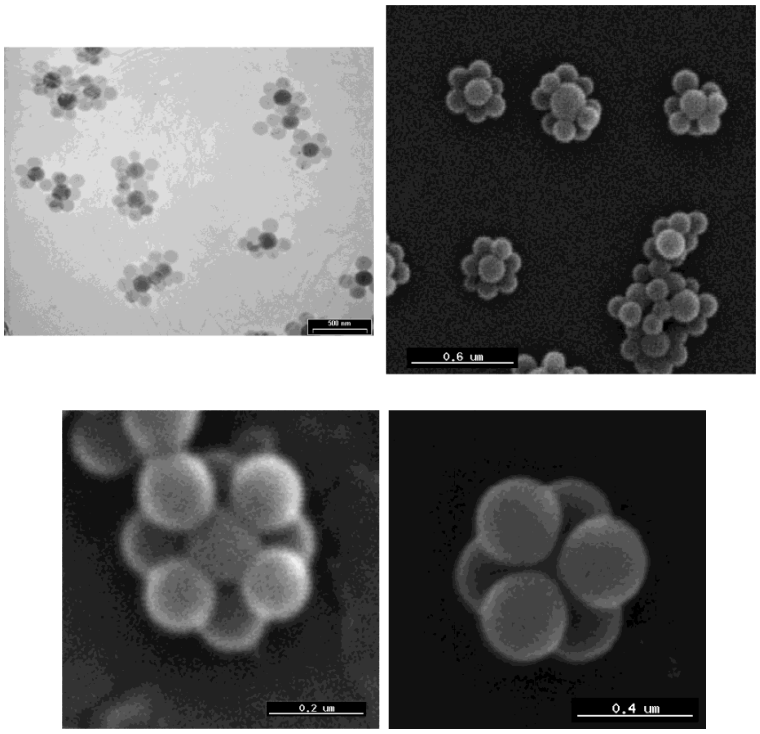

Figure 2.11 (a) Illustration of formation pathway of silica-polystyrene composite particles with daisy-shaped and multipod-shaped. (b) TEM and SEM images of silica-polystyrene composite particles with daisy shape and multipod shape. Adapted from Reference 73.

Reports show that AuNPs have the potential capability of serving as seeds for seeded emulsion polymerization. Several publications demonstrate a moderate interaction between aromatic rings and AuNP surface.[2, 75-76] Miyamura et al find that polystyrene ligands could serve as stabilizing reagent to avoid aggregation of AuNP clusters. Kumar et al suggest the reduction of π electrons clouds density of aromatic rings will result in negligible binding of the substituted benzenes with AuNP surface. Ohnuma et al find asymmetric gold-polystyrene composite particles are synthesized via precipitation polymerizations, with the aids of cross-linkers.[77] A seeded formation mechanism is proposed where polystyrene polymers are able to provide aromatic rings to interact with the surface of AuNPs. Therefore it is possible that for reactions involving AuNPs and monomers with aromatic components, seeded-growth formation is taken place, where monomers/oligomers dispersed in water phase are able to provide π electrons from aromatic rings to interact with AuNPs in water phase.

2.3 Gold Nanoparticles with their Optical and Catalytic Properties.

2.3.1 Surface Plasmon Resonance

Surface Plasmon Resonance (SPR) is the collective resonant oscillation of the conduction electrons of noble metals.[78] Figure 2.13 (left) is the illustration of how resonant electric field triggers displacement of conduction electrons. For AuNPs, SPR enables a sharp and intense absorption band in the visible range. Figure 2.13 (right) is the UV-Vis absorption spectrum of 20 nm AuNPs.

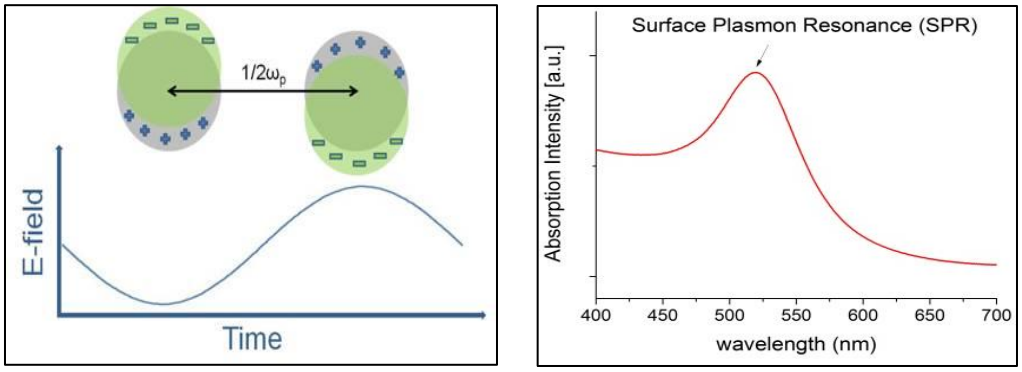

Figure 2.12 (Left) Illustration of SPR oscillations triggered by an oscillating E-field. The periodic displacement of the conduction band electrons (green) from the nuclei (gray) is demonstrated. ω_p is the SPR frequency. (Right) Typical extinction spectrum of 20 nm AuNPs based on SPR. The absorption peak locates at wavelength of 523 nm. Adapted from Reference 78.

For spherical nanoparticles with size much smaller than incident light wavelength, the dipole approximation of Mie theory explains how oscillating electric field triggers the displacement of electrons in conduction band. In dipole approximation of Mie theory, the scattering and absorption of particles will induce energy loss in the light propagation direction. This energy loss is quantified via extinction cross section as a function of wavelength. Equation 2 is the extinction cross section of a single metal particle,

$$C_ext(\lambda) = \frac{24\pi^2 R^3 \varepsilon_m^{3/2}}{\lambda} \frac{\varepsilon''(\lambda)}{(\varepsilon'(\lambda) + 2\varepsilon_m) + \varepsilon''(\lambda)^2} \quad (2)$$

where λ is the incident light wavelength, $\varepsilon(\lambda)$ is dielectric function of the particle $\varepsilon(\lambda) = \varepsilon'(\lambda) + i\varepsilon(\lambda)$, ε_m is the dielectric constant of the medium. R is particle radius.

From this equation, the extinction cross-section is determined by dielectric function of metal and dielectric constant of medium. In terms of dielectric function of metal nanoparticles, this dependence enables metal nanoparticles distinctive absorption and scattering properties. The dielectric constant of the medium also plays an important role on extinction properties of metal nanoparticles. Take AuNPs as an example; a common phenomenon is that the color of AuNP solution varies with different solvent being used, as the dielectric constant of the solvent is changed. This phenomenon is investigated by UV-Vis spectrometer by Underwood et al.[79] They test 16 nm AuNPs dissolved in a list of solvents with different dielectric constants and the results show the absorption peak red-shift from 520 nm to 545 nm, as the solvent refractive index changes from 1.3 to 1.6. This result agrees well with the predicted value of dipole approximation of Mie theory.

2.3.2 Catalytic Properties.

Sustainable chemistry is a major concern in 21st century.[80-81] Tremendous efforts have been devoted to energy conservation and saving resources such as fossil fuel. Compared to stoichiometric reactions which require multiple steps with high E-factor (weight ratio of by product to desired product) of 5-10, simple reactions with low E-factor and minimum energy loss are preferred. The term "green" process is defined as process at room temperature and atmospheric pressure, in water solution or solvent-free conditions, and utilizing air and hydrogen gas as oxidant and reductant, respectively.

Gold in bulk phase has been considered as chemical inert material for thousand years, suitable for art and luxury items. However, researchers have found that as the size reduced to nanoscale, gold materials have exhibit an excellent catalytic properties

towards various types of reactions.[82] For most cases, AuNPs have exhibited higher catalytic activity, stability and selectivity under lower temperature condition, compared to palladium and platinum counterpart. This shows great potential for sustainable process. Zhang et al.[83] have summarized the contribution of AuNP catalysts toward chemical synthesis. First, AuNPs are found to have capability of removing environmentally harmful materials at room temperature and atmospheric pressure. (e.g. carbon monoxide, nitrogen oxides, volatile organic compounds (VOC)). Second, unlike conventional noble metal catalysts Pd, Ru etc., which are difficult to catalyze important reactions such as hydrochlorination of alkynes, epoxidation of terminal olefins, AuNPs have shown excellent catalytic performance towards these reactions. Moreover, it is found that a unique Au-Pd alloy catalytic system is capable of improving efficiency and selectivity in selective oxidation reaction, which might be a breakthrough in the catalyst industry.

For selective hydrogenation reaction, Okumura et al synthesize a series of AuNP supported by alumina substrate via different methods, and investigate their catalytic performance on the 1,3-butadiene hydrogenation reaction.[84] They find that through the application of deposition-precipitation method, synthesized AuNPs achieve the best performance, where 1,3-butadiene conversion is approximate 100%, with good selectivity (over 60%) to the desired 1-butene (side product 2-butene). Excellent catalytic performance is also shown in α,β-unsaturated aldehyde hydrogenation, nitro group hydrogenation, anhydride hydrogenation and aromatic ring hydrogenation.[83] For selective oxidation reactions, AuNPs have shown good performances towards selective oxidation of alkanes, epoxidation reactions, alcohols oxidations, aldehydes oxidations, silanes oxidations and hydrosilylation reactions, as well as biomass transformation to fine

chemicals.[83] For reactions involving addition to multiple C-C bonds, AuNPs demonstrates an important role as Lewis acid towards multiple C-C bonds.[85] For addition to alkynes, the coordination of AuNPs with carbon triple bonds is very effective.[85-88] As shown in Figure 2.14, alkyne turns into activated nucleophiles, where the final step is the Au-C bond cleavage. For hydroamination of multiple C-C bonds of AuNPs, several publications are reported. Recently, AuNPs exhibit high catalytic activity towards hydrosilylation of multiple C-C bonds.[89-90] For addition to olefins, past catalysts do not give desirable results, as unsaturated C-C bonds, in specific C=C bonds, favored to react with electrophiles. However, AuNPs demonstrate that alkenes can be activated by AuNPs catalysts, where $CuCl_2$ is needed for stabilization of AuNPs reason.[91-92] For alkylation of heterocycles by carbonylic reagent, cyclization reactions, AuNPs are considered as desirable catalysts for furan condensation by carbonyl compounds under mild conditions.[93-95] For green chemistry considerations, AuNPs are more desirable compared to Brensted acids.

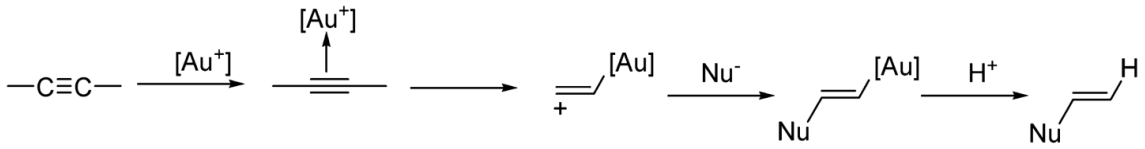

Figure 2.13 Illustration of summary of reaction mechanism for nucleophilic addition to carbon-carbon triple bonds catalyzed by gold nanomaterials. Adapted from Reference 85.

For cyclization reactions, the conversion of 2-substituted furans into phenol derivatives by gold salt is reported by Hashmi et al, where a unique ring expansion shows promising potentials for modification of phenols from furans.(Figure 2.15)[95-96] For

benzannulation reactions, gold salts are capable to catalyze benzannulation reactions such as enynal, enynones and alkynoates substructures with carbon multiple bonds.[97-98] AuNPs are suitable for green chemistry purpose. For C-C coupling reactions, reports show AuNPs are capable of serving as catalysts for Suzuki-Miyaura coupling reaction, the same role of the past Pd catalysts.[99] Corma et al report that Gold/CeO_2 serves as catalysts towards Sonogashira cross-coupling reaction and excellent yield with a very high selectivity of 99% is obtained.[100]

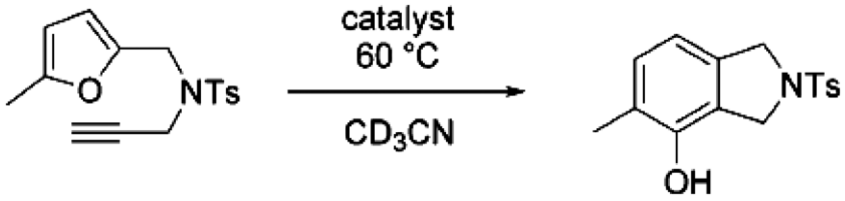

Figure 2.14 Illustration of the rearrangement reaction of o-alkynyl substituted furans into phenols catalyzed by gold nanomaterials. Adapted from Reference 85.

Nowadays green chemistry demands us to apply oxygen as preferred oxidation reagent for oxidation reactions. Here AuNPs show capability of serving as catalysts for oxidation reaction utilizing oxygen reagents. It is reported that supported AuNPs demonstrate superior catalytic selectivity of 99% for propylene oxidation reaction in the presence of hydrogen.[101-112] However, the limitation exists that it is hard to achieve high selectivity with conversion above 1 %.

Supported AuNPs

Compared to pure dispersed AuNPs, the primary role of composite gold particles is to reduce the nanoparticle agglomeration problem and increase particle recyclability. For

pure AuNPs, the nanoparticles tend to agglomerate, leading to decreased catalyst activity and recyclability with short shelf lifetime.[85] In addition, supports are found to participate directly or indirectly in catalytic reaction to improve catalytic activity.[85]

Supported gold composite particles have been synthesized with different structures. ishida et al summarize four typical structures of supported AuNPs.[113] (See Figure 2.16) Tsukuda et al.[114] synthesize poly(N-vinylpyrrolidone) (PVP)-capped AuNPs with diameters 1.3 nm. These AuNPs successfully catalyze benzyl alcohol oxidation reaction to produce benzaldehyde. The reaction proceeds in water under 30 ℃ with O_2 as oxidant. They demonstrate the TOF value increases as AuNP's size decreases from 6 nm to below 3 nm. However, due to their small size, these AuNPs are difficult to recycle. Figure 2.16b is the polyacrylic resin (poly-2-(methylthio)ethyl methacrylate-N,N-dimethyl acrylamide-N,N-methylene bisacrylamide (MTEMA-DMAA-4-8))-supported AuNPs with gel structure.[5] The aggregation problem is avoided as the gel pore size (2.5 nm) is just slightly larger than AuNPs (2.2 nm). They demonstrate that these gel-type particles successfully catalyze pentanal oxidation reaction to produce pentanoic acid with 95% conversion. Figure 2.16c is polystyrene-encapsulated AuNPs where AuNPs are stabilized with aromatic rings of polystyrene substrate.[2] These particles demonstrate excellent recyclability and catalytic activity at room temperature. Deng and Haruta[115] develop a simple way to synthesize polymer-supported AuNPs via surface functional group of anion-exchange resin. The AuNPs are stabilized on the surface of anion-exchange resin as illustrated in Figure 2.16d. These supported AuNPs demonstrate excellent TOF (turnover frequency) value for glucose oxidation reaction in water solution.

Supported AuNP catalysts provide a path to bridge the space between homogeneous and heterogeneous catalysis. The combination of gold nanoparticles and support provides new options of catalysts because the properties of these composite particles could not be achieved from support nor bare gold nanoparticles alone. In addition, gold nanoparticles are able to interact with support via electron transfer within their pathways. This interaction provides stabilization of charged species on support's surface serving as Lewis acids as they serve in corresponding salts in solution.[85, 116-117]

AuNPs are reported to exhibit strong interactions with supports, as evidenced by the presence of charged gold detected from several spectroscopies, and the fact that these AuNPs are able to catalyze reactions which requires charged gold species.[85] This indicates that even argument exists that charged species are not located on support, one has to admit that there must be some unsaturated gold atoms in support capable of polarizing reaction molecules in a similar pathway as Au(III) and Au (I) serve in homogeneous solution. This property indicates that AuNPs potentially provide catalytic applications expanding to new reactions. In addition, it is desirable to utilize these unsaturated AuNPs to interact with chiral ligands, forming chiral AuNP active sites. This property also provides possibility of new research direction involving synthesizing multifunctional AuNP catalysts as new product, as well as one-pot reaction with multi-steps.

The successful applications of AuNPs as catalysts also provide insights on stabilization and control the formation of other surface charged noble metals such as Pt, Ir, Rh, Pd, etc. Therefore, similar to Au species, other surface charged noble metals are possible to transfer from homogeneous species to solid catalysts and subsequently heterogeneous

catalysts like supported catalysts. This could potentially serve as a bridge between homogeneous catalysts and heterogeneous catalysts.

Application of AuNPs is limited due to their cost and availability. However, AuNPs provide promising potentials for industrial applications, considering the fact that the main concern in industry is catalyst effectiveness related to catalyst activity and selectivity. This productivity influences supported AuNPs' stability and durability. For the same reason, other noble metals such as Pt, Ir, Rh, Pd, etc. could be used where estimated catalysts cost is acceptable and effectiveness of catalysts is more concerned. Reports demonstrate that AuNPs, like other precious noble metals could be recollected and recycled. Currently, market data show that comparing to other noble metals such as Pt, Pd, Au is more available with stable price. Therefore, compared to other precious noble metal catalysts, application of AuNPs might be more effective.

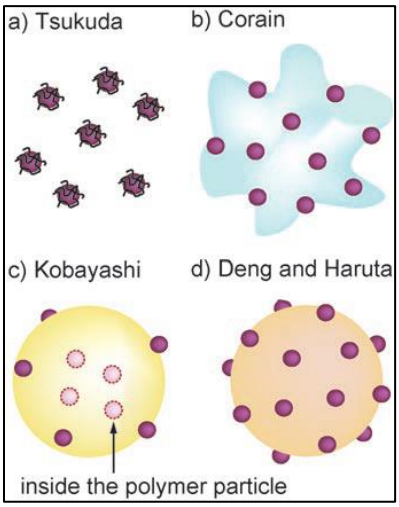

Figure 2.15 Schematic illustration of polymer-supported AuNPs. a) Polymer (PVP)-capped AuNPs b) Functionalized resin-supported AuNPs. AuNPs are anchored within the resin pores c) AuNPs embedded inside the polymer substrate, and d) AuNPs supported on the surface of polymer particle substrate. Adapted from Reference 113.

2.4 Motivations

2.4.1 Core-shell Polystyrene-Gold Composite Particles via Pickering Emulsion Polymerization.

In recent years, the idea of customizing design of material's optical properties has attracted increasing research interest. Surface plasmon resonance properties of noble metal are found to be tunable by controlling the design of geometry of polymer-gold composite particles. Halas and coworkers are pioneers for designing core-shell structured gold composite particles with specific surface plasmon resonance properties. For core-shell nanocomposite particles with a dielectric core and an AuNPs shell, the particles exhibit unique SPR properties corresponding to their dimension ratio of the core and the shell [10-13] or the interparticle distance between adjacent AuNPs[118-119] (See Figure 2.17). This dependence is attributed to the plasmons hybridization interaction between the inner gold-core interface and outer gold-surrounding medium interface of the AuNP shell layer. This tunable SPR wavelength feature is attractive for applications in solar energy harvesting (tune the SPR wavelength to infrared region where the major part of the sunlight energy can be absorbed), conducting polymer devices (tune the SPR wavelength to polymer's triplet exiton to quench the triplet exiton thus reduce photo-oxidation problem), drug delivery (tune the SPR wavelength to infrared region to transfer absorbing light to heat therefore rendering drug release with the help of "smart" thermo-responsive material.), and biosensors (tune the SPR wavelength infrared region).[14,16-18,120]

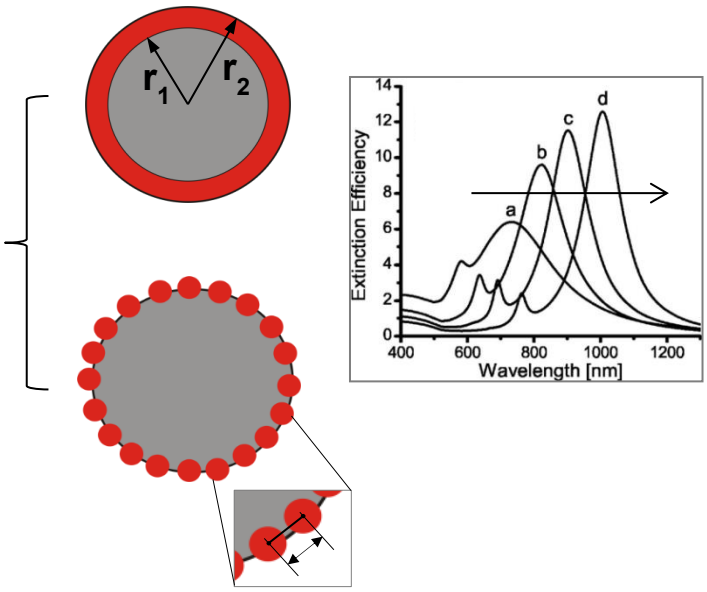

Figure 2.16 Schematic illustration of tunable surface plasmon resonance properties of core-shell structured polymer-gold composite particles.

To date, the conventional synthesis methods of core-shell structured gold composite particles are mainly based on chemical binding or electrostatic attraction interaction, which often require multiple steps with sophisticated instruments. That is, preforming AuNPs and driving them to coat the substrate particles[10-11, 42] or directly forming the AuNPs at the substrate particles' surface.[43-45] During these processes, modifying the substrate particle or AuNP's surface is required. For the synthesis of polymer-gold core-shell composite particles, Pickering emulsion polymerization method has its advantages. Pickering emulsion polymerization enables core-shell structured composite particles to be formed in one step, using a simple reaction set-up. Recently, we have developed the one-step Pickering emulsion polymerization route to synthesize silica core-shell nanocomposite particles.[46-47] Driven by the necessity of developing a new and simple route of synthesizing polymer-gold core-shell particles, we employ the one-step

Pickering emulsion polymerization to synthesize the desired core-shell composite particles.

Currently, solid stabilizers that utilized in Pickering emulsion polymerization are limited to silica particles, titania particles and laponite platelets. The common advantage of these three solid stabilizers is that high concentration of the particles is available with low cost. As mentioned before, high particle concentration in the reaction is able to increase the surface coverage of the solid stabilizers to provide emulsion stability. In addition, it is reported that the excess of solid stabilizers are able to provide 3-D network surrounding emulsions to provide emulsion stability. On the other hand, to our best knowledge, it remains challenging for AuNPs to be utilized as stabilizers in Pickering emulsions. The high Hamaker constant of AuNPs prevent them from forming stable Pickering emulsions.[121] Pozzo and coworkers successfully stabilize water-hexadecane emulsions by using functionalized AuNPs, where the AuNPs' surface is modified by hydrophilic polyethylene glycol-thiol ligand and hydrophobic alkane-thiol ligand.[122] However, due to the chemical inertness of hexadecane as the oil phase, emulsion polymerization could not proceed.

To the best of our knowledge, the morphology study of core-shell polymer-gold composite particles is not of research interests. This is mainly because for core-shell polymer-gold composite particles synthesized via conventional route described above, AuNPs generally distributed randomly on the surface of polymer core, as no uniform interaction force is present between AuNPs. On the other hand, here it is intriguing to investigate the morphology of core-shell polymer-gold composite particles synthesized via Pickering emulsion polymerization. This is because for Pickering emulsions, solid

stabilizers are able to self-assemble at the emulsion's oil-water interface with a long-ranged lattice structure.[140-141] It is possible that the ordered lattice structure could be maintained during Pickering emulsion polymerization to give core-shell composite particles with ordered lattice structure on the surface.

2.4.2 "Smart" PNIPAm-Gold Composite Particles with Tunable Optical Properties

2.4.2.1 Tunable Surface Plasmon Resonance of Polymer-gold Composite Particles.

The advent of synergistic combination of "smart" polymers (thermo-responsive PNIPAm polymers in particular) and inorganic nanomaterials triggers increasing research attentions in recent years. Several PNIPAm-gold composite materials have been synthesized with unique structures, showing that the material's optical properties can be tuned based on PNIPAm's thermo-responsiveness. For example, Tagliazucchi et al. present a model demonstrating that for PNIPAm-coated AuNPs, as the coated PNIPAm layer collapses above the LCST, the change of refractive index of the PNIPAm medium leads to a slight red-shift of the particle's SPR wavelength.[27] Sorrell et al. fabricate a color-tunable film in which the PNIPAm microgel layer is sandwiched by two Au substrates. The color-tunable property is based on tuned interference properties.[30, 123]

Recently, Lv et al proposed a potential application based on this tunable SPR properties.[120] This tunable SPR properties is based on Equation (3):

$$\frac{r_1}{r_2} = \left[1 + \frac{3}{2}\frac{\varepsilon_2'(\lambda)(\varepsilon_1 + 2\varepsilon_3)}{\varepsilon_2'(\lambda)^2 - \varepsilon_2'(\lambda)(\varepsilon_1 + \varepsilon_3) + \varepsilon_1\varepsilon_3 - \varepsilon_2''(\lambda)^2}\right]^{1/3} \quad (3)$$

where λ is the wavelength corresponding to the diameter ratio. ε_2' and $\varepsilon_2''$is the real and imaginary part of AuNP dielectric function respectively. $\varepsilon_1$and $\varepsilon_3$are the dielectric functions of the core and surrounding medium respectively.

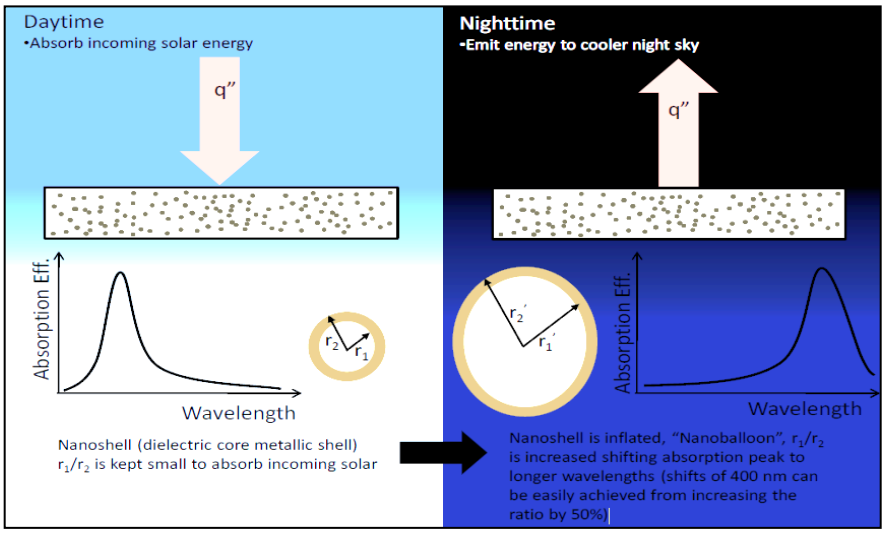

Figure 2.17 Schematic illustration of dual use solar thermal collector/night-sky radiator. Adapted from Reference 120.

The potential application leads towards two directions. The first is that radiative properties are dynamically controllable, providing potential technological opportunities for nanofluid application. A theoretical design is a "dual use solar thermal collector/night-sky radiator" (Figure 2.18). In the day time (T>32 °C), r_1/r_2 ratio is kept small with absorption/emission wavelength blue-shifted to the high energy range; in the night time (T<32 °C). r_1/r_2 ratio increases with absorption/emission wavelength red-shifted to the infra-red range. As the absorption peak wavelength is dynamically controllable, it is possible to create a system t receives solar energy during the daytime (absorption receiver), and releases energy during the nighttime for cooling purpose (radiator).

Another interesting application is to utilize the particles in a thermo-optical switch, which could serve as a nanofluid filter switching between opaque and transparent status.

2.4.2.2 Tunable Scattering Intensity of Polymer-Gold Composite Particles

Light intensity is a key factor for optical devices and could be utilized as signals for intensity-based optical sensors, which is potentially the simplest optical sensor.[124] For example, particles with switchable scattering intensity could be utilized in thermal sensor, in which the thermo-responsive scattering intensity serves as signals. However, currently tuning or utilizing the particle's scattering intensity remains less-explored.

Mie theory explains the principle of particle light scattering.[125] The oscillating electrons induce dipole reradiations. These dipole reradiations overlay each other, leading to net scattering light. The Mie's solution to particle light scattering involves two parameters, n_r (so-called "magnitude of refractive index mismatch") and x (size parameter):

$$n_r = n_p/n_{med} \quad (4)$$

n_r is the refractive index ratio of the refractive index of particle to surrounding medium.

$$x = 2\pi a/(\lambda /n_{med}) \quad (5)$$

where a is particle radius, λ is light wavelength

Based on Mie theory, the scattering intensity depends on particle size and refractive index contrast between particles and surrounding medium. The scattering coefficient increases as particle size increases, or as refractive index contrast increases.[28, 126-127] The

particle density and refractive index increase significantly, leading to a large refractive index contrast between the particles and the water phase.

Motivated by the success of synthesizing "smart" polystyrene/PNIPAm-silica core-shell composite particles in our group, we will demonstrate the synthesis of "smart" polystyrene/PNIPAm-gold core-shell composite particle. Due to the thermal responsiveness of PNIPAm polymers, both particle's size and refractive index change according to Mie theory. Therefore, we will investigate the tunable optical properties focusing on scattering intensity issue.

2.4.3 Gold-Polymer Composite Particles with Complex Structure and their Self-modulated Catalytic Activities

Nanoscale particles with complex structure have drawn an increasing research interests in recent years. Particles can be synthesized with different structure (e.g. dumbbell shape, multipetal shape etc. Figure 2.19), composition and functionality, enabling them to serve as building blocks for advanced ordered and hierarchical materials. For instance, polystyrene particles could be designed and assembled into micro-clusters functionalized with DNA patches.[128] These colloidal particles possess a variety of three-dimensional structure with specific directional bondings, imitating hybridized atomic orbitals (including sp, sp^2, sp^3). This suggests the possibility of assembling micron-sized particles in a way where molecules self-assemble in the molecule domain. In addition, particles with complex structure (e.g. multipetal shape) provide high surface roughness and large specific surface area. These unique properties might lead to potential applications such as super-hydrophobic and super-hydrophilic surfaces.[24-25] For

dumbbell-shaped composite particles, applications such as photonic band-gap materials, nanopatterns by colloidal lithography are reported.[22-23]

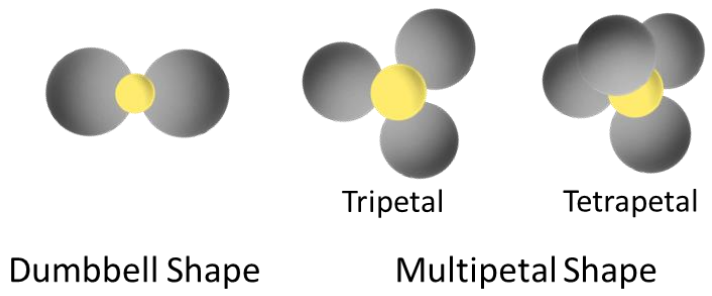

Figure 2.18 Illustration of composite particles with dumbbell and multipetal shapes.

To date, reports for synthesis of multipetal-shaped composite particles are quite rare, and the synthesis of organic-inorganic hybrid multipetal-shaped composite particles is limited to utilization of silica nanoparticle as center particle. Utilization of gold nanoparticles to synthesize multipetal-shaped composite particles is not reported. AuNPs are well-known for their unique optical and catalytic properties. As for the above-mentioned applications in building blocks for ordered and hierarchical materials, utilizing AuNP for synthesis of multipetal-structured and dumbbell-structured composite particles might provide advanced feature, potentially useful for applications in SERS substrate, etc.. Moreover, multipetal-structured and dumbbell-structured gold-polymer composite particles might serve as supported catalysts. Here we propose to employ AuNPs as seeds for one-step seeded emulsion polymerization route to synthesize of gold-center/polystyrene-petal multipetal-shaped and dumbbell-shaped composite particles.

AuNPs are well-known for their superior catalytic activity towards homogeneous reaction and heterogeneous reaction.[82, 85] Studies on synergistic catalytic function

contributed by AuNPs and thermo-responsive PNIPAm is seldom-reported. The possibility of self-controlling the catalytic properties of AuNPs is promising. Here we propose a one-step seeded emulsion polymerization route for synthesis of PNIPAm-gold composite particles. The catalytic properties of these composite particles will be investigated.

2.4.4 "Smart" Nanofluids with Self-controlled Temperature.

Solar energy collectors are widely used nowadays and are the tools for "green" solar energy harvesting. However, a common problem exists for solar energy collector: overheating problem caused by stagnation (a region in a flow field where the local velocity of the fluid is zero) of heat transfer fluids.[137] Caused by power or equipment failures or during routine shut-downs when a reduced energy is required, mid-temperature flat-plate solar collectors may reach temperatures in excess of 180 ℃.[138] During this no-flow condition, commonly referred as stagnation condition, serious damage is possible for solar collectors and system components. The harmful high temperature caused by stagnation condition might cause the following problem: accelerated degradation of collector components (ranging from visual appearance to degradation of the optical properties of the absorber coating) and heat transfer fluids; excessive pressures in absorber mountings or within the absorber structure itself (due to thermal expansion).(Figure 2.20) High temperatures in other components of the solar collector, particularly if different materials or complex geometries are used (e.g., insulation, gaskets and sealants) may also result in accelerated material degradation or outgassing of volatile compounds that may condense on the optical surfaces of the

collector, (e.g., the surface of absorber or the interior of glazings); scalding temperatures, a potential danger for residents.[137]

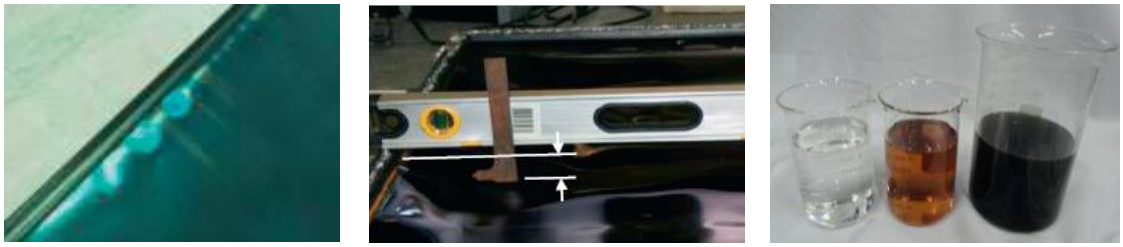

Figure 2.19 (left) Deformation and bending of absorber plate at edge due to its constrained thermal expansion during stagnation; (middle) permanent deflection of absorber plate due to constrained thermal expansion of solar collector absorber plate; (right) degradation of propylene-glycol/water solution after increased time-exposure to high temperatures. Photos adapted from Reference 137.

Nanofluids are dilute dispersions of particles with nanometer size. Nanofluids are found to be potentially useful as heat transfer fluid due to their enhanced heat transfer coefficient.[139] In particular, it is possible to employ nanofluid materials to serve as heat transfer fluids in solar collector system. Recently, Dr. Otanicar has developed a theoretical model of "smart" nanofluids with self-regulated temperature (Figure 2.21). These "smart" self-temperature-controlled nanofluids are proposed with capability of reducing temperature under stagnation condition. These nanofluids are composed of thermo-responsive PNIPAm-gold (or other inorganics) core-shell structured composite particles. Due to the thermo-responsiveness of PNIPAm, particles in dispersions are in swollen stage under normal operation conditions, below LCST; when stagnation occurs (above LCST), particles are in shrinkage stage. According to the model, the absorbed

energy is proportional to particle diameter and absorption efficiency (Equation 7). Assume the absorption efficiency is constant, as particles undergo size decrease, the volume fraction decreased, leading to decreased absorbed energy. Figure 2.22 shows decreased absorbed energy leads to decreased temperature decrease. Therefore, the self-temperature-control property of nanofluids is achieved.

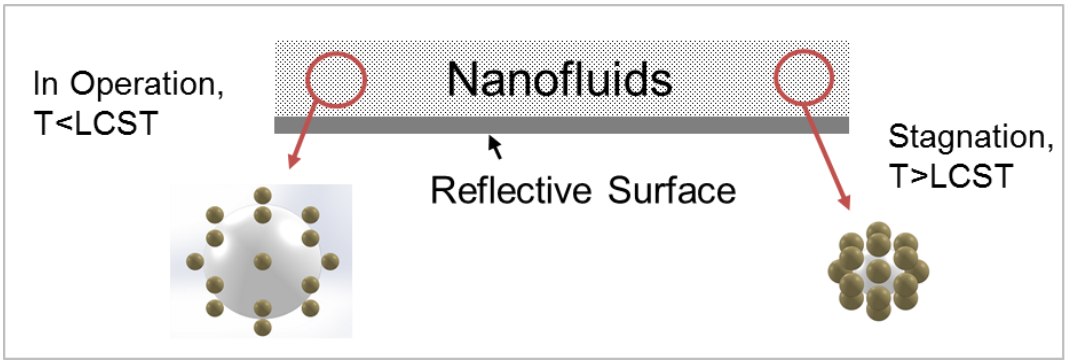

Figure 2.20 Schematic illustration of performance of "smart" nanofluids of PNIPAm-gold core-shell particles. Figure adapted from (Otanicar, 2014)

$$\text{Absorbed Energy} \propto D^2 Q_{abs} \tag{6}$$

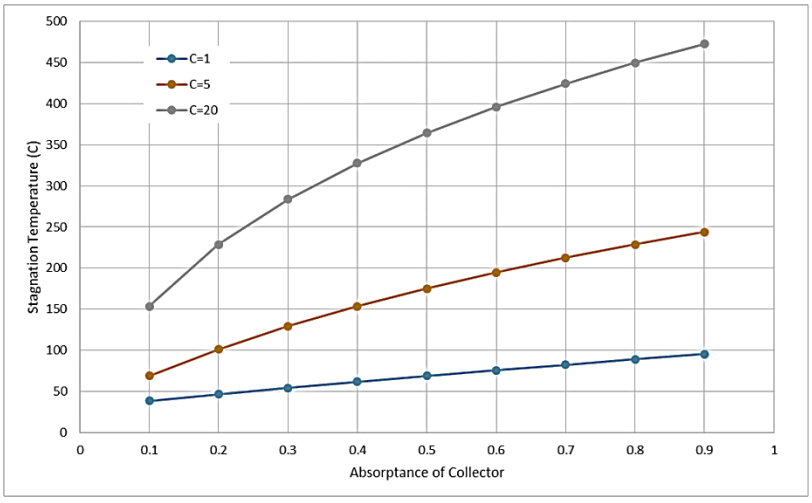

Figure 2.21 Relationship between stagnation temperature and absorption of heat transfer fluids. Figure adapted from (Otanicar, 2014)

Here we propose to experimentally develop "smart" nanofluids with the self-temperature-control ability. We plan to synthesize core-shell PNIPAm-gold composite particles with increased thermo-responsiveness. Given by the current limitation of synthesizing core-shell composite particles with significant thermo-responsiveness, we will consider modifying the synthesis recipe. For example, the reaction solution will be ended at the early stage. Kinetic study shows PNIPAm and polystyrene react at different stage: PNIPAm first, then polystyrene.[55] In addition, methods of decreasing particles size are considered, as the numerical model is based on particle size below 200 nm. Here we will decrease the styrene and PNIPAm concentration or increase initiator concentration to achieve this, based on the following theory of emulsion polymerization.[69] In Equation 8 below, M_n is the number-weighted molecule weight of particles, directly related to particle size. M_0 is monomer concentration, and $[I]_0$ is initiator concentration.

$$M_n \sim R_p e^{k_d t} M_o / k_d [I]_o \quad (7)$$

However, there is a potential problem that Q_{abs} is not constant for PNIPAm-gold core-shell particles. As shown in Figure 2.23, as temperature increases, particles shrink with absorption significantly increased. This is undesirable for temperature control. Here we propose to try some alternative particle stabilizers such as carbon black and graphite to synthesize thermo-responsive core-shell PNIPAm-carbon black/graphite composite particles. Undesirable increase of absorption efficiency will be avoided, because carbon black/graphite shows no SPR properties in this functioning wavelength range.

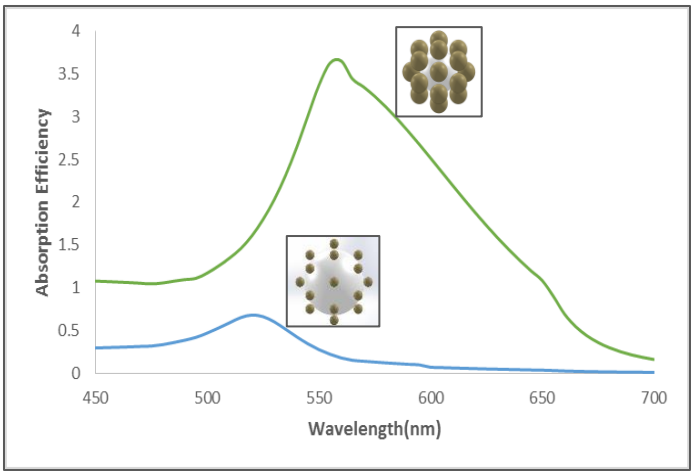

Figure 2.22 Numerical results of absorption efficiency for PNIPAm-gold core-shell particles below LCST (blue) and above LCST (green). Figure adapted from (Otanicar, 2014).

Chapter 3

METHODOLOGY

3.1 Materials

Spherical AuNPs, (20 nm, wt% of 3.0%, capping agent Nsol (alkyl acrylate), Nanopartz Inc.), styrene monomer (99.9%, Fisher), N-isopropylacrylamide monomer (NIPAAm, 97%, Aldrich), nonionic initiator VA-086 (98%, 2,2-azobis(2-methyl-N-(2-hydroxyethyl) propionamide), Wako Chemicals), and water (HPLC grade, Acros Organics) are utilized in the Pickering emulsion polymerization process without further purification. N,N'-methylene-bis-acrylamide (MBA) (MP Biomedical LLC.) is used as cross linker. Carbon black (99.9%, Alfa Aesar)

3.2 Particle Synthesis

For synthesis of polystyrene-gold composite particles, 0.1 g AuNPs dispersion, 6 ml water and 0.1 g styrene are sonicated by a VCX 500 ultrasound sonicator (amplitude 21%) to form the emulsion. For synthesis of polystyrene/PNIPAm-gold composite particles, 0.05 g AuNPs dispersion, 15 ml water and different proportion of styrene (0.1g-0.5g), different proportion of NIPAAm (0.05g-0.5g) are sonicated by a VCX 500 ultrasound sonicator to form the emulsion. The emulsion is then immediately moved to a 3-neck 15 ml flask and degassed with nitrogen for 15 minutes. After the solution is heated to 65 ℃, 0.028 g VA-086 initiator in 0.3 ml water solution is injected. The reaction lasts for 4 hours. Before characterization, the synthesized sample is washed with water by three centrifugation-redispersion cycle to remove unreacted monomers/oligomers and unattached AuNPs. The core-shell and asymmetric particles are separated by

centrifugation with speed of 5,000 rpm for 20 minutes. The core-shell particles settle down after centrifugation; the pure asymmetric particles are collected from the upper solution. For the control experiment with cross linkers, 5% (mole percentage) of MBA is added with styrene and NIPAAm monomers. For synthesis of CB-PNIPAm/polystyrene composite particles, 0.33g CB powder, 0.67g styrene, 3.3g NIPAAm, initiator VA086 0.254g, water 31.6g are sonicated by a VCX 500 ultrasound sonicator to form the emulsion. The amplitude of ultrasound sonicator is set at 31 % to avoid styrene-CB paste forming. Reaction lasts for 4 hrs.

3.3 Catalytic Study of Gold Composite Particles

Typically, 5 ml Rhodamine B solution (4×10^{-5} mol/L) are mixed with 2×10^{-3}g $NaBH_4$, and gold composite particles (AuNP concentration is 9.2×10^{-4} wt %) are added as the catalyst. UV-Vis analysis is employed to perform a time study on the reaction. For catalysts recyclability study, after each reaction cycle, the complete solution is transferred to centrifugation tube; the gold composite particles are recollected after washing with water by three centrifugation-redispersion cycles. The recyclability of the particles is determined by analyzing the conversion of Rhodamine B for each reaction cycle, via measuring the absorption intensity of Rhodamine B at the beginning and end of the reaction using a UV-Vis spectrometer.

3.4 Characterization Techniques

Particle size distributions are analyzed by a NICOMP 380 ZLS via the dynamic light scattering (DLS) technique. The transmission electron microscopy (TEM) images are obtained via an environmental TEM Tecnai F20. The TEM specimen is prepared by

placing one droplet of the solution onto TEM grids and air-drying the specimen. The energy-dispersive X-ray spectroscopy (EDX) spectra are obtained by using the TEM's adjunct X-ray detector. The specimens for the scanning electron microscope (SEM) are sputter coated with gold for 100 seconds and viewed by a SEM-XL30 (FEI). Specimens are prepared by placing a droplet of the samples onto mica substrates and allowing them to air-dry. An AR-G2 rheometer is used to measure the viscosity of solutions of asymmetric particles under steady-state flow procedure, where a 25mm plate-plate geometry is used. The UV-Vis extinction properties of the sample are analyzed via a Cary 300 Bio UV-VIS spectrophotometer. The temperature control function is utilized to study the temperature transition property of NIPAAm-incorporated particles. Extinction intensity data is taken from a Cary 300 Bio UV-VIS spectrophotometer with a laser wavelength of 639 nm. Scattering intensity data are taken from the NICOMP 380 DLS machine with laser wavelength of 639 nm.

Chapter 4

RESULTS AND DISCUSSION

4.1 Core-Shell and Asymmetric Polystyrene-Gold Composite Particles via One-Step Pickering Emulsion Polymerization.

4.1.1 Core-shell Polystyrene-Gold Composite Particles

The core-shell polystyrene-gold composite particles are successfully synthesized via one-step Pickering emulsion polymerization. Figure 4.1a is the SEM image of the synthesized particles with AuNP concentration 0.092 wt%. The core-shell gold composite particles are present with diameters of 300 nm - 470 nm. The images show that the AuNPs are covering the polystyrene substrate particle surface in an ordered hexagonal pattern. Figure 4.1b shows the TEM image of a synthesized particle with the same AuNP concentration. We focus the electron beam on the particle to perform EDS analysis and the result (Figure 4.1c) confirms the presence of gold element. To the best of our knowledge, it is the first time that an ordered lattice structure is formed and maintained during Pickering emulsion polymerization. Previously, an ordered lattice structure had only been investigated at the oil-water interfaces. Micron-sized particles like modified polystyrene particles and silica particles are able to self-assemble at the emulsion's oil-water interface with a long-ranged lattice structure.[140-141] The center-to-center distance between adjacent particles is usually several times of the particle diameter. Here it's interesting to find that after the emulsion polymerization, the ordered lattice structure maintains at the nano-scale range with short center-to-center distance (approximately 40 nm). Although multiple publications investigate the origin of this lattice structure at oil-water interfaces, it is yet not conclusive. It has been suggested that the dominant forces

are non-screened Columbic forces occurring at the oil-particle interface, due to surface residual charges at the oil-particle interface, [141-142] other than dipole-dipole repulsion due to asymmetric distribution of electrical double layer.[143] The successful formation of polystyrene-gold composite particles covered with nanoscale lattice structure provides a new way of fabricating materials with advanced functionality, such as photonic crystals and SERS substrates.

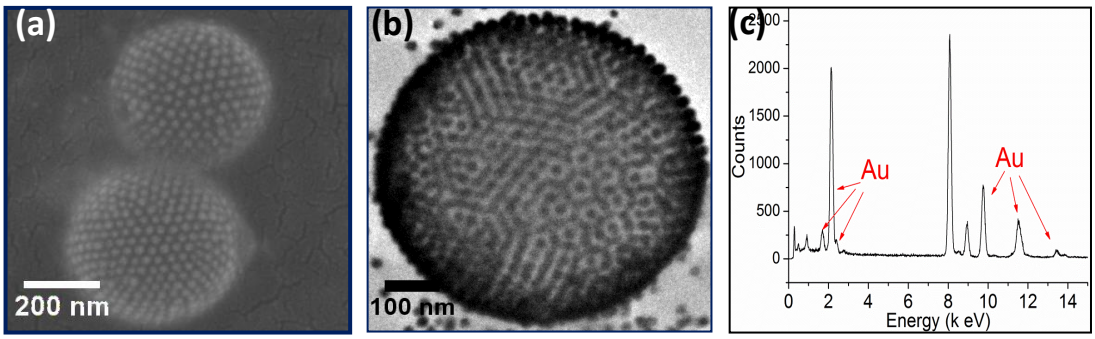

Figure 4.1 (a) SEM images of core-shell gold-polystyrene composite particles. (b) TEM image of core-shell gold-polystyrene composite particles. (c) Corresponding EDS spectrum of particles in (b). Corresponding AuNP concentration is 0.092 wt%.

We perform the surface coverage study and find that the surface coverage of core-shell polystyrene-gold composite particles is influenced by AuNP hydrophobicity and AuNPs concentration. Two types of AuNPs have been tested here to investigate the influence of hydrophobicity. The first type is AuNPs dispersed in organic solvent isopropanol with Nsol (alkyl acrylate) capping agent. The second type is AuNPs with hydrophilic capping agent, polyvinylpyrollidone (PVP). The measured zeta potential for isopropanol-dispersible AuNPs and PVP-capped AuNPs are -25 mV and -20mV

respectively. We compare the unwashed synthesized composite particles with different type of AuNPs mentioned above, under the same AuNP concentration and reaction condition. It is found that for Nsol-capped AuNPs, the polystyrene particles are covered with AuNPs and there is no residue of unattached AuNP (Figure 4.2a). In contrast, as shown in Figure 4.2b, the PVP-capped AuNPs are not attached onto but around the polystyrene core. From Figure 4.2c (left) and 2d (left), it is clearly seen that before emulsion polymerization, the Nsol-capped AuNPs distribute in both the top styrene phase and bottom water phase, indicating moderate hydrophobicity; whereas the PVP-capped AuNPs distribute mostly in the water phase, suggesting low hydrophobicity. These results are consistent with both experimental[63] and theoretical study[57], where it is found that particles with intermediate hydrophobicity require more energy to desorb from the oil-water interface, thus producing the most stable emulsions. After polymerization reaction, the Nsol-capped AuNPs solutions have a milky purple color, in contrast with the milky pink color of PVP-capped AuNPs solution. The color variation might arise from the tuned surface plasmon resonance band,[11, 144] (discussed in the next paragraph) as a result of the formation of the core-shell structure (Figure 2a). This further confirms AuNPs with intermediate hydrophobicity give enhanced AuNPs surface coverage.

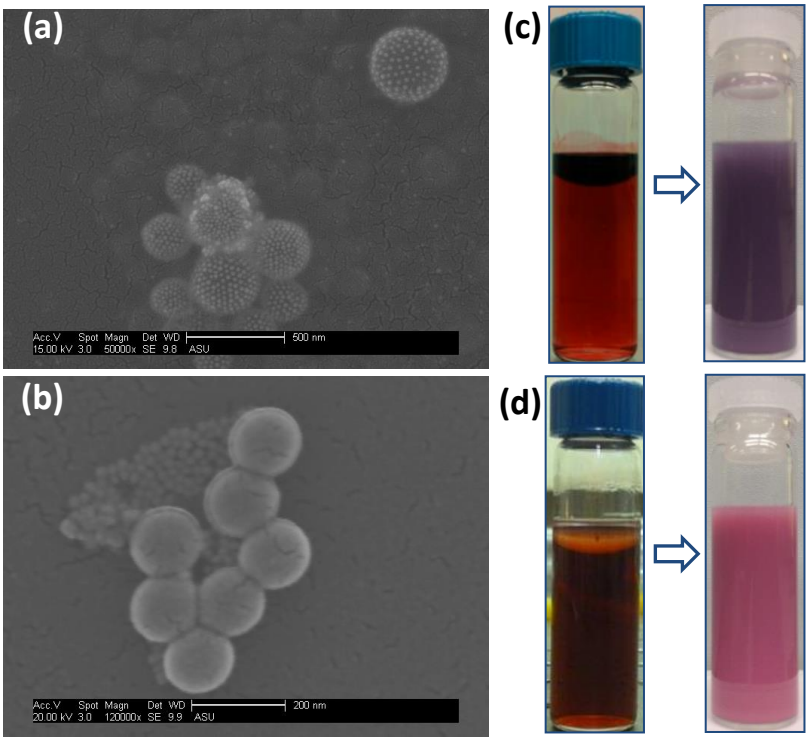

Figure 4.2 Comparison of synthesized product using different types of AuNPs. (a) SEM image of composite particles synthesized by Nsol-capped (alkyl acrylate) AuNPs (AuNP diameter: 20 nm). (b) SEM image of composite particles synthesized by PVP-capped AuNPs. (AuNP diameter: 20 nm) (c) and (d): corresponding photos for solutions before (left) and after (right) emulsion polymerization with Nsol-capped AuNPs and PVP-capped AuNPs respectively. AuNP concentration for both type of AuNPs are 0.092 wt%.

Figure 4.3 shows the effect of Nsol-capped AuNPs concentration on composite particles' surface coverage. In Figure 3a, each TEM figure shows representative particle under AuNPs concentrations of 0.009 wt%, 0.019 wt%, 0.046 wt%, 0.07 wt%, and 0.092 wt%, respectively. The surface coverage is analyzed via the grain analysis function in ImageJ®, by selecting 10 TEM images for each AuNPs concentration and taking the averaged reduced surface coverage value. The calculation is carried out using the following formula:

$$\text{Reduced Surface Coverage} = \frac{\text{Total Grain Area}}{\text{Surface area of Spherical Particle}} \qquad (8)$$

Figure 4.3 shows the reduced surface coverage is increased as AuNPs concentration is increased. We name it "reduced surface coverage" because the upper limit for this calculation method is 25%, due to the particle overlaying issue of the TEM images. For the image representing the particle with AuNPs concentration of 0.092 wt%, the average surface coverage is 20.8 %. From this coverage, we roughly estimate the center-to-center distance between adjacent AuNPs as the length of two AuNP diameters (40 nm). The interparticle distance is confirmed by the SEM image in Figure 4.1a. Figure 4.3b demonstrates the influence of AuNPs surface coverage on composite particle's SPR properties. For the three samples with AuNPs concentration below 0.046 wt%, the absorption spectra do not change. The peak at 530 nm belongs to distributed AuNPs on composite particles with low coverage, and the single AuNP on asymmetric composite particle (illustrated in next section). As AuNPs concentration further increases, separate peaks appear at 602 nm and 705 nm for AuNPs concentration of 0.07 wt%, 0.092 wt% respectively, indicating the tunable SPR properties due to increased AuNPs coverage as

the non-continuous shell. As surface coverage increases, AuNPs become close-packed, leading to enhanced electromagnetic interaction between the adjacent AuNPs; therefore, the plasmon resonance band shifts to higher wavelength. The result is consistent with Yong et al, where the SPR wavelength shifts from 698 nm to 931nm for polystyrene-gold composite particles with diameter of 543 nm, as the AuNPs shell is tuned from noncontinuous shell to continuous one.[11] A significant peak-broadening is shown for peak 705 nm, attributed to aggregated gold clusters with different aspect ratios on the composite particle's surface.[145] Although it has been reported that compared to silica nanoparticles or polymer particles, the formation of stable AuNP-stabilized emulsion is difficult due to low AuNPs concentration (0.053 wt%) and high Hamaker constant for gold surfaces interacting across water or polymers.[121] Here we demonstrate by utilizing AuNPs with intermediate hydrophobicity, the gold core-shell composite particles can be successfully synthesized under low nanoparticle concentration.

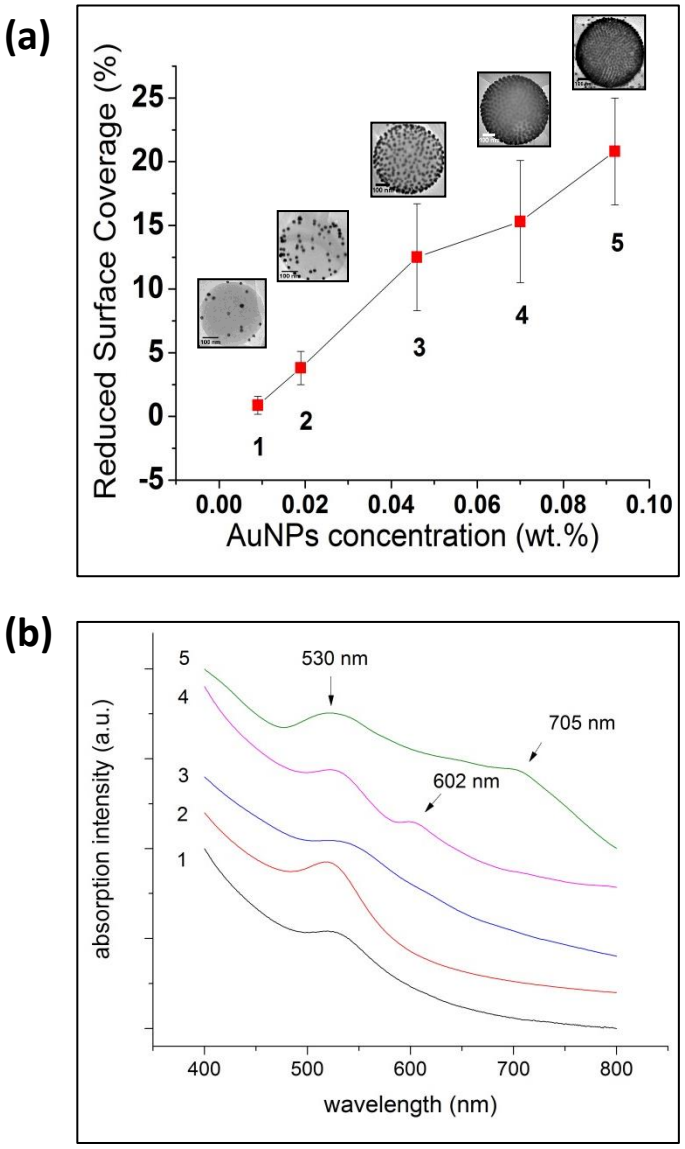

Figure 4.3 (a) Influence of AuNPs concentration on reduced surface coverage of core-shell gold-polystyrene particles. The scale bar for each TEM image is 100 nm. Corresponding AuNPs concentration is 0.009 wt%, 0.019 wt%, 0.046 wt%, 0.07 wt%, 0.092 wt%, respectively. Capping agent: Nsol (alkyl acrylate). Styrene monomer concentration is kept as constant. (b) Corresponding UV-Vis spectra of composite particles for Figure 4.3a.

4.1.2 Asymmetric Polystyrene-Gold Composite Particles and Their Formation Mechanism

During the Pickering emulsion polymerization to synthesize the desired core-shell polystyrene-gold composite particles, an intriguing observation is that under low AuNPs concentration (0.009 wt%, 0.019 wt%, and 0.046 wt%, Nsol AuNPs are utilized here), asymmetric polystyrene-gold nanocomposite particles are simultaneously formed, as shown in Figures 4.4 and 4.5. Figure 4.4a is the TEM image of the synthesized particles under AuNPs concentration of 0.046 wt%. In addition to the core-shell composite particles pictured in Figure 4.4a, the asymmetric particles are present in which only one AuNP covers each polystyrene microparticle. The DLS result in Figure 4.4b shows a bimodal distribution where two peaks are present located at 180 nm and 460 nm, representing asymmetric composite particles and core-shell composite particles respectively. The DLS result shows the asymmetric composite particles have a number-weighted percentage of 75%, and core-shell composite particles have a number-weighted percentage of 25%. As shown in Figures 4.5a and 4.5b, the asymmetric particles have a uniform size distribution. In Figure 4.5c, curve 1 represents pure asymmetric gold composite particles after filtration. The absorbance wavelength of 530 nm for asymmetric particles is approximately the same with pure AuNPs (curve 2).

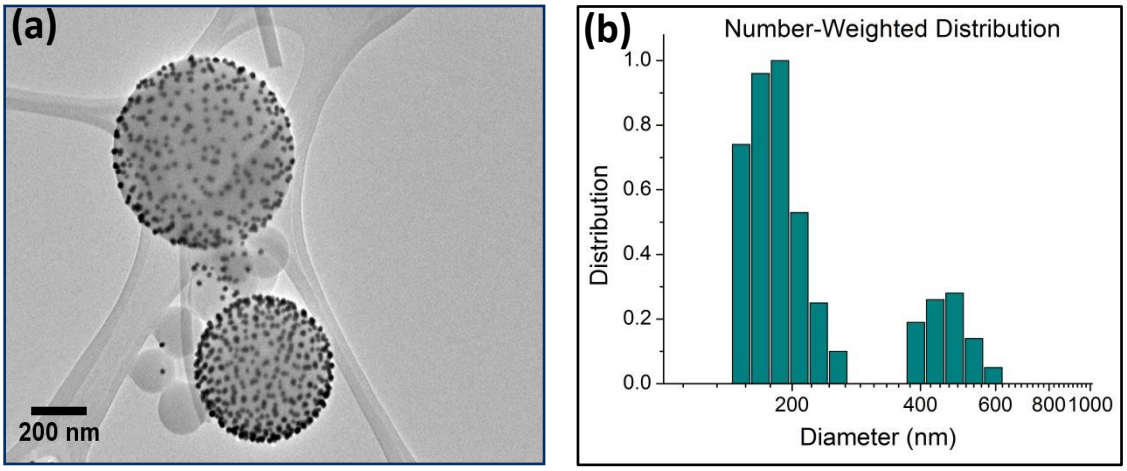

Figure 4.4 (a) TEM of the bimodal size distribution of polystyrene-gold composite particles. (b) DLS of the bimodal size distribution of polystyrene-gold composite particles. Corresponding AuNPs concentration is 0.046 wt%.

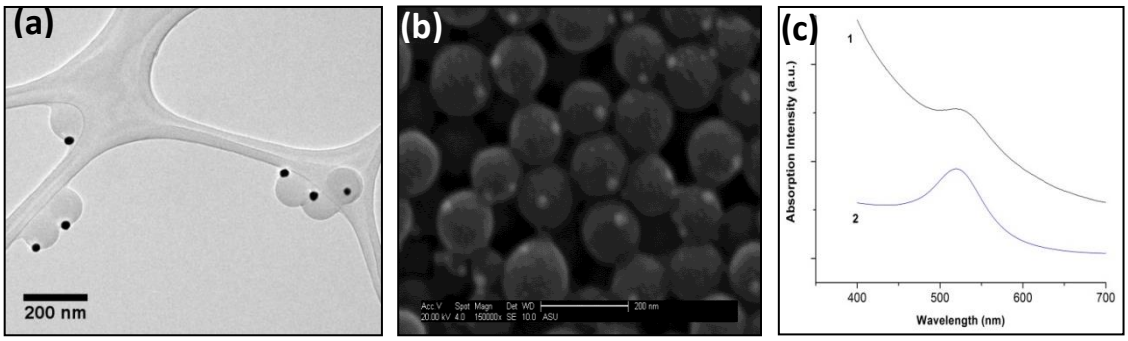

Figure 4.5 (a) TEM images of the asymmetric gold-polystyrene particles. (b) SEM images of the asymmetric gold-polystyrene particles. Corresponding AuNPs concentration is 0.009 wt%. (c) UV-Vis spectra of asymmetric particles (curve 1) and pure gold nanoparticles (curve 2).

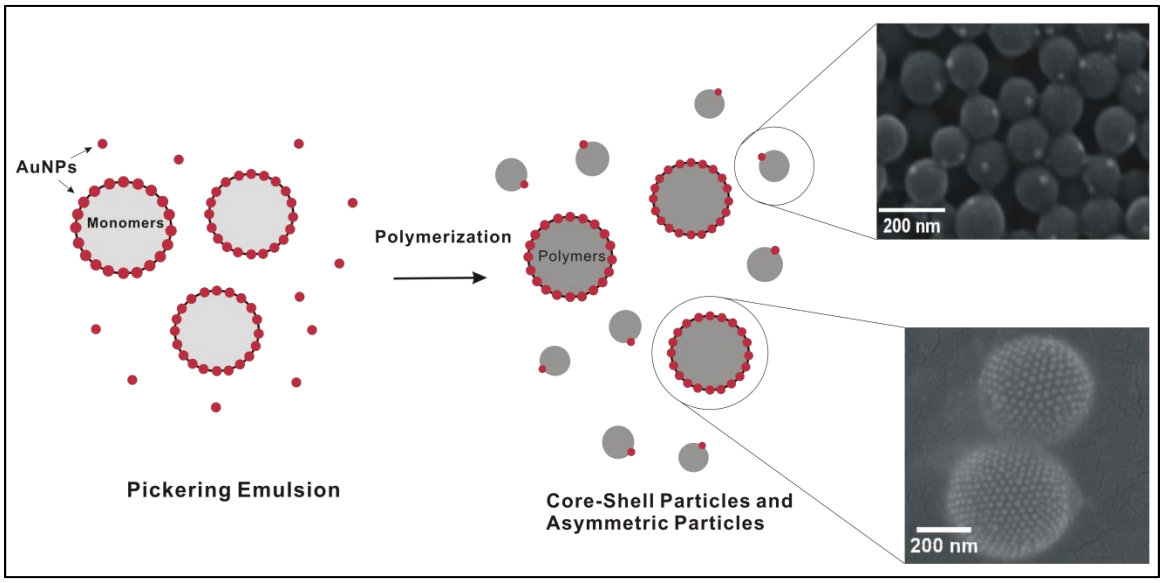

Figure 4.6 Schematic illustration of formation of core-shell structured and asymmetric polystyrene-gold composite particles via Pickering emulsion polymerization.

In order to explore the formation mechanism of the asymmetric polystyrene-gold composite particles, a time study is conducted in which we sample the reaction batch at 0.5 hour, 1 hour, and then collect the final 4 hour reaction product. For the 0.5 and 1 hour reaction samples, small particles are found where the AuNPs serve as the seeds, allowing styrene monomers/oligomers to continue to grow on the seeds (Figure 4.7). No core-shell particle with large sizes is found in these early stages. The particle's asymmetric structure is similar to what has been found by Ohnuma et al, where polystyrene-gold composite particles are synthesized via precipitation polymerization with the aid of cross-linker.[77, 146] A seeded-growth formation mechanism is also found during their synthesis. For the synthesis chemistry, they find the seeded-growth could not take place since polystyrene oligomers could not replace the original stabilizing ligands on AuNPs if the stabilizing

ligand has a strong binding to the AuNP surface (such as ligand with thiol group). Therefore it is likely that for the synthesized asymmetric particles, a moderate chemical binding causes polystyrene to grow on the AuNP surface. Several publications demonstrate a moderate interaction between aromatic rings and AuNP surface.[2, 75-76] Miyamura et al find that polystyrene ligands could serve as stabilizing reagent to avoid aggregation of AuNP clusters. Kumar et al suggests the reduction of π electrons clouds density of aromatic rings will result in negligible binding of the substituted benzenes with AuNP surface. Therefore it is possible that during the seeded-growth formation of asymmetric particles, styrene monomers/oligomers dispersed in water phase are able to provide π electrons from aromatic rings to interact with AuNPs in water phase. Currently, the AuNP surface modification is mostly based on thiol-Au interaction;[147] here we demonstrate an alternative route of AuNP surface modification. Asymmetric composite particles are capable of meeting the rising demand of fabricating advanced building blocks for functional materials, with the potential applications in self-assembly,[19-20] opto-electronics,[21] etc. For example, if the asymmetric particles are synthesized with anisotropic distribution of electric charges, the particles can self-assemble into an electric-field-oriented pattern under a given electric field.

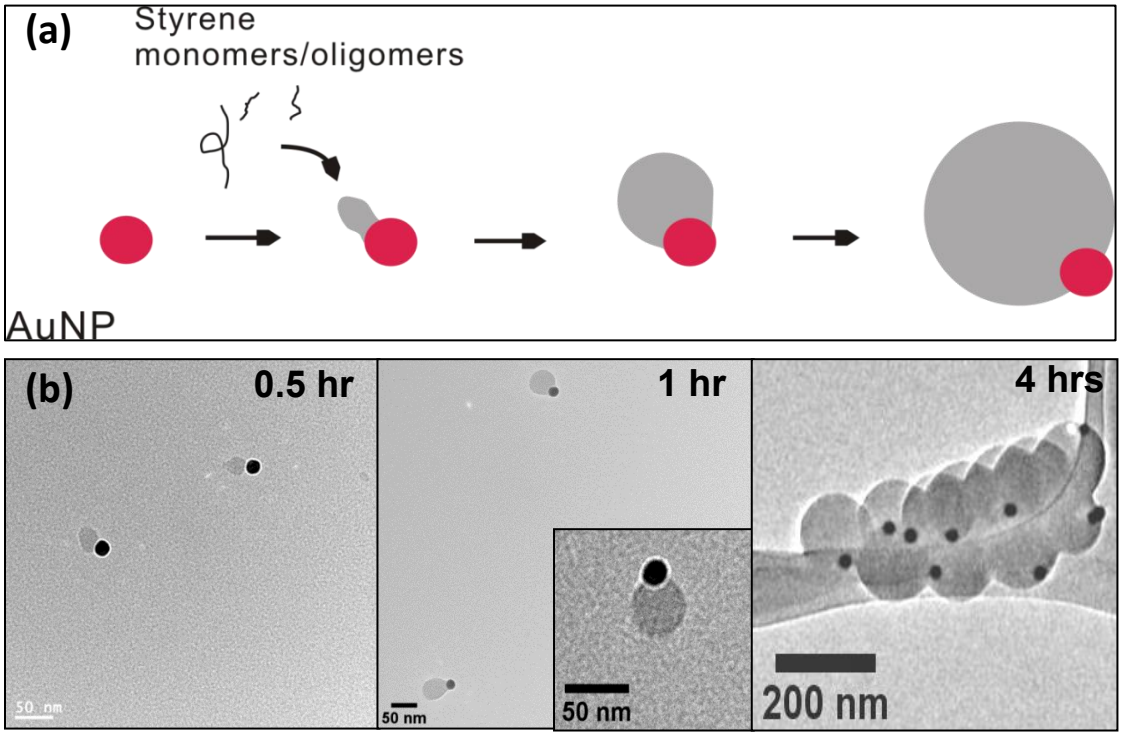

Figure 4.7 Formation mechanism of asymmetric particles: seeded growth. (a) Proposed seeded growth mechanism. (b) TEM images of particles sampled at reaction time of 0.5 hour, 1 hour, 4 hours, respectively.

4.1.3 Catalytic Study of Polystyrene-Gold Composite Particles

Compared to pure metallic nanoparticles, the primary role of composite particles is to reduce the nanoparticle agglomeration problem and increase particle recyclability. For pure AuNPs, the nanoparticles tend to agglomerate, leading to decreased catalyst activity and recyclability with short shelf lifetime.[85] Here we utilize a redox reaction of Rhodamine B as the model reaction to investigate the particle's catalytic performance. Results show that both core-shell and asymmetric polystyrene-gold composite particles successfully catalyze the redox reaction of Rhodamine B reduced by $NaBH_4$. Figure 4.8 is UV-Vis spectra of time study on redox reaction and the peak located at 552 nm belongs to Rhodamine B. As reaction time increases, the absorbance intensity decreased, and finally vanishes after 9 mins. The inset pictures show the pink color diminishes after the catalytic reaction finished. The vanishing of solution color indicates the Rhodamine B successfully reduces to its lueco form via hydrogenation, as has been studied in detail in previous publications.[148] A control experiment is conducted where the reaction solution is without polystyrene-gold composite particles. Even under excess amount of reductant $NaBH_4$, the color remains unchanged for 24 hours test period. The AuNPs on the polystyrene core are believed to serve as electron relay for oxidant Rhodamine B and reductant $NaBH_4$, such that $NaBH_4$ donates electrons to AuNPs and Rhodamine B captures electrons from AuNPs.[149-150] In addition, the performance of asymmetric particles and pure AuNPs under the same AuNPs concentration and reaction condition are tested (Figure 4.9). The absorption intensity of Rhodamine B reduces to zero after 20 minutes and 1.1 minutes for asymmetric particles and pure AuNPs respectively. Compared with pure AuNPs, the reduced catalytic activity is possibly due to the

restriction of the AuNP geometry. It has been reported that polymers[151] and molecules with bulky group[152] attached on catalyst surface could give steric hindrance to reduce the accessibility of functioning catalytic surface to the reacting molecules.

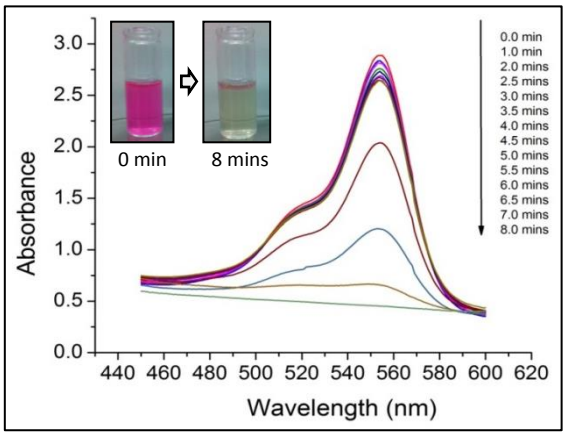

Figure 4.8 Time study on UV-Vis absorbance of Rhodamine B under redox reaction catalyzed by core-shell polystyrene-gold composite particles catalysts. Inset photos are taken before reaction (left) and after reaction (right) respectively.

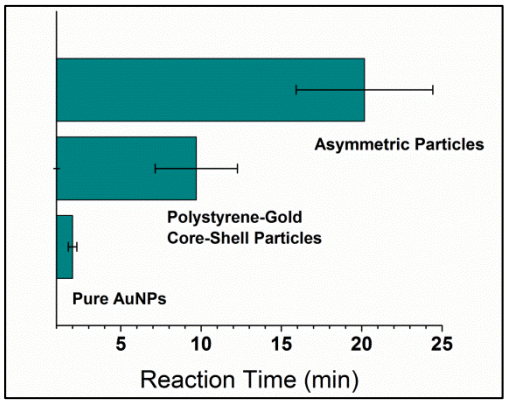

Figure 4.9 Comparison of the reaction time for three types of AuNPs. Reaction condition: [RhB] = 4×10^{-5} mol/L, [$NaBH_4$] =5×10^{-2} mol/L, concentration of the three types of AuNPs particles are kept at 9.2×10^{-4} wt %.

Figure 4.10 is the recyclability study of core-shell particles, asymmetric particles and pure AuNPs. Both the core-shell particles and asymmetric particles have maintained 80% conversion after 5 cycles, indicating good catalyst reusability. The slight loss of

conversion is possibly due to catalysts deactivation[151] as several cycles have repeated. For pure AuNPs, we find recycling is difficult; the conversion is lowered to 40% after 5 reaction cycles. The significant loss of conversion is likely due to AuNPs agglomeration, evidenced from the TEM images (Figure 4.11), the agglomeration problem increases with repeating cycles. At the 5th reaction cycle, particles agglomerate into bulk. The significant reduction of AuNPs functioning area leads to the loss of recyclability. For core-shell and asymmetric composite particles, no significant AuNP leaching problem has been observed from TEM. In addition, we conduct the control experiment to test whether the remaining solution after recollecting the particles can catalyze the reaction. From UV Vis measurement we find that for different reaction cycles, the redox reaction cannot proceed. From DLS measurement, no small size particle (20 nm) could be detected from the remaining solution, indicating AuNPs are stably anchored on the composite particle surface.

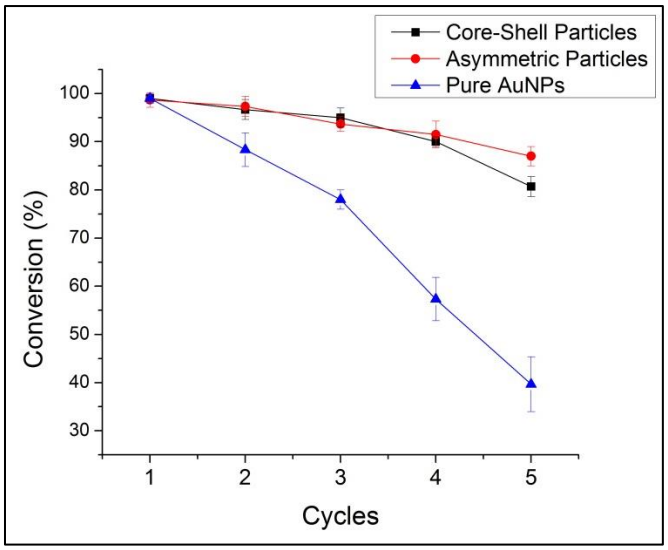

Figure 4.10 Catalysts recyclability study: comparison of the final conversion of RhB for core-shell particles, asymmetric particles and pure AuNPs.

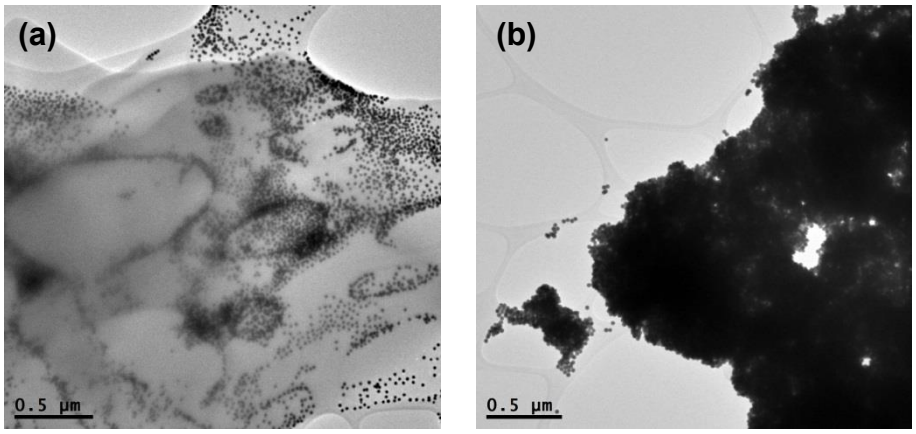

Figure 4.11 TEM images of pure AuNPs recollected after (a) 3rd reaction cycle and (b) 5th reaction cycle for particle recyclability study.

4.2 Thermo-responsiveness and Optical Properties of Asymmetric Polystyrene/PNIPAm-Gold Composite Particles.

4.2.1 Bimodal Size Distribution of Polystyrene/PNIPAm-gold Composite Particles

We successfully synthesize polystyrene/PNIPAm-gold composite particles with a bimodal size distribution. (Figure 4.12) Figure 4.13a is the TEM images of core-shell structured and asymmetric composite particles. Figure 4.13b is the bimodal size distribution of synthesized particles measured by DLS. The core-shell structured composite particles have randomly distributed AuNPs on the surface; the asymmetric particles have a single AuNP attached on each polystyrene-PNIPAm substrate core. Figure 4.13c and 13d show both core-shell and asymmetric composite particles have a relatively uniform size distribution. The DLS result is consistent with the TEM image, in which the core-shell and asymmetric composite particles have average diameters of 440 nm and 230 nm, respectively; the number-weighted percentage of core-shell and asymmetric composite particles are 26% and 74% respectively. In Figure 4.13e and 4.13f, the EDX spectra show that the representive peak for the element nitrogen is present as the electron beam is focusing on the particle whereas the nitrogen peak does not exist as the beam is focused on the blank area. This indicates that PNIPAm is successfully incorporated into the composite particles. The core-shell polystyrene/PNIPAm-gold composite particles are formed via polymerization of AuNPs stabilized Pickering emulsion; in contrast, the asymmetric composite particles are formed via seeded-growth mechanism, in which styrene monomers/oligomers dispersed in water phase are able to provide π electrons from aromatic rings to form a stable binding with AuNP surface.

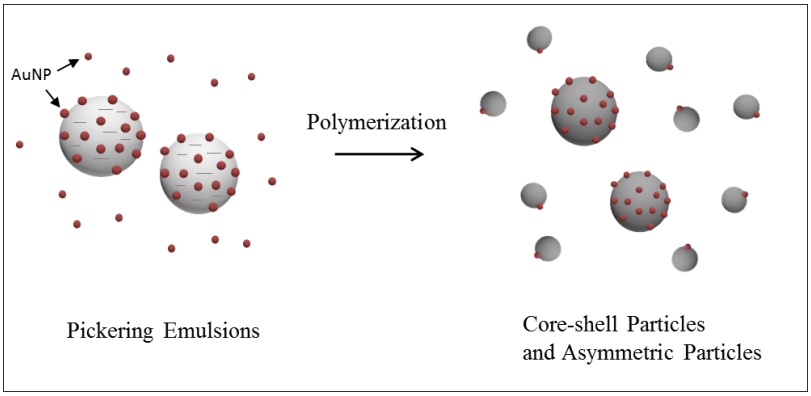

Figure 4.12 Scheme of core-shell and asymmetric polystyrene/PNIPAm-gold composite particles formation via Pickering emulsion polymerization.

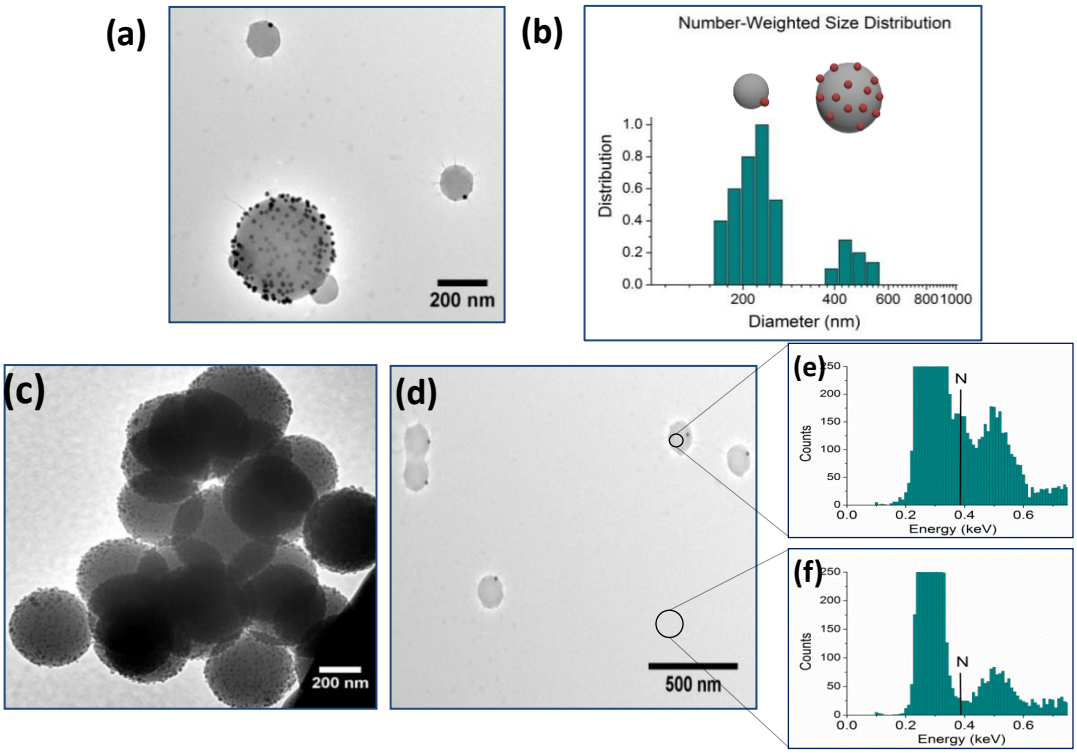

Figure 4.13 Bimodal size distribution of polystyrene/PNIPAm-gold composite particles. (a) is the TEM image of bimodal-sized polystyrene/PNIPAm-gold composite particles. (b) is the number-weighted size distribution from the DLS measurement. (c) and (d) are the filtrated core-shell composite particles and filtrated asymmetric particles respectively. (e) and (f) represent EDS analysis focused on the asymmetric particles and blank area respectively in image (d).

4.2.2 Thermo-responsiveness of Polystyrene/PNIPAm-Gold Composite Particles

The thermo-responsiveness of core-shell and asymmetric polystyrene/PNIPAm-gold composite particles is investigated via DLS analysis with a temperature control function. Particle size is measured over a temperature range of 23 ℃ - 40 ℃. In Figure 4.14a and 4.14b, both the core-shell and asymmetric composite particles exhibit a trend where size decreases with increasing temperature. For batches with NIPAAm content of 33% and 50%, the LCST is determined as 31 ℃ for core-shell and asymmetric particles, by taking the derivative of each curve. For batches with NIPAAm content of 71% and 83% (results are shown in Figure 4a), the LCST remains 31 ℃. This indicates the influence of copolymerization with styrene to LCST variation is small. The result is consistent with previous results found in our group, where the LCST of polystyrene/PNIPAm-silica composite particles synthesized via the same approach are not affected by copolymerization of styrene.[56] A possible explanation is that phase separation inside the core particles exists between polystyrene and PNIPAm polymers. Duracher et al propose that phase separation exists inside particles that contain a PNIPAm-rich core and polystyrene-rich shell.[55]

Figure 4.14c summarizes the comparison of the shrinking ratio between core-shell and asymmetric composite particles based on Figure 4.14a and b (The shrinking ratio is the ratio of particle diameter at a given temperature to particle diameter at 40 ℃). Under the same NIPAAm content (33 wt% and 50 wt%), the core-shell composite particles have a small shrinking ratios of 1.07 and 1.14; the asymmetric particles have a larger shrinking ratios of 1.22 and 1.41 for NIPAAm content of 33 wt% and 50 wt% respectively. The difference in shrinking ratio between core-shell and asymmetric particles is likely due to

different formation mechanisms. The emulsion polymerization takes place in the styrene phase, whereas the seeded-growth for asymmetric particles takes place in the water phase, where the majority of NIPAAm monomers are present. Therefore, NIPAAm monomers are more likely to participate in seeded growth copolymerization for asymmetric particles.

The thermo-responsiveness of asymmetric particles could be enhanced as we further increase the NIPAAm content. Figure 4.15 is a summary of the thermo-responsiveness of asymmetric composite particles for different NIPAAm concentrations. As the NIPAAm content increases, the size of the asymmetric particles is increased at 25 ℃; above the LCST, particles undergo more significant size decrease with an increase in the NIPAAm content. At the NIPAAm content of 83 wt%, particles have a size decrease from 1,180 nm to 237 nm (80% size decrease). The significant shrinking ability of PNIPAm-included particles could be visually observed in TEM images of asymmetric particles with different PNIPAm content (Figure 4.15c). Images are taken via environmental TEM, which allows the sample to be analyzed even with a trace amount of water present in the sample. For particles with 71 wt% PNIPAm, clear shrinking trails appear underneath the particles. For particles with 83 wt% PNIPAm, particles have lost their spherical shape and are accompanied by comet-like tails due to shrinking. These indicate that as the PNIPAm content increases, particles become more flexible and deformable; as the electron beam hits the particles in the TEM column, the particles' temperature increases beyond the LCST, repelling the remaining water and shrinking from their original structure.

It should be noted that compared with the microgel synthesis with the aid of cross linker,[28, 153-154] the composite particles here are synthesized via cross-linker-free Pickering

emulsion polymerization and have shown a higher size-decrease percentage. To investigate the influence of a cross linker, we applied MBA as cross linker for synthesis under the same reaction condition with NIPAAm content of 83 wt%. It is clearly seen that the influence of cross linkers is significant, where particles undergo only 27.6% size decrease, a much smaller size decrease percentage compared to the 80% diameter decrease of the counterpart without cross-linkers (Figure 4.16). This result is consistent with previous work, suggesting that cross-linkers restrict particles' flexibility to swell/shrink.[153,155] Figure 4.17 shows viscosity measurements of asymmetric composite particles suspensions with a particle concentration of 3 wt%. Shear thinning characteristic are shown for both samples with NIPAAm content of 83 wt% (Figure 4.17a) and 71 wt% (Figure 4.17b). For batches with 83 wt% NIPAAm content, as temperature increases from 20 ℃ to 40 ℃, the viscosity undergoes an average of 8.6 times decrease over the shear rate range of 10 s^{-1} - 40 s^{-1}. The same viscosity decrease trend is shown for batches with 71 wt% NIPAAm content, where the viscosity decreases approximately 3.5 times over the shear rate range of 10 s^{-1} - 40 s^{-1}. As the particles undergo large size decrease, the volume fraction decreases significantly, leading to the solution's viscosity decrease.

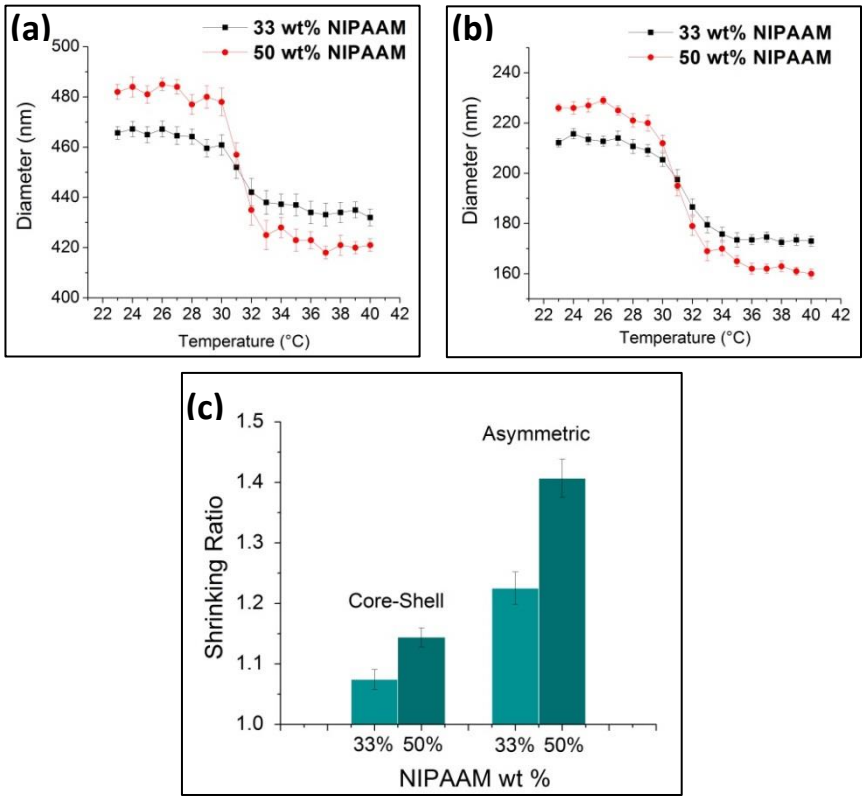

Figure 4.14 (a) (b) represent DLS result of core-shell and asymmetric polystyrene/PNIPAm-gold composite particles respectively. (c) Comparison of shrinking ratio between core-shell and asymmetric polystyrene/PNIPAm-gold composite particles with NIPAAm content of 33 wt% and 50 wt%. The shrinking ratio is the ratio of particle diameter at a given temperature to particle diameter at 40 ℃

(a)

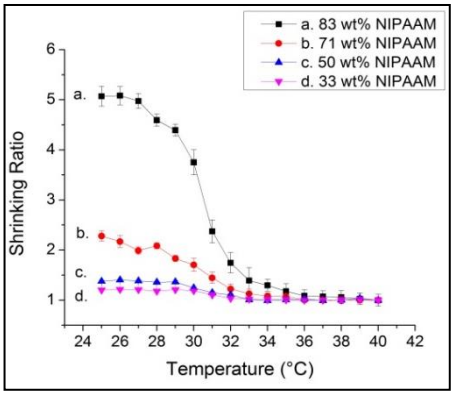

(b)

Corresponding Curve	a	b	c	d
$D_{25\,°C}$ (nm)	1180	392	227	212
$D_{40\,°C}$ (nm)	237	170	161	173

(c)

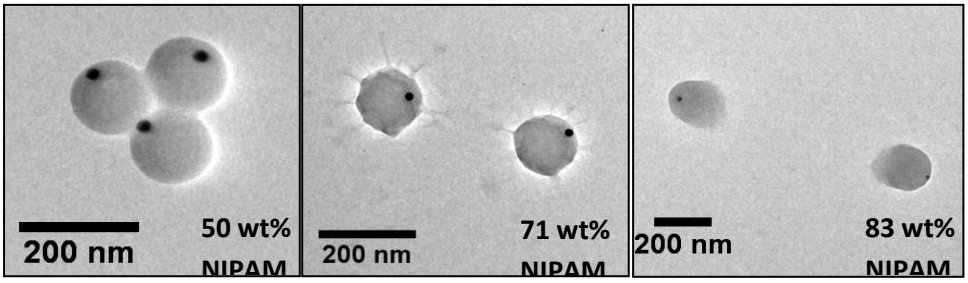

Figure 4.15 (a) Shrinking ratio of asymmetric polystyrene-NIPAAm-gold composite particles with different NIPAAm content. (b) Corresponding particle diameter at 25 ℃ and 40 ℃. (c) TEM images of asymmetric particles with 50 wt%, 71 wt%, 83 wt% NIPAAm content. Under the electron beam, particles' temperature increases above their LCST of 31 ℃

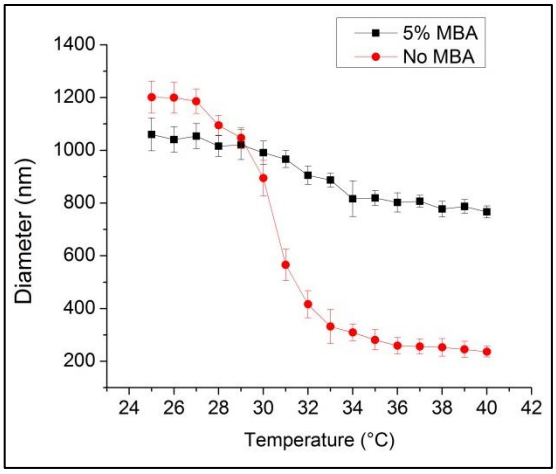

Figure 4.16 Influence of a cross-linker on thermo-responsiveness. Comparison of thermo-responsiveness of asymmetric polystyrene/PNIPAm-gold composite particles synthesized with 5% MBA and without MBA. NIPAAm content for both types of particles is 83 wt%.

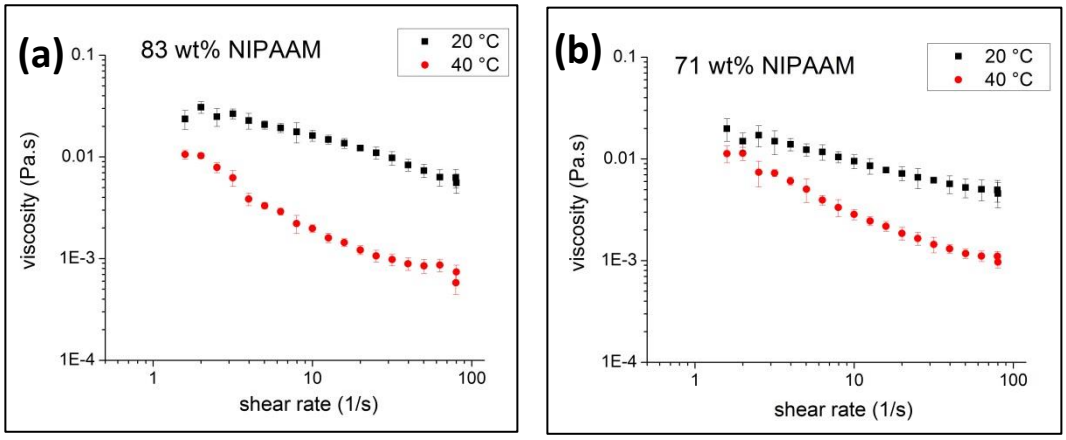

Figure 4.17 Viscosity measurement of asymmetric polystyrene-NIPAAm-gold composite particles suspension with NIPAAm content of 83 wt% (a) and 71 wt% (b) under 20 ℃ and 40 ℃. Particle concentration for (a) and (b) is kept at 3 wt%.

4.2.3 Tunable Optical Properties of Asymmetric Polystyrene/PNIPAm-Gold Composite Particles

Due to the thermo-responsiveness of the PNIPAm, the optical properties of asymmetric particles are found to be tunable by adjusting the temperature. For the core-shell structured particles, we find that the thermo-responsiveness is not sufficient to give a considerable size variation; therefore, no obvious optical change is observed. Particles with large variation in scattering intensity could be directly utilized as signals for intensity-based optical sensors,[124] leading to great potential for bio-imaging and bio-sensing, as well as thermo-responsive optics. Light intensity is also an important factor for photo-catalytic reactions.[156-157] By controlling the photo-catalytic reaction's light intensity, the reaction rate could be adjusted. Figure 4.18 shows that the extinction and scattering intensities of the asymmetric particles are sensitive to temperature. It should be noted that the extinction intensity measured from the UV-Vis spectrometer includes absorbing and scattering light intensities,[158] where the scattering light becomes dominant as the temperature increases above the LCST. The dramatic extinction/scattering intensity increase starts at PNIPAm's LCST of 31°C, as shown in Figure 4.18a. The extinction intensity at 40 ℃ is ~12 times that at 20 ℃; the scattering intensity at 40 ℃ is ~7 times that at 20 ℃. Figure 4.18b shows the comparison between the sample at 20 ℃ (control vial left) and 40 ℃ (heated vial right). The sample changes from clear pink color to milky pink with increasing brightness and turbidity, indicating a significant increase of scattering intensity. An air bubble is located at the bottom of vial at 20 ℃; however, it does not influence observation. In Figure 4.18c, we report that the increase of extinction/scattering intensity is affected by the NIPAAm content. For the sample without

NIPAAm, the extinction/scattering intensity remains unchanged as temperature increases; this indicates the significant increase of extinction/scattering intensity is due to the presence of PNIPAm which causes the large size decrease of the asymmetric particles. This significant intensity change is attributed to the refractive index change of the PNIPAm-containing core particles. Below the LCST, the polymer backbone is stretched and the particles are swollen with up to 97% water, with refractive index matching the surrounding water phase.[119, 159-160] As temperature increases above the LCST, the PNIPAm backbone collapses with inter-chain clustering, and the particles repel most of the water, undergoing a significant shrinking in diameter from 1180 nm to 237 nm (80% size decrease percentage). The particle density and refractive index increase significantly, leading to a large refractive index contrast between the particles and the water phase. From a recent ellipsometry study,[30, 31] the refractive index of PNIPAm microgels increases from 1.34 to 1.40, for a relatively small size decrease (30% - 50% diameter decrease percentage). This large refractive index contrast is responsible for the extinction and scattering intensity increase, as predicted by Mie theory.[28, 125-127] Figure 4.18d is the reusability study of particles' switchable optical properties. The significant extinction and scattering intensity increase is completely reversible as the sample undergo three cycles between 20 ℃ and 40 ℃, indicating their good reusability for sensing applications. For gold-PNIPAm particles, investigations have mainly focused on adjusting the SPR absorption properties of AuNPs via tuning the inter-particle distance[29, 31, 119] and refractive index of the AuNP's surrounding medium.[27-28, 154] However, tuning or utilizing the particle's scattering intensity remains less-explored. light intensity is a key factor for optical devices and could be utilized as signals for intensity-based optical sensors, which

is potentially the simplest optical sensor[124]. For example, particles with switchable scattering intensity could be utilized in thermal sensor, in which the thermo-responsive scattering intensity serves as signals. Aslan et al. developed a wavelength-ratiometric resonance light scattering technique for glucose sensing based on AuNPs aggregation and dissociation. Instead of absorption signals, the plasmon resonance scattering signals of AuNPs are analyzed for glucose sensing.[161] In addition, the switchable light intensity properties provide potential applications in photo-catalytic reactions, considering light intensity is an important factor for such reactions.[156-157]

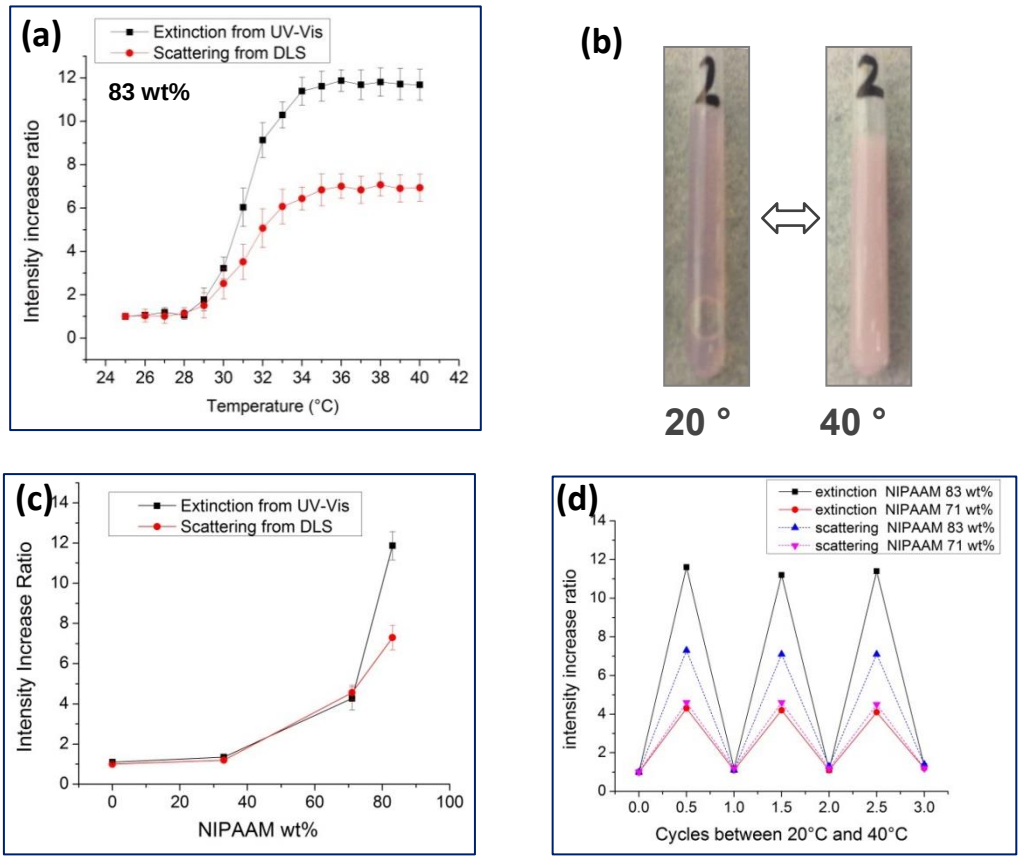

Figure 4.18 Thermal responsiveness of extinction and scattering intensity. (a) Extinction and scattering intensity at different temperatures with NIPAAm content of 83 wt%. The laser wavelength for the extinction/scattering intensity measurement is kept at 639 nm. (b) Photos of asymmetric particle sample at 20 ℃ and 40 ℃. (c) Effect of different NIPAAm content on extinction/scattering intensity increase ratio. (d) reusability study of asymmetric polystyrene/NIPAAm-gold composite particles.

Other than the change of refractive index contrast between PNIPAm-containing core particles and surrounding water, the change of local refractive index of PNIPAm that surrounds AuNP leads to variation of AuNP's SPR properties. Figure 4.19a is the normalized extinction spectra of asymmetric particles with 83 wt% NIPAAm at 20 ℃

and 40 ℃. The representative peak of 20 nm AuNPs at 520 nm is not distinguishable at 20 ℃. At 40 ℃, the representative peak is shown with the peak broadening and shifting to 527 nm. As temperature increases above the LCST, the local refractive index of PNIPAm substrate around AuNPs is increased, as the PNIPAm substrate covering around the AuNPs collapses and becomes denser.[28, 154] The slight red-shift of the SPR band is consistent with theoretical[27] and other experimental[28] results. Tagliazucchi et al. conclude from the theoretical results that the shift caused by the local refractive index change is of the order of several nanometers (<10 nm). The variation of the extinction spectrum is reversible as it undergoes several heating-cooling cycles. In addition, the PNIPAm content is found to influence the absorption properties of the asymmetric particles. Figure 4.19b and 4.19c show the absorption spectra of asymmetric particles with different NIPAAm content at 20 ℃ and 40 ℃ respectively. It is shown in Figure 4.19b, with decreasing NIPAAm content, the representive peak becomes more distinguishable and shifts to 530 nm. It has been reported that at 20 ℃, the refractive index of polystyrene particle is 1.58,[162] compared with 1.34 for PNIPAm particles (quite close to that of water: 1.33 at 20 ℃). At 40 ℃, the refractive index of PNIPAm increases, resulting in a slight plasmon band shifting to 527 nm. This extinction spectra result further supports that the variation of refractive index of the substrate gives rise to the change of SPR properties of the asymmetric particles.

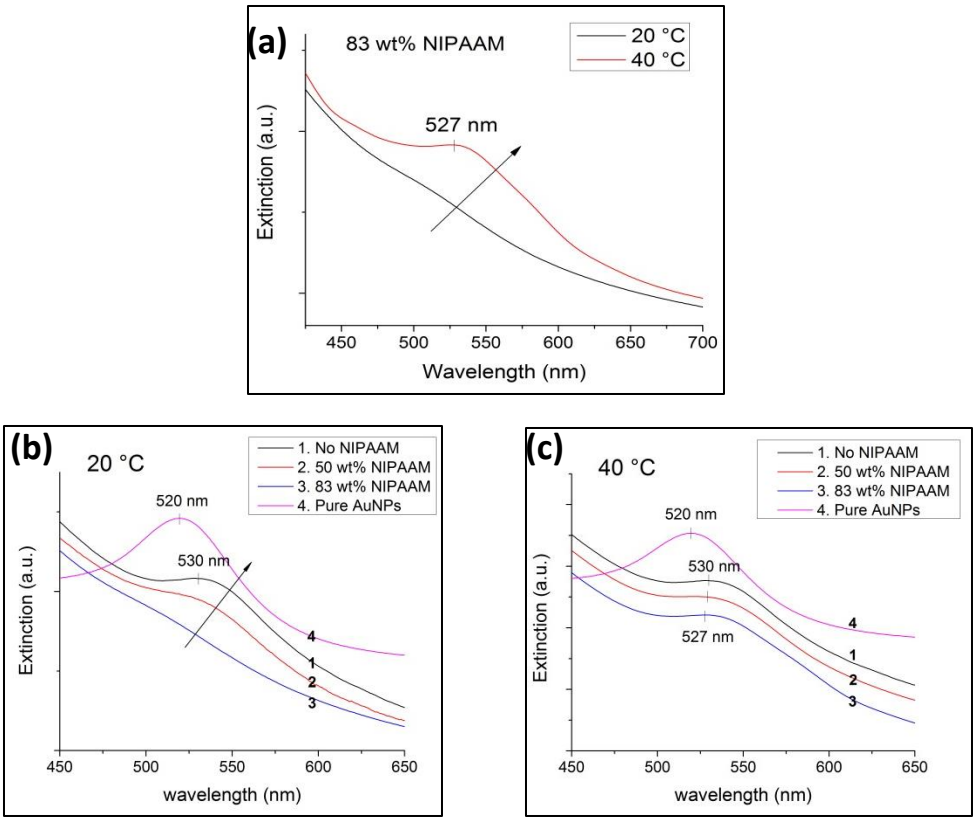

Figure 4.19 (a) Normalized extinction spectra of asymmetric particles synthesized under NIPAAm content of 83 wt% at 20 ℃ and 40 ℃. The arrow represents the variation trend of plots from 20 ℃ to 40 ℃. (b) and (c) are normalized extinction spectra of pure AuNPs and asymmetric particles with different NIPAAm-styrene feed ratio at 20 ℃ and 40 ℃, respectively. The arrow in (b) represents variation trend of plots from 83wt% NIPAAm content to 0% NIPAAm content.

4.3 Multipetal-shaped and Dumbbell-shaped Gold-Polymer Composite Particles with Modulatable Catalytic Activity.

4.3.1 Multipetal-Shaped and Dumbell-Shaped Gold-Polystyrene Composite Particles.

Multipetal-structured and dumbbell-structured gold-polystyrene composite particles are successfully synthesized via seeded emulsion polymerization. Figure 4.20 shows the transmission electron microscopy (TEM) and scanning electron microscopy (SEM) images of synthesized particle sample with 125 nm AuNPs after 1 hour (hr) ((a) and (b), tetrapetal structure) and with 80 nm AuNPs after 1 hour ((c) and (d), tripetal structure), 4 hrs reaction time ((e) and (f), dumbbell-structure) respectively. In Figures 4.20a and 4.20b, each AuNP center is surrounded with 3-5 polystyrene "petals" in non-specific direction, showing a flower-like structure. Similar results are shown in Figure 4.20c and 4.20d. Close observation shows most petals of multipetal-structured particles are distributed in three dimensions. TEM and SEM images in Figure 1e and 1f show that the synthesized particles have dumbbell structure. It is intriguing to find that for most of the dumbbell-structured particles, the two polystyrene petals are aligned with near-perfect 180 °angle. The observed particle sizes of multipetal-structured and dumbbell-structured composite particles from TEM images match well with dynamic light scattering (DLS) results (362 nm, 324 nm and 563 nm for tetrapetal-structured, tripetal-structured and dumbbell-structured composite particles respectively). To the best of our knowledge, utilization of AuNP for synthesis of multipetal-structured gold-polystyrene composite particles is first reported here. Previously, utilization of silica nanoparticle for synthesis of multipetal-structured silica-polystyrene composite particles are reported by Reculusa et al, where 170 nm silica nanoparticles serve as seeds for seeded emulsion

polymerization.[73] The multipetal-structured and dumbbell-structured gold-polystyrene composite particles could potentially serve as building blocks for advanced hierarchical and supra-colloidal materials.

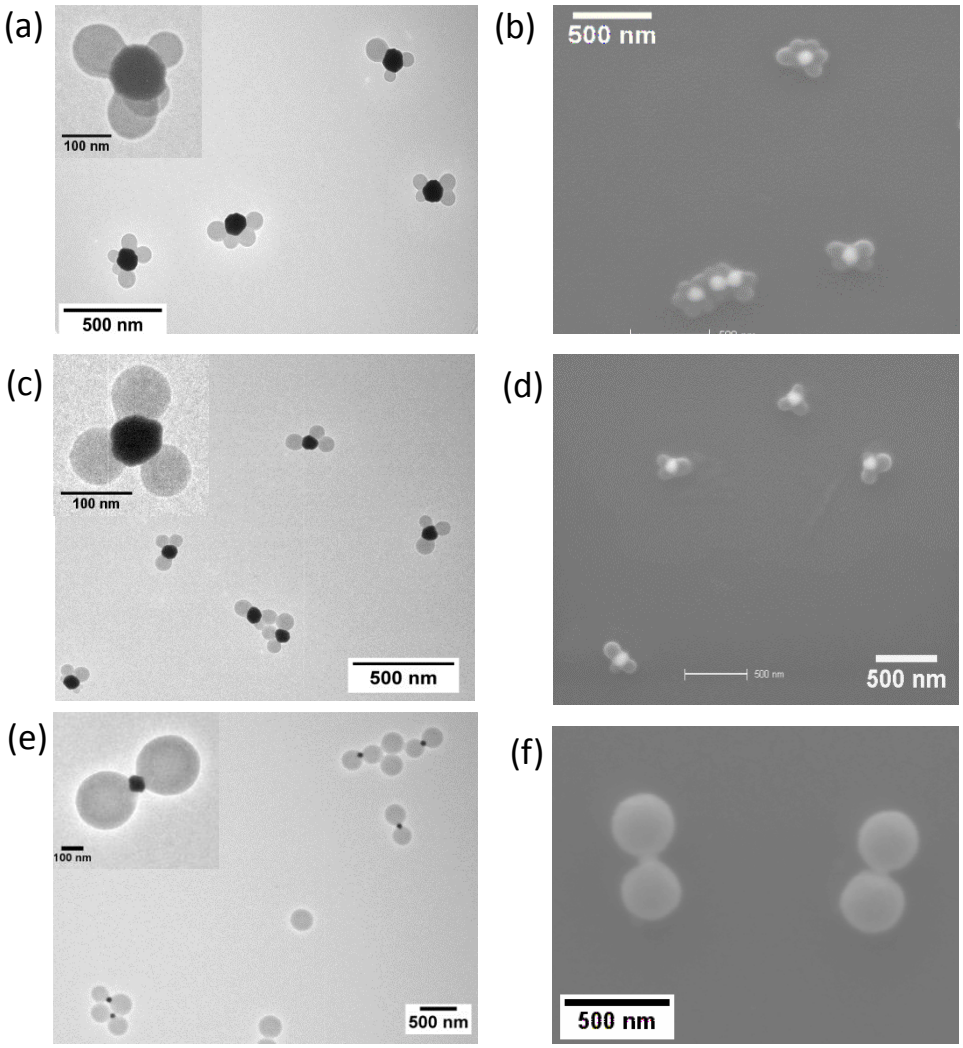

Figure 4.20 TEM and SEM images of multipetal-structured and dumbbell-structured gold-polystyrene composite particles. (a)(b) Particles with tetrapetal structure. (particles synthesized with 125 nm AuNPs, 1 hr reaction time). (c)(d) Tripetal-structured particles. (particles synthesized with 80 nm AuNPs, 1 hr reaction time). (e)(f) Dumbbell-structured particles. (particles synthesized with 80 nm AuNPs, 4 hrs reaction time)

4.3.2 Effect of Reaction Time on Particle Morphology

The morphology of gold-polystyrene composite particles is found to be controlled by reaction time. Figure 4.21 is the TEM images of particles sampled at different reaction time (1hr, 2 hrs, 4 hr). The morphology of particles gradually changes from multipetal shape to dumbbell shape for 1 hr, 2 hrs and 4 hrs sample. For 1 hr sample, each AuNP center is surrounded with an average of 2.9 polystyrene petals with diameter of ca. 80 nm (the counting and calculation of number of petals on each AuNP center is based on 10 TEM images for each sample). For 2 hrs sample, the polystyrene petals are growing larger; more than a half of particles are dumbbell-shaped particles. For 4 hrs sample, we find nearly all the composite particles are dumbbell-shaped; in addition, we observe many bare polystyrene particles with the same size of polystyrene petals. It is reasonable to propose that the morphology change is due to that as reaction proceeds, the growing of polystyrene petals gives more steric hindrance; this causes the polystyrene petals to drop off the AuNP center, and eventually, the dumbbell-shaped particles are formed with 180 ° angle of petal distribution for the most kinetic preference.

The same trend is shown in Figure 4.21 d-f for 125 nm AuNP composite particle system. The average number of polystyrene petals on each AuNP center gradually decreases from 3.9, 2.8, to 1.9 for 1hr, 2 hr and 4 hr sample, with the morphology change from multipetal shape to dumbbell shape. An increasing number of bare polystyrene particles are also observed as we investigate from 1hr sample, 2 hr sample to 4 hr sample. This confirms that the morphology change is due to increased steric hindrance of growing polystyrene petals, leading to petals' dropping off from the AuNP center. Again, we find

nearly all the composite particles are dumbbell-shaped particles with 180 °angle of petal distribution due to kinetic preference.

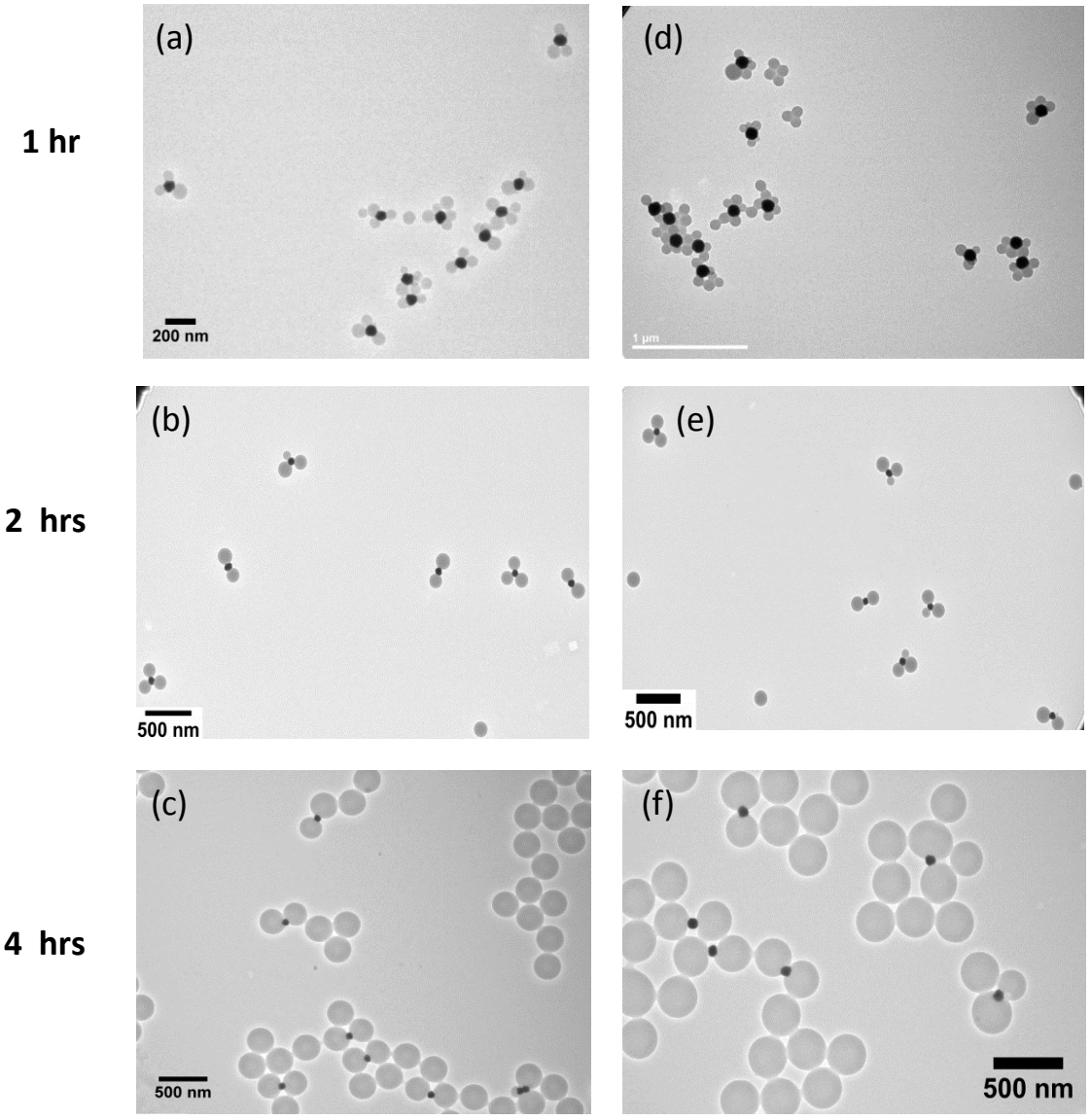

Figure 4.21 TEM images of gold-polystyrene composite particles sampling after different reaction time (1hr, 2 hr, 4 hr) (a)(b)(c) are samples synthesized with 80 nm AuNP, (d)(e)(f) are samples synthesized with 125 nm AuNP.

From tetra-petal, tri-petal composite particles to dumbbell-shaped composite particle, these composite particles show distributed bonding between AuNP center and polystyrene petals. These particles show similarity with hybridized atomic orbitals including sp^3, sp^2, and sp. This triggers an idea of designing and fabricating advanced materials with three-dimensional structures in the colloidal domain, mimicking molecule assembly in atomic domain. Currently, fabricating three-dimensional advanced materials is hard, due to the lack of directional bonding. Previously, Pine's group reports polystyrene micro-clusters functionalized with DNA patches.[128] The complementary DNA patches show high affinity to each other, allowing particles to self-assemble into supra-colloidal particles with specific directional bonding, which imitates hybridized atomic orbitals. Inspired from their method, here the multipetal-shaped and dumbbell-shaped colloidal particles with directional bonding might provide possibility of fabricating three-dimensional advanced materials.

4.3.3 Effect of AuNP size on Particle Morphology

Figure 4.22 shows the influence of AuNP size on particle morphology. Figure 4.22 compares the number of polystyrene petals on each AuNP center between 80 nm AuNPs system and 125 nm AuNPs system from 1hr to 4 hrs reaction time. At the early stage of the reaction, it is shown that as the diameter of AuNP increases, the number of polystyrene petals on each AuNP increases. This is because AuNPs with larger size provide more sites for seeded-growing polystyrene petals and reduce the possibility of petals' dropping caused by steric hindrance. For 1 hr sample of 125 nm AuNP system, we even observe a small amount (<5%) of AuNPs attached by 6 polystyrene petals, as shown

in Figure 4.22b,c. At the final stage of reaction, Figure 4.22a shows for both 125 nm AuNPs system and 80 nm AuNPs system, the number of polystyrene petals on each AuNP finally decreases to 2 showing dumbbell morphology after 4 hrs reaction time. The number of polystyrene petals on each AuNP center is less influenced by AuNP size; this indicates as polystyrene petals grow larger, steric hindrance gives more influence than AuNP size.

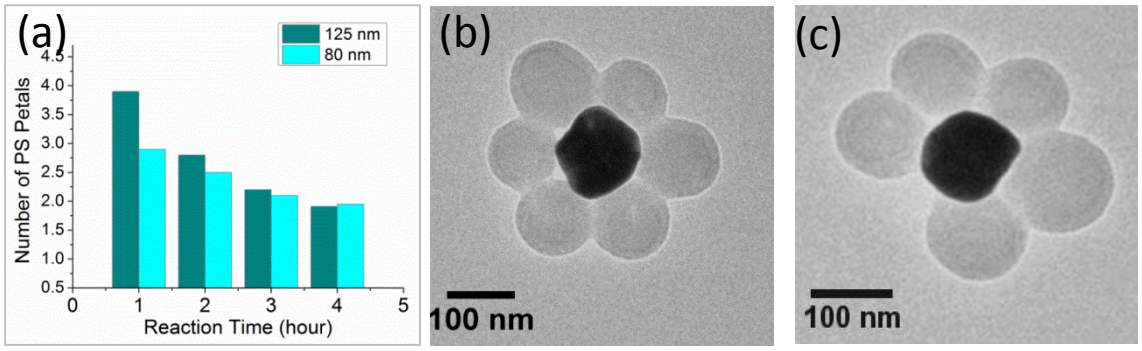

Figure 4.22 Influence of AuNP size on particle morphology. (a) Comparison of number of polystyrene petals on a single AuNPs between 80 nm AuNP system and 125 nm AuNP system. The counting and calculation of number of petals on each AuNP center is based on 10 TEM images for each sample. (b) multipetal-shaped gold-polystyrene particle with 125 nm AuNPs, where 6 polystyrene petals attach on a single AuNP.

4.3.4 Formation Mechanism of Multipetal-shaped and Dumbbell-shaped Gold-Polystyrene Composite Particles.

In order to find the formation mechanism, we perform a time study of the reaction product, sampling at 15 min, 45 min and 1.5 hrs during the reaction. Figure 4.23 is the TEM images of the sample at the early stage of the reaction. It is found that polystyrene monomers/oligomers are growing on the surface of AuNP surface. At 15 mins, three

small petals are observed on AuNP surface. As time increase to 45 mins and 1.5 hrs, polystyrene petals grow bigger and a spherical shape is formed. This phenomenon is similar to what we find in our previous study about the formation mechanism of asymmetric gold-polystyrene particles.[163-164] Therefore, the seeded growth formation mechanism is proposed. It is possible that during the seeded-growth formation, styrene monomers/oligomers dispersed in water phase are able to provide π electrons from aromatic rings to interact with AuNPs in water phase.[2, 163]

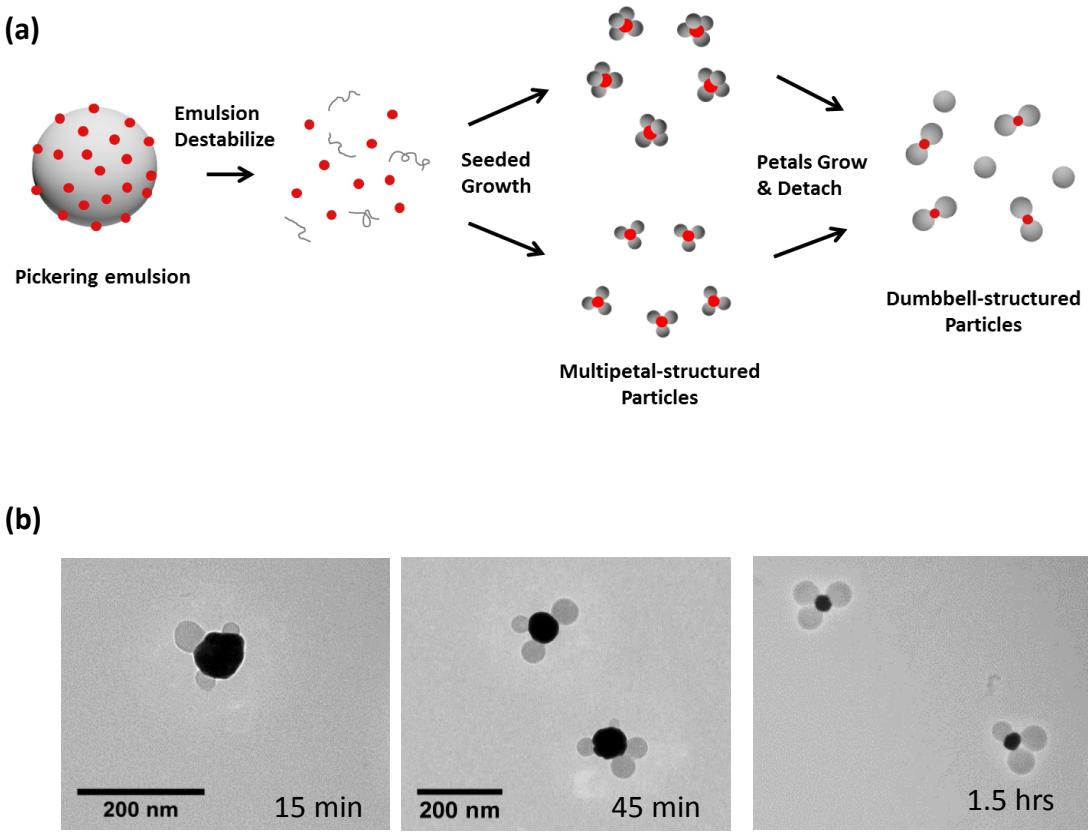

Figure 4.23 Illustration of formation pathway of (a) multipetal-shaped and dumbbell-shaped gold-polystyrene composite particles and (b) seeded growth formation mechanism of multipetal-shaped gold-polystyrene composite particles.

Figure 4.23a shows the illustration of formation of gold-polystyrene multipetal-shaped and dumbbell-shaped particles. It is very interesting to note that the multipetal-shaped and dumbbell-shaped particles are found by accident, as we investigate the influence of AuNP size on Pickering emulsion (emulsions stabilized by AuNPs) stability under emulsion polymerization. Our previous reports demonstrate the formation of core-shell structured gold-polystyrene composite particles, utilizing 20 nm AuNPs as emulsion

stabilizers for Pickering emulsion polymerization; as the AuNP size is increased from 20 nm to 80 nm and 125 nm, to our surprise, the expected core-shell structured gold-polystyrene composite particles are not found via TEM and DLS results. This indicates the size of particle stabilizer possibly influences the stability of emulsions, as AuNPs with larger size tend to destroy the emulsions. This result is consistent with experimental results found by Binks and Lumsdon et al suggesting that particles with bigger size tend to have less emulsion stability.[165] Also, Tambe et al studied the effect of particle size on emulsion stability utilizing alumina particles on decane-water system. They found the larger particles (47 μm) could not stabilize the emulsions, whereas smaller particles (4 μm) are able to stabilize them.[60]

4.3.5 Thermo-responsiveness of Dumbbell-Structured Gold-PNIPAm/polystyrene Composite Particles

Previously in our group, we have successfully incorporated thermo-responsive PNIPAm polymers for synthesis of asymmetric thermo-responsive gold-PNIPAm/polystyrene composite particles via seeded emulsion polymerization. Here we show the successful incorporation of PNIPAm for synthesis of the dumbbell-structured gold-PNIPAm/polystyrene composite particles via seeded emulsion polymerization with significant thermo-responsiveness. It is found the dumbbell-structured particles are formed in both 4 hrs samples with 83 wt% and 91 wt% NIPAAm content, consistent with previous results of non-PNIPAm incorporated gold-polystyrene composite particles. Figure 4.24 shows the thermo-responsiveness and morphology of dumbbell-structured gold-PNIPAm/polystyrene composite particles with different NIPAAm content (image of

4 hrs samples with 91 wt% NIPAAm content are shown in Figure 4.25). By the comparison of the TEM images, it is clearly observed that the addition of PNIPAm into particle petals result in "softness" and deformability of the petals. In TEM microscope, these PNIPAm-incorporated particles are already dehydrated and shrunk, as TEM samples are placed in vacuum environment and are further heated by electron beam. An important thing to notice is that as shown in TEM images, compared to particles without PNIPAm incorporation, the PNIPAm-polystyrene petals cover most of AuNP surface (also evidenced in Figure 4.25, TEM image of 4 hrs samples with 83 wt % and 91 wt% NIPAAm content). This full coverage of AuNP surface by PNIPAm petals helps to achieve modulatable catalytic activity of the composite particles, as will be discussed in next section.

In Figure 4.24, the DLS results show the size variation around LCST of 31 ℃. Particles with 83 wt% NIPAAm content has a size decrease from 1080 nm (25 ℃) to 480 nm (40 ℃) in diameter (55.6 % diameter decrease percentage); particles with 91 wt% NIPAAm content has a size decrease from 1780 nm (25 ℃) to 510 nm (40 ℃) in diameter (71.3 % diameter decrease percentage). The results suggest the composite particles' thermo-responsiveness increases with increased NIPAAm content. For 91 wt% PNIPAm content dumbbell-shaped gold-PNIPAm/polystyrene composite particles, the 71% size decrease percentage is significant; in comparison, the size variation of other reported thermo-responsive PNIPAm particles are mainly less than 60 %.[28, 119, 155, 160]

In addition, 1 hr sample of the composite particles with 83 wt% and 91 wt% NIPAAm content are analyzed.(see Figure 4.25) The DLS results show the composite particles with 83 wt% and 91 wt% NIPAAm content have size of 320 nm and 400 nm,

respectively, and the size does not change with temperature variation around LCST. Also, from the TEM images of 1 hr samples, no deformation of petals is observed compared to 4 hrs sample. The fact that no thermo-responsiveness in the early stage of the reaction possibly indicates PNIPAm polymers are participating the copolymerization within the composite particles after polystyrene's seeded growth stage. This is supported by formation chemistry that it is aromatic rings provided by styrene monomers/oligomers dispersed in water phase that interact with the surface of AuNPs.[29, 31]

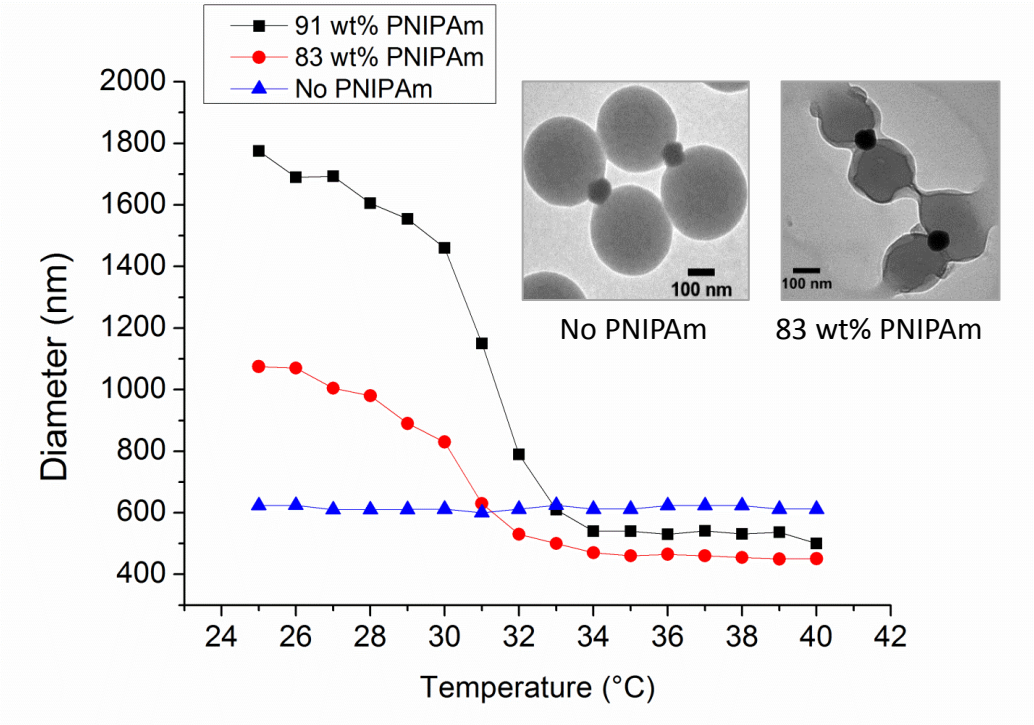

Figure 4.24 Thermo-responsiveness of dumbbell-shaped gold-polymer composite particles with different PNIPAm content. DLS results show relationship between particle size and temperature for particles with 83 wt% and 91 wt% PNIPAm content. Inset TEM images show morphology comparisons between dumbbell-shaped gold-polymer composite particles without PNIPAm content (left) and with 83 wt% PNIPAm content (right).

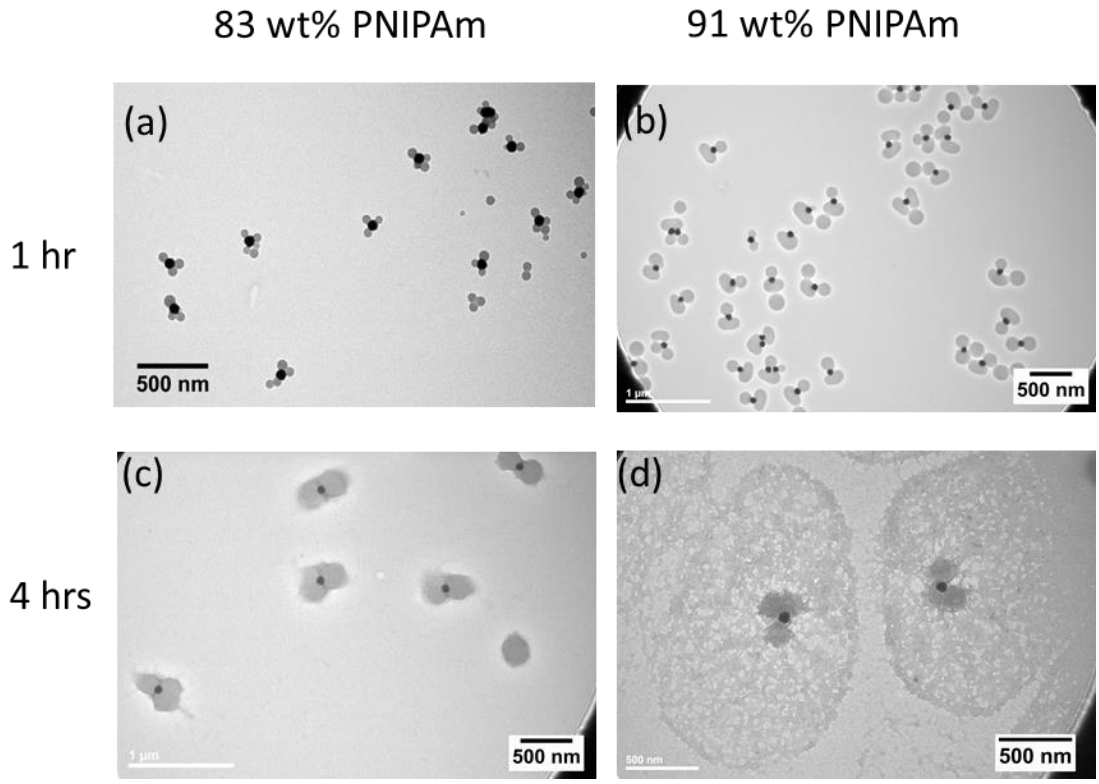

Figure 4.25 TEM images of gold-PNIPAm/polystyrene composite particles with 83 wt% (left) and 91 wt% (right) PNIPAm content, respectively. Samples are taken after 1hr and 4 hrs reaction time.

4.3.6 Modulatable Catalytic Activity of Dumbbell-shaped Gold-PNIPAm/polystyrene Composite Particles

Currently, for polymer-gold/silver composite particles, much research efforts utilizing the size variation ability of PNIPAm polymers are focused on tuning optical properties of particles.[29, 119, 166] In our previous work, PNIPAm-gold composite particles with asymmetric structure demonstrate to switch scattering intensity significantly due to the thermo-responsiveness of PNIPAm polymer.[164] However, the PNIPAm's ability to modulate catalytic activity of noble metals is seldom-reported. Here, we demonstrate the catalytic activity of dumbbell-shaped gold-PNIPAm/polystyrene composite particles is found to be modulatable around the LCST of 31 ℃. A redox reaction of Rhodamine B (RhB) is applied as the model reaction to investigate the particle's catalytic performance. In this reaction, under the catalysis of dumbbell-shaped gold-PNIPAm/polystyrene composite particles, RhB is reduced by $NaBH_4$ to its lueco form via hydrogenation with its pink color changed to transparent. Figure 4.26 shows the UV-Vis results of this reaction. In Figure 4.26a, the RhB peak at 552 nm gradually decreases, and disappears as reaction finishes. Figure 4.26b and 4.26c show the relationship between reaction temperature and reaction rate for particles with 83 wt% NIPAAm content and 91 wt% NIPAAm content (The reaction time is counted from the addition of particle catalysts to the point where the RhB peak at 552 nm disappears completely). For both particles with 83 wt% NIPAAm content and 91 wt% NIPAAm content, instead of linear increase of the reaction speed with increased temperature, the reaction speed decreases starting at 29 ℃ and remain stable until further increase after 35 ℃. Figure 4.26e shows the comparison of catalyst activity decrease between 83 wt% and 91 wt% NIPAAm content dumbbell-

shaped composite particles, the particles with 83 wt% NIPAAm content have a 12 % activity decrease, smaller than 18% for particles 91 wt% NIPAAm content. This indicates the thermo-responsive PNIPAm polymers are responsible for catalyst activity decrease. In contrast, we find for dumbbell-shaped polystyrene-gold composite particles without NIPAAm incorporation, the reaction speed increases linearly with temperature (Figure 4.26d). This indicates a modulated catalytic activity around LCST of 31 ℃, as a result of PNIPAm's thermo-responsiveness. This modulatable catalytic property presents a concept of automatically controlling reaction speed, providing potential applications where limiting reaction rate at high temperature is necessary. For instance, industry might require limiting reaction rate in daytime to a range similar to reaction rate in nighttime.

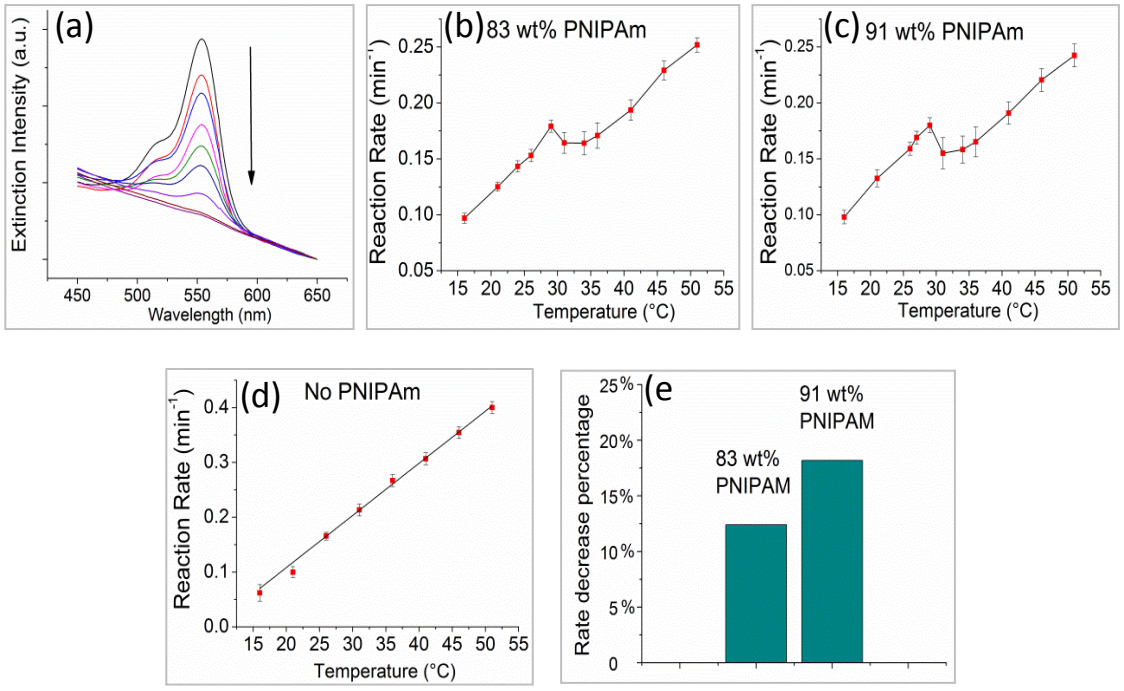

Figure 4.26 UV-Vis results of the RhB reduction reaction catalyzed by gold-PNIPAm/polystyrene particles. (a) UV-Vis spectra of sample with 91 wt% PNIPAm during reaction at 31 ℃. Spectrum is measured every 40 seconds until RhB peak disappears completely. (b) (c) (d) relationships between reaction temperature and reaction rate for particles with 83 wt% 91 wt%, and 0 wt% NIPAAm content respectively. (e) Comparison of catalyst activity decrease percentage between 83 wt% and 91 wt% NIPAAm content composite particles. Rate decrease percentage is calculated based on the following equation: $Rate\ decrease\ percentage = \frac{r_{32.5°C\ predicted} - r_{32.5\,°C\ real}}{r_{32.5°C\ predicted}} \times 100\%$. $r_{32.5\,℃\ predicted}$ is the predicted reaction rate assuming it linearly increases with temperature, obtained via linear fitting the measured reaction rate from 16 ℃ to 29 ℃. $r_{32.5\,℃\ real}$ is the average of $r_{31°C}$ and $r_{34°C}$

For the reason of why PNIPAm's thermo-responsiveness contributes to the modulated catalytic activity, we believe the significant shrinkage of PNIPAm petals block the access of Rhodamine B and $NaBH_4$ to the surface of AuNPs at temperature above LCST of 31 ℃ (See Figure 4.27). Shi et al[28] and Kim et al[18] find that PNIPAm-gold composite particles reduce catalytic reaction rate above LCST. They suggest that the shrinkage of PNIPAm particles possibly limits the diffusion of reaction molecules to AuNP surface. However, no experimental work is conducted to further investigate the cause. Compared to their microgel particle structure where many AuNPs are buried inside one PNIPAm microgel, the composite particles applied here have dumbbell-shaped structure, where two PNIPAm-containing petals anchor on a single AuNP center. For validating the hypothesis that shrunk PNIPAm petals block the diffusion of reaction molecules to the active surface of AuNPs, an effective way is to analyze the refractive index change of PNIPAm petals, which demonstrates petals' density change. Here we use UV-Vis spectrometer and DLS instrument to measure the scattering intensity variation around LCST of 31 ℃. The scattering intensity variation is caused by the change of refractive index contrast between PNIPAm petals and surrounding waters, as predicted by Mie theory.[28, 126-127] As shown in Figure 4.28, the scattering intensity increases 2.45 time and 3.4 time for 83 wt% and 91 wt% NIPAAm content composite particles, respectively. These trends are also observed in extinction spectra obtained by UV-Vis spectrometer (see Figure 4.29. It should be noted that the extinction intensity measured from the UV-Vis spectrometer includes absorbing and scattering light intensities,[158] where the scattering light becomes dominant as the temperature increases above the LCST.) The particle density and refractive index increase significantly, leading to a large refractive

index contrast between the particles and the water phase. From a recent ellipsometry study,[30, 31] the refractive index of PNIPAm microgels increases from 1.34 to 1.40, for a relatively small size decrease (30% - 50% diameter decrease percentage, compared to 55.6% and 71.3% diameter decrease percentage of our 83 wt% and 91 wt% PNIPAm content dumbbell-shaped composite particles). The large refractive index contrast is responsible for the extinction and scattering intensity increase. The increased refractive index of PNIPAm petals indicates increased particle density to reduce the diffusivity of Rhodamine B and $NaBH_4$ to the AuNP surface. Figure 5 c-e are the normalized UV-Vis spectra for dumbbell-shaped particles with PNIPAm content of 0 wt%, 83 wt% and 91 wt% respectively with temperature range of 25 ℃ - 37 ℃. For dumbbell-shaped particles with 0 wt% PNIPAm content, the AuNP extinction peaks at 580 nm remain unchanged. For particles with 83 wt% PNIPAm content, the peaks gradually decrease, merged by PNIPAm substrate curves. This trend becomes more obvious in extinction spectra of 91 wt% PNIPAm particles, where the SPR peaks at 570 nm are merged completely by PNIPAm substrate curves as temperature increases above LCST of 31 ℃. The merge of AuNP extinction peak is due to increased scattering intensity of PNIPAm petals, consistent with scattering intensity increase results shown in Figure 5a and 5b.

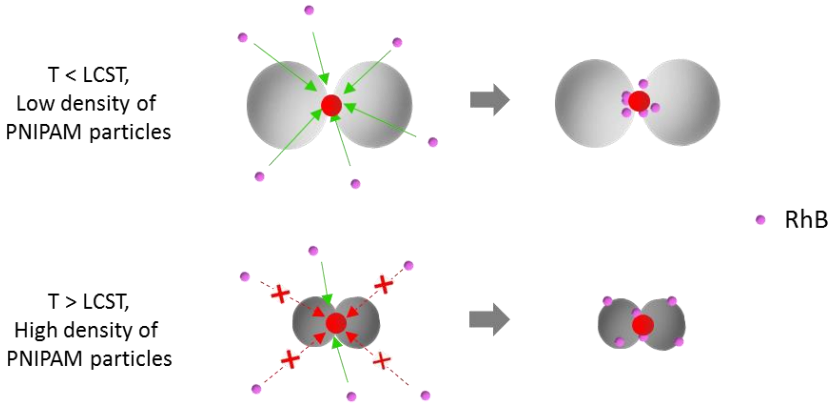

Figure 4.27 Illustration of proposed reason of modulatable catalytic activity of gold-PNIPAm/polystyrene dumbbell-shaped composite particles.

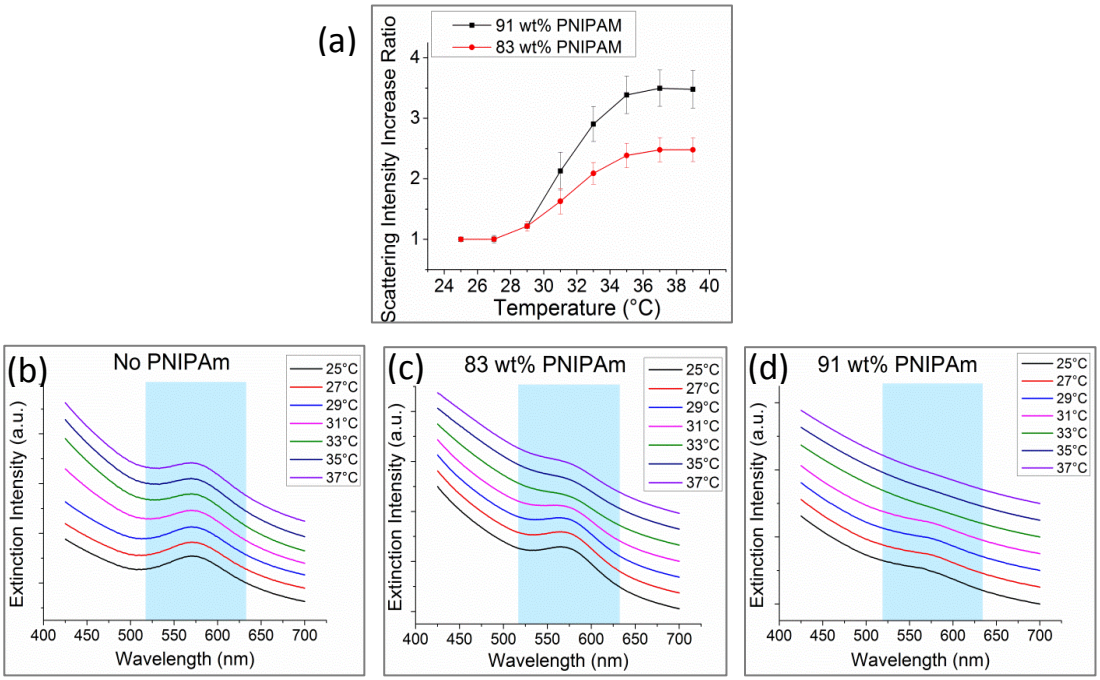

Figure 4.28 Relationship of scattering intensity of dumbbell-structured gold-PNIPAm/polystyrene composite particles with temperature. (a) DLS result of scattering intensity increase ratio for temperature range of 25 ℃ – 39 ℃ for particles with 83 wt% and 91 wt% PNIPAm content respectively. (b) (c) (d) are the normalized extinction spectra measured via UV-Vis spectrometer for particles with PNIPAm content of 0 wt%, 83 wt% and 91 wt% respectively with temperature range of 25 ℃ - 37 ℃. The extinction intensity measured from the UV-Vis spectrometer includes scattering and absorbing intensities.

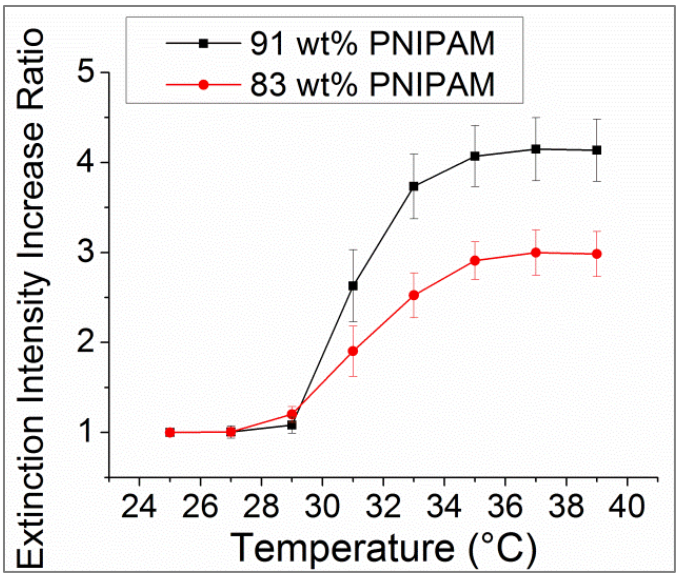

Figure 4.29 Relationship of extinction intensity of dumbbell-shaped gold-PNIPAm/polystyrene composite particles with temperature obtained via UV-Vis spectrometer. Extinction intensity increase ratio for temperature range of 25 ℃ – 39 ℃ for particles with 83 wt% and 91 wt% PNIPAm content respectively. The extinction intensity measured from the UV-Vis spectrometer includes scattering and absorbing intensities.

4.3.7 Conclusion

We first report a successful synthesis of gold-polymer composite particles with controlled structure (tetrapetal-structured, tripetal-structured and dumbbell-structured). Multipetal-structured and dumbbell-structured gold-polystyrene composite are obtained separately at the early stage and final stage of seeded emulsion polymerization, respectively. As AuNP diameter increases, the number of petals on each single AuNP increases (from tripetal structure to tetrapetal structure). The particles are found to be formed via seeded-growth formation mechanism. These particles show potential applications as building blocks for advanced ordered and hierarchical materials. Further incorporation of PNIPAm polymers gives thermo-responsive dumbbell-structured gold-PNIPAm/polystyrene particles. Significant size variation is shown for particles with 83 wt% and 91 wt% PNIPAm content around LCST. These significant size variations give rise to self-controlled catalytic activity around LCST, potentially useful for applications where automatically controlling catalytic activity is needed. This is because above LCST, the significant shrinkage of particles limits diffusion of reaction molecules to the surface of AuNPs, leading to a reduced catalytic activity.

4.4 “Smart” Core-Shell Structured CB-PNIPAm/polystyrene Composite Particles

4.4.1 Synthesis of Core-shell Structured CB-PNIPAm/polystyrene Composite Particles

Core-shell structured CB-PNIPAm/polystyrene composite particles are successfully synthesized via one-step Pickering emulsion polymerizations. To the best of our knowledge, it is the first time to report that Pickering emulsion polymerization route are capable of synthesizing CB-polymer composite particles. Figure 4.30 is TEM image of synthesized CB-PNIPAm/polystyrene composite particles sampled at 2 hrs reaction time. From the TEM images, it is found the majority of core-shell composite particles have a size of ~ 60 nm. A clear core-shell structure is observed. We believe the shell part of these particles are composed of CB, because the density of CB is ~2 g/cm3, much higher than PNIPAm/polystyrene’s density of ~1 g/cm3 giving a clear contrast in TEM microscope, where dark parts indicate CB is dominant. It should be noted that the particles structure is not strictly spherical as shown in these images. It is observed that as the electron beam hits on the particles, this CB shells start to deform. In addition, EDX analysis is performed. As shown in Figure 4.30c, d, the presence of nitrogen elements is evidenced by a characteristic peak as the electron beam is focused on the center part of particle, while this nitrogen peak are not shown when the electron beam is focused on the blank space of TEM film. This indicates the successful incorporation of PNIPAm into the composite particles.

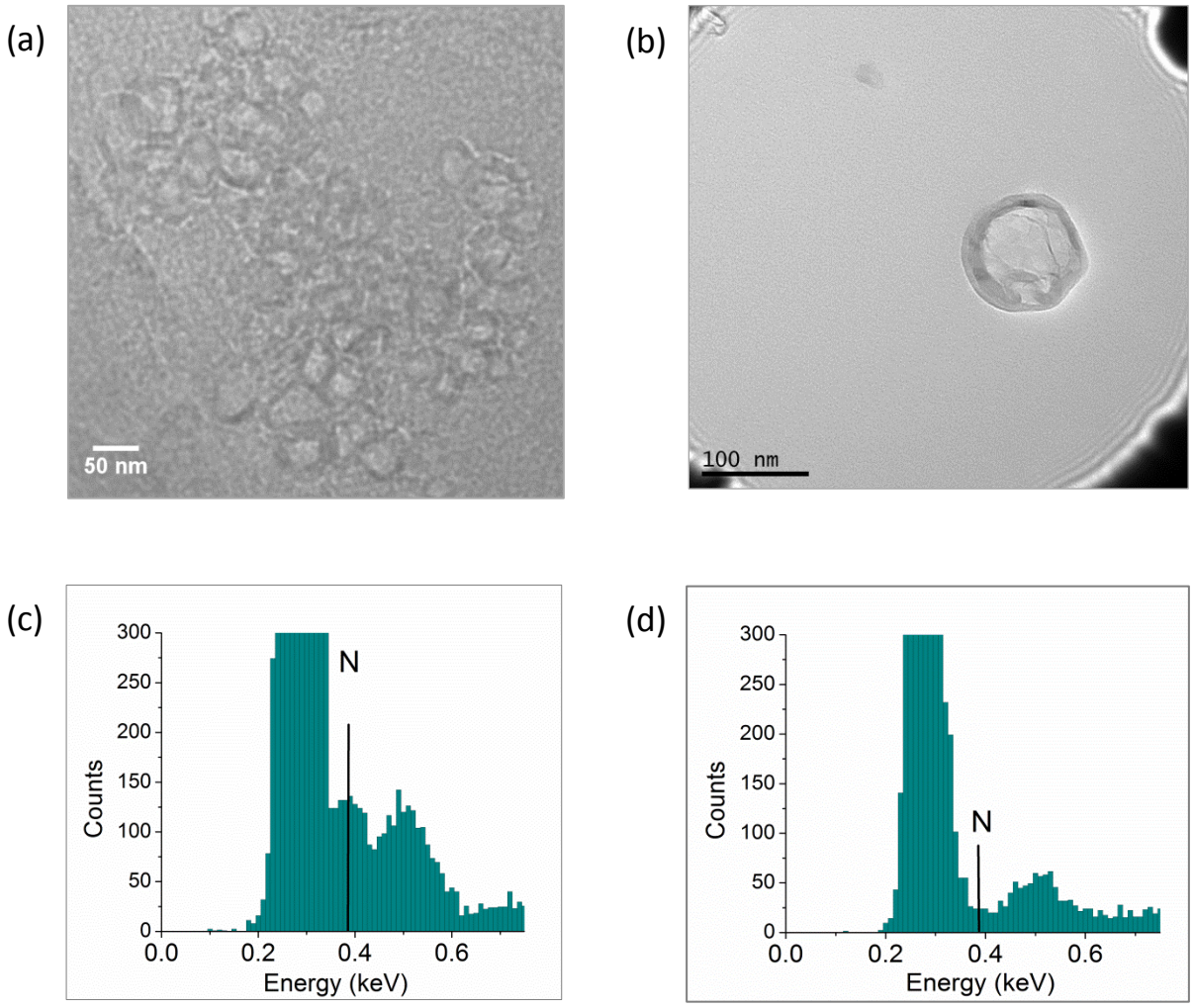

Figure 4.30 (a)(b) TEM images of CB-PNIPAm/polystyrene composite particles. (c)(d) EDX results of CB-PNIPAm/polystyrene composite particles. The left and right EDX results represent results where electron beam is focused on the particles and the blank space, respectively.

4.4.2 Thermo-responsiveness of Core-Shell Structured CB-PNIPAm/polystyrene Composite Particles

Following the successful validation of the AuNP system's thermos-responsiveness as described in previous sections, here the thermos-responsiveness of core-shell CB-PNIPAm/polystyrene composite particles is analyzed by DLS techniques. Figure 4.31 demonstrates the size variation of samples taken at different reaction time during Pickering emulsion polymerization. These particles are synthesized with 83 wt% PNIPAm monomer content (17 % polystyrene content). For the sample with 1 hr reaction time, the particle size is 71 nm and no size variation is observed via DLS. For the sample with 2 hrs reaction time, a typical size decrease curve is observed, where particles undergo size decrease from 78 nm to 55 nm above the LCST of 31 ℃. This trend is consistent with the previous results of PNIPAm-gold composite particle systems.[164] For the sample with 3 hrs reaction time, the particle size decreases from 190 nm to 78 nm at the LCST. For the sample with 4 hrs reaction time, the particle size decreases from 525 nm to 150 nm going through the LCST. Figure 4.31e at the bottom is the comparison of shrinkage ratio of samples with different reaction time. The shrinkage ratio is the ratio of particle diameter at a given temperature to particle diameter at 40 ℃. As the reaction time increase, the thermo-responsiveness of the CB-PNIPAm/polystyrene composite particles becomes more and more significant. At 4 hrs reaction time, a shrinkage ratio of 3.5 is detected. The fact that no thermo-responsiveness in the early stage of the reaction possibly indicates that PNIPAm polymers are participating the copolymerization within the composite particles later than styrene's polymerization stage. The observation here is also supported by report by Duracher et al.. [55]

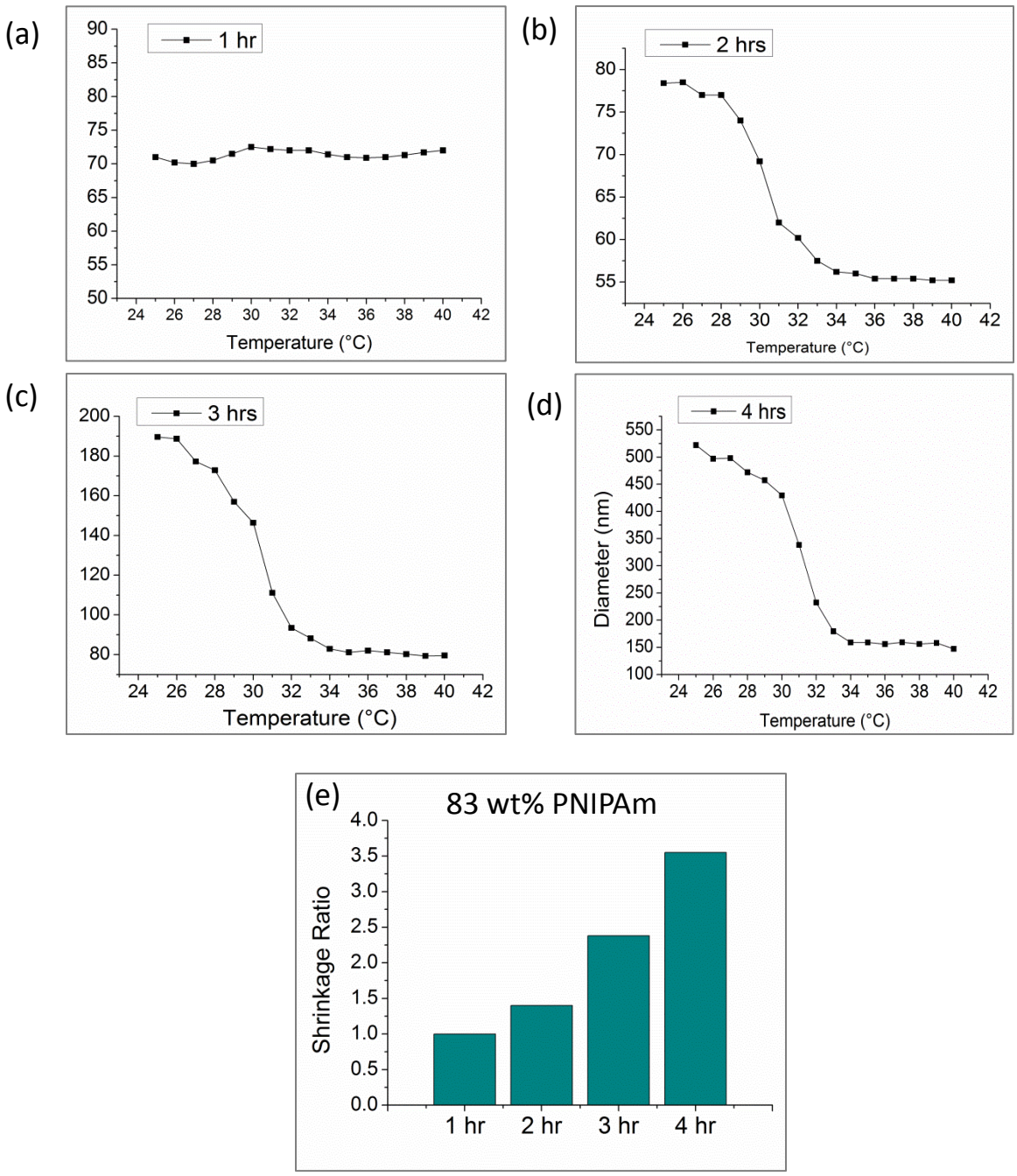

Figure 4.31 DLS analysis of CB-PNIPAm/polystyrene composite particles with 83 wt% PNIPAm content under increasing temperatures. (a)(b)(c)(d) represent results of samples with 1 hr, 2 hrs, 3 hrs and 4 hrs reaction time, respectively. (e) comparison of shrinkage ratio of the above four samples with 83 wt% PNIPAm content under increasing temperatures.

4.4.3 Study of Optical properties of Core-Shell Structured CB -PNIPAm/polystyrene Composite Particles

The absorption characteristics of the CB-PNIPAm/polystyrene composite particles are analyzed via UV-Vis spectrometers (Figure 4.32). For the sample with 1 hr reaction time, the extinction spectra are the same at 20 ℃ and 40 ℃. This indicates no PNIPAm incorporation at this stage, consistent with previous DLS particle size measurements. For the sample with 2 hrs reaction time, a decrease of extinction intensity is observed at 40 ℃, due to decreased volume fraction of the sample dispersion as particles undergo size decrease. For example, at the wavelength of 500 nm, the extinction intensity decreases from 0.69 to 0.65 with decrease percentage of 5.8 %. This result is consistent with numerical model created by Dr. Otanicar. For the sample with 3 hrs reaction time, a significant increase of extinction intensity is observed at 40 ℃. For the sample with 4 hrs reaction time, the extinction intensity increases even more dramatically from 20 ℃ to 40 ℃. It should be noted that the extinction intensity measured from the UV-Vis spectrometer includes absorbing and scattering light intensities,[158] where the scattering light becomes dominant as the temperature increases above the LCST. This result is consistent with previous study on PNIPAm/polystyrene-gold asymmetric composite particles. The significant increase of extinction/scattering intensity is due to the presence of PNIPAm which causes the large size decrease of the CB-PNIPAm/polystyrene composite particles. This significant intensity change is attributed to the refractive index change of the PNIPAm-containing core particles. Reports show below the LCST, the polymer backbone is stretched and the particles are swollen with up to 97% water, with the refractive index matching the surrounding water phase.[119, 159-160] Our results show as

temperature increases above the LCST, the PNIPAm backbone collapses with inter-chain clustering, and the particles repel most of the water, undergoing a significant shrinking in diameter from 525 nm to 150 nm (71.4% size decrease percentage). The particle density and refractive index increase significantly, leading to a large refractive index contrast between the particles and the water phase. From a recent ellipsometry study,[30, 31] the refractive index of PNIPAm microgels increases from 1.34 to 1.40, for a relatively small size decrease (30% - 50% diameter decrease percentage). This large refractive index contrast is responsible for the extinction and scattering intensity increase, as predicted by Mie theory.[28, 125-127] Therefore, we believe the increased refractive index contrast between PNIPAm particles and surrounding water phase is more influential than the decrease of volume fraction of CB-PNIPAm/polystyrene composite particles, which causes an increase of extinction intensity.

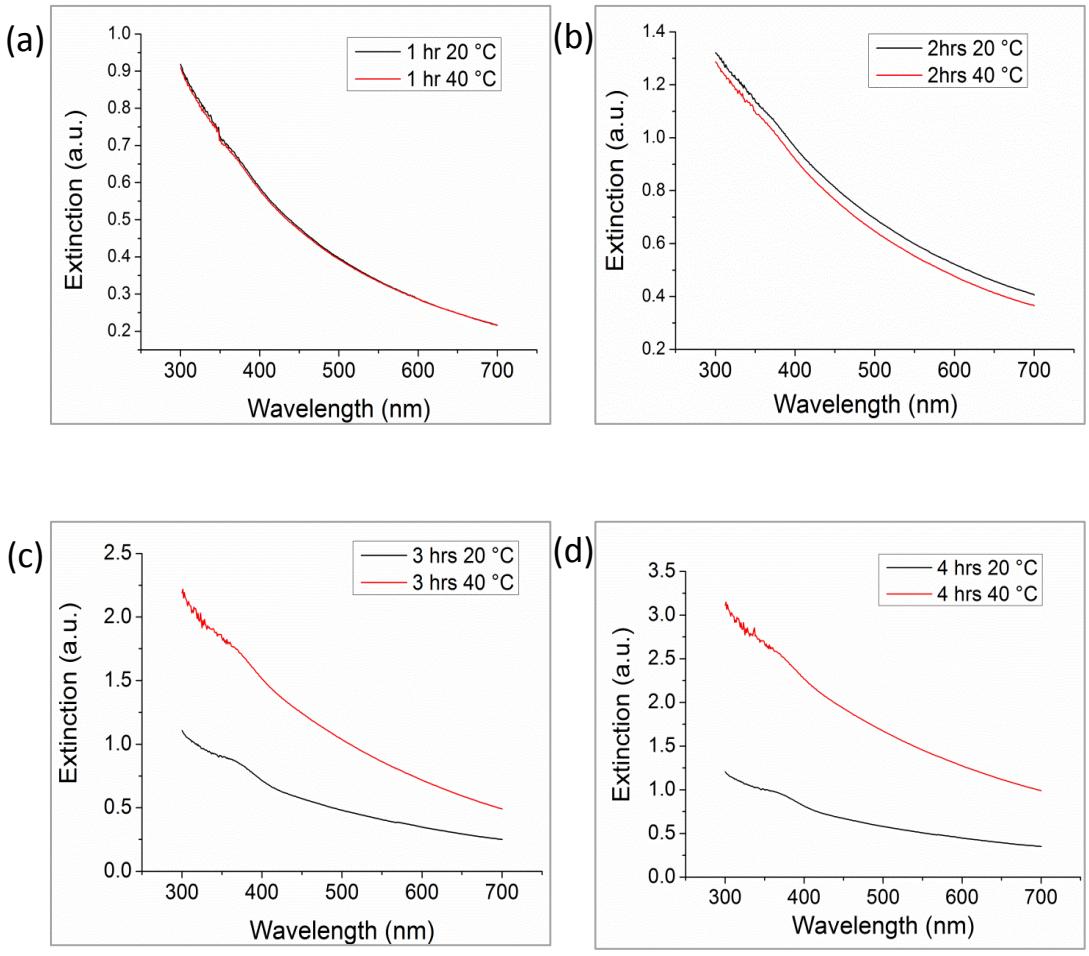

Figure 4.32 UV-Vis spectrometer analyses of CB-PNIPAm/polystyrene composite particles with 83 wt% PNIPAm content at 20 ℃ and 40 ℃. (a)(b)(c)(d) represent samples with 1 hr, 2 hrs, 3 hrs and 4 hrs reaction time, respectively.

The scattering intensity response is further validated via DLS instrument's scattering intensity records, as shown in Figure 4.33. For samples with 1 hrs and 2 hrs reaction time, no scattering increase is observed as the temperature is increased from 25 ℃ to 40 ℃, because not enough PNIPAm is incorporated to give increase of refractive index contrast between PNIPAm particles and surrounding water phase. This is consistent with the

above-mentioned UV-Vis results. For samples with 3 hrs and 4 hrs reaction time, a significant increase of scattering intensity is observed over the same temperature range, with scattering intensity increasing by a factor of 2.6 and 3.6 for 3 hrs and 4 hrs samples, respectively, as temperature is increased from 25 ℃ to 40 ℃. This is consistent with size variation around the LCST temperature confirmed by DLS's particle size measurement.

$$\text{Absorbed Energy} \propto D^2 Q_{abs} \tag{6}$$

Equation 6 shows the influence of particle size and absorption efficiency on absorbed energy.

Based on this equation, for the sample with 2 hrs reaction time, the estimated decrease percentage of absorbed energy is 53%. For sample with 3 hrs reaction time and 4 hrs reaction time, the particle size exceeds the limit (< 100 nm) of numerical model by Otanicar et al. Figure 2.21 in the motivation section shows the relationship between stagnation temperature and absorption of heat transfer fluids. For each of three batches with different concentrations, stagnation temperature decreases as absorbed energy decreases. The results indicate dispersions of CB-PNIPAm/polystyrene composite particles synthesized with 2 hrs reaction time shows potential to be utilized as nanofluids with self-controlled temperature to solve stagnation problems.

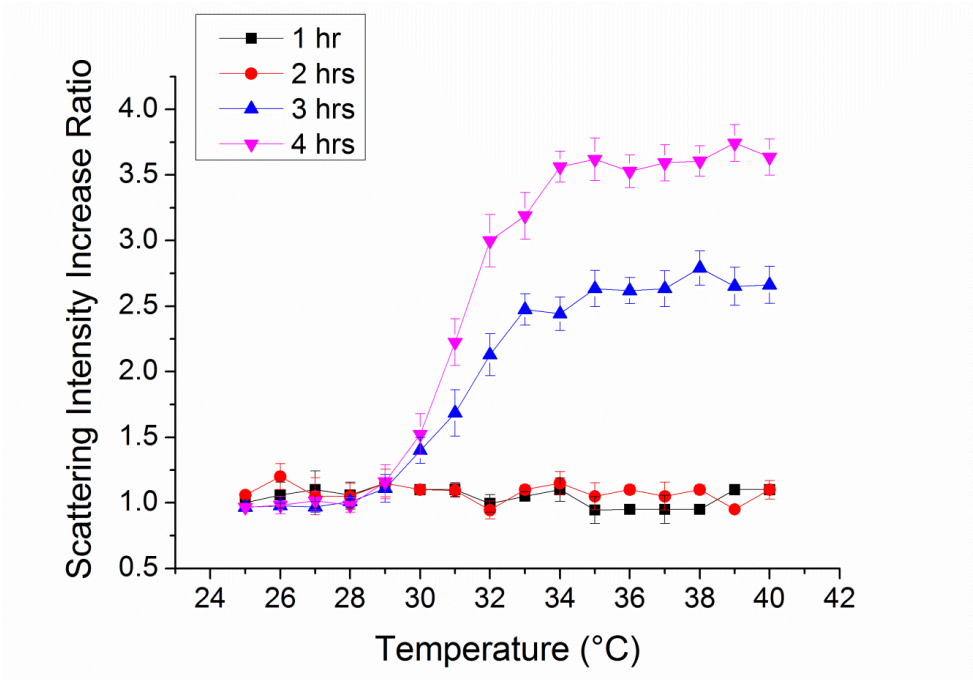

Figure 4.33 Relationship between scattering intensity increase ratio and temperatures of CB-PNIPAm/polystyrene composite particles with 83 wt% PNIPAm. The four plots represent samples with 1 hr, 2 hrs, 3 hrs and 4 hrs reaction time, respectively. The laser wavelength of DLS for scattering intensity measurement is kept at 639 nm.

4.4.4 Conclusion

"Smart" core-shell CB-PNIPAm/polystyrene composite particles are successfully synthesized via Pickering emulsion polymerization methods. These particles are around 78 nm in diameter where the incorporation of PNIPAm is confirmed by an EDX analysis. The thermo-responsiveness of core-shell CB-PNIPAm/polystyrene composite particles is validated via a DLS particle size measurement, where an increasing size variation is found for samples with 83 wt% PNIPAm content after 2 hrs, 3 hrs and 4 hrs reaction time. The extinction intensity is found to be influenced by both the volume fraction of particles and the refractive index contrast between PNIPAm particles and surrounding water phase; as the volume fraction decreases or refractive index contrast decreases, the extinction intensity increases. This is further confirmed by direct scattering intensity analysis via the DLS scattering intensity measurement. Previous numerical model suggests absorbed energy of heat transfer fluids is proportional to particle size and absorption efficiency. Dispersions of core-shell CB-PNIPAm/polystyrene composite particles with 2 hrs reaction time is found to be able to serve as potential nanofluids with self-controlled temperature to solve stagnation problems of heat transfer fluids.

Chapter 5

SUMMARY AND FUTURE WORK

5.1 Summary

Gold core-shell composite particles are successfully synthesized via one-step Pickering emulsion polymerization route. The surface coverage is found to be improved with increasing AuNP hydrophobicity and AuNP concentration. Under high AuNPs concentration (0.092 wt%), it's intriguing to find that AuNPs exhibit an ordered hexagonal pattern on polystyrene substrate surface, likely due to electrostatic repulsion during the emulsion polymerization progress. Other than the desired gold core-shell composite particles, interestingly we find that at low AuNPs concentrations, there is a bimodal size distribution in which asymmetric nanocomposite particles and gold core-shell composite particles are both present with an averaged diameter of 180 nm and 460 nm respectively. We conduct a time study and propose the seeded-growth mechanism for the formation of asymmetric particles. The core-shell and asymmetric polystyrene-gold composite particles show potential applications in catalysts as they successfully catalyzed the redox reaction of Rhodamine B with stable performance. Both core-shell and asymmetric composite particles show high recyclability.

We successfully employed emulsion polymerization method to synthesize polystyrene/PNIPAm-gold composite particles. Core-shell and asymmetric structured particles are simultaneously formed during the polymerization process. Compared with core-shell structured composite particles, the asymmetric composite particles have a higher thermo-responsiveness as a result of different formation mechanism. With an increasing NIPAAm content, the size decrease of an asymmetric composite particles

becomes more significant. Compared with traditional gold-PNIPAm particles synthesized with the aid of cross-linking agent, the asymmetric particles synthesized here without cross linker show significant particle size and viscosity variations around the LCST. The significant size decrease of the asymmetric composite particles gives rise to meaningful scattering intensity increase due to an increased refractive index contrast between the PNIPAm substrate particles and surrounding water. The resulting size decrease also leads to tunable surface plasmon resonance properties, as a result of the local refractive index change of the PNIPAm medium surrounding AuNP. The switchable scattering intensity gives the asymmetric particles great potential for intensity-based thermal sensor.

We successful synthesized multipetal-shaped and dumbbell-shaped gold-polystyrene composite particles. The multipetal-shaped and dumbbell-shaped gold-polystyrene composite particles are obtained separately at the early stage and final stage of seeded emulsion polymerization, respectively. As the AuNP diameter increases, the number of the petals on each single AuNP increases. The particles are found to be formed via seeded-growth formation mechanism. No core-shell particles are formed, indicating that the increased AuNP size here leads to decreased emulsion stability. Further incorporation of PNIPAm polymers gives thermo-responsive dumbbell-shaped gold-PNIPAm/polystyrene particles. Significant size variation is shown for particles with 83 wt% and 91 wt% PNIPAm content around LCST. These significant size variations give rise to a modulatable catalytic activity around LCST. This is hypothesized that above LCST, the significant shrinkage of particles limits diffusion of reaction molecules to the surface of AuNPs, leading to a reduced catalytic activity.

Moreover, non-metal inorganic material carbon black is found to be able to serve as Pickering emulsion stabilizer for the synthesis of "smart" core-shell CB-PNIPAm/polystyrene composite particles via Pickering emulsion polymerization methods. These particles are around 78 nm in diameter at room temperature where the incorporation of PNIPAm is confirmed by EDX analysis. The thermo-responsiveness of core-shell CB-PNIPAm/polystyrene composite particles is validated via DLS particle size measurement, where an increasing size variation is found for samples with 83 wt% PNIPAm content of 2 hrs, 3 hrs, and 4 hrs reaction time. The extinction intensity is found to be influenced by both volume fraction of particles and refractive index contrast between PNIPAm particles and surrounding water phase, where as volume fraction decreases or refractive index contrast decreases, extinction intensity increases. This is further confirmed by direct scattering intensity analysis via the DLS scattering intensity measurement. Previous numerical model suggests the absorbed energy of heat transfer fluids is proportional with particle size and absorption efficiency. As the absorbed energy decreases, the temperature decreases. Dispersions of core-shell CB-PNIPAm/polystyrene composite particles with 2 hrs reaction time is found to be able to serve as potential nanofluids with self-controlled temperature to solve the stagnation problems of heat transfer fluids.

5.2 Future Work

5.2.1 "Smart" Core-Shell PNIPAm/polystyrene-Gold Composite Particles

Previously we successfully synthesize PNIPAm/polystyrene-gold composite particles, where AuNPs form a discontinuous shell layer. Another synthesis route shows potential for synthesizing PNIPAm/polystyrene-gold composite particles with a continuous Au shell, where the shell thickness is controllable. Yong et al successfully synthesized core-shell structured polystyrene-gold composite particles via chemical binding between gold and thiol group.[11] This indicates the possibility of incorporation of PNIPAm polymers via copolymerization of styrene and NIPAAm under chemical synthesis of polystyrene-gold composite particles via chemical binding between gold and thiol group. The advantage of their method is that a continuous shell is forming where the shell thickness is controlled by time of chemical reduction reaction of gold salts; therefore, by controlling the reaction time, the absorption properties of composite particles is tuned.

The first goal proposed here is to synthesize thiol-terminate PNIPAm-polystyrene core-shell structured particles. As reported before, reaction kinetics show styrene monomers polymerize at the first stage; at the later stage, NIPAAm monomer starts to polymerize. As a result, these particles have a PNIPAm core and a polystyrene shell. This is supported by the fact that the LCST of polystyrene/PNIPAm-silica composite particles synthesized via the same approach are not affected by copolymerization of styrene.[56] For asymmetric PNIPAm/polystyrene-gold composite particles with NIPAAm content of 71% and 83% (results are shown in Figure 4a), the LCST remains 31 ℃.[164] This indicates the influence of copolymerization with styrene to LCST variation is small. A possible explanation is that phase separation inside the core particles exists between polystyrene

and PNIPAm polymers. Duracher et al propose that phase separation exists inside particles that contain a PNIPAm-rich core and polystyrene-rich shell.[55] Here, surfactants with thiol end group might be chosen to stabilize the emulsions to form thiol terminated PNIPAm-polystyrene core-shell particles. The next step is proposed as chemical deposition of gold salt via thiol-gold binding, as described by Yong et al.

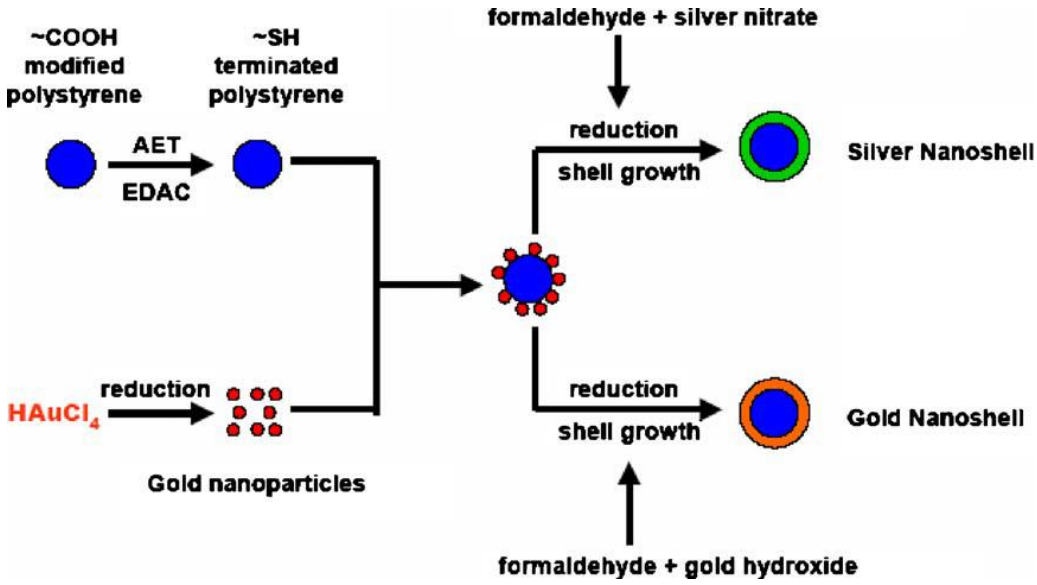

Figure 5.1 Formation pathway of polystyrene-gold core-shell composite particles. Adapted from Reference 11.

5.2.2 Self-controlled Natural Convection of Nanofluids Composed of Asymmetric PNIPAm/polystyrene-Gold Composite Particles

The significant thermo-responsiveness of asymmetric PNIPAm/polystyrene composite particles contributes to switchable scattering intensity properties of particles, as described previously. Another potential application utilizing the significant thermos-responsiveness of asymmetric PNIPAm/polystyrene composite particles is nanofluids with self-controlled natural heat transfer. Considering the significant variation of viscosity for asymmetric PNIPAm/polystyrene composite particles with 83 wt% and 71 wt% PNIPAm content, the natural convection heat transfer coefficient is presumed to change as well. For instance, this "smart" nanofluid is suitable for applications in which increased heat transfer is needed in the daytime (above the LCST of 31°C) for the purpose of releasing energy, while decreased heat transfer is needed in the nighttime (below the LCST of 31°C) for the purpose of storing energy. As a result, this nanofluid is potentially helpful for systems that must be maintained at a constant temperature.

Gunawan et al in Dr. Phelan's group previously conducted theoretical and experimental studies on the amplifying effect of natural convection on power generation of thermogalvanic cells.[167-168] The device (shown in Figure 5.2) is capable of running natural convection heat transfer experiments without galvanic setups. Both vertical alignment and horizontal alignment (shown in Figure 5.2c) are proposed for measurements. For experiments measuring systems above LCST of 31 °C, the temperature at hot end might be set at 50 °C, cold end at 40 °C; for experiments measuring systems below LCST of 31 °C, the temperature at hot end might be set at 20 °C, cold end at 10 °C.

The calculation of Nusselt number for the device in Figure 5.2 is shown below.[169-172]

$$\mathrm{Gr_T} = g\beta(T_h - T_c)L^3/\nu^2$$
$$\mathrm{Pr} = \frac{\nu}{\alpha} \tag{9}$$

For horizontal orientation,

$$\mathrm{Nu}\frac{L}{H} = 1 + \left\{ \left[\frac{((\mathrm{Gr_C Pr})H/L)^2}{362880} \right]^{-0.386} + \left(0.623(\mathrm{Gr_C Pr})^{1/5} \frac{L}{H} \right)^{-0.386} \right\}^{1/-0.386}$$
$$\mathrm{Gr_C Pr} \lesssim 10^9 \tag{10}$$

For vertical orientation,

$$\mathrm{Nu} = 0.147(\mathrm{Gr_C Pr})^{0.247}, \quad 2 \times 10^4 < \mathrm{Gr_C Pr} < 5 \times 10^5 \tag{11}$$

where $\mathrm{Gr_T}$ is thermal Grashof number and Pr is Prandtl number, β is the coefficient of volume expansion, g is gravitational acceleration, T_h is temperature at hot end, T_c temperature at cold end, ν the kinematic viscosity, α the thermal diffusivity.

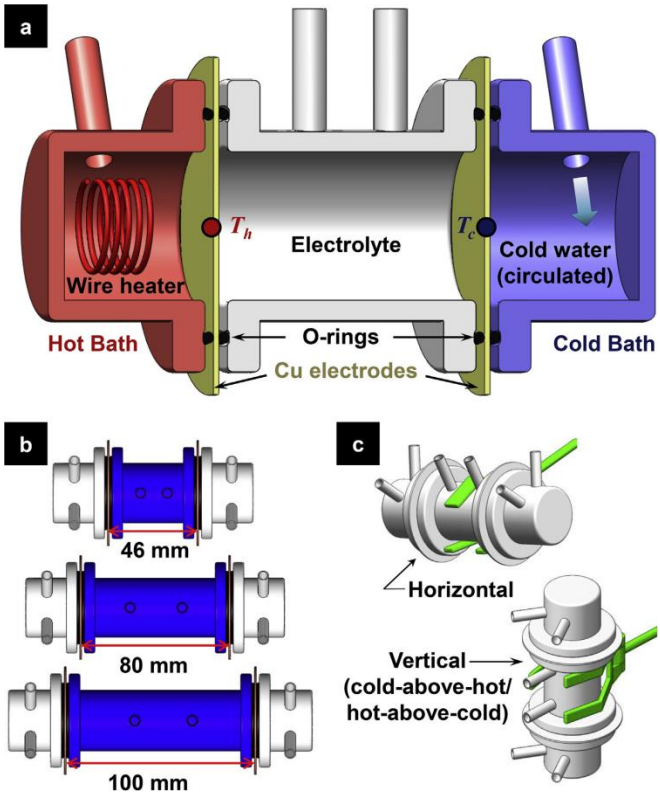

Figure 5.2 Illustration of glass cell setups for natural convection heat transfer. (a) cross-section of of the cell's three compartments; (b) interchangeable middle compartments which are made to fit different electrode spacing distance; (c) the cell setups are stabilized in horizontal and vertical orientation, providing three potential orientations for measurements. Adapted from Reference 167.

REFERENCES

1. Xuan, S. H.; Wang, Y. X. J.; Yu, J. C.; Leung, K. C. F. Preparation, Characterization, and Catalytic Activity of Core/Shell Fe_3O_4@Polyaniline@Au Nanocomposites. *Langmuir* 2009, *25* (19), 11835-11843.

2. Miyamura, H.; Matsubara, R.; Miyazaki, Y.; Kobayashi, S. Aerobic oxidation of alcohols at room temperature and atmospheric conditions catalyzed by reusable gold nanoclusters stabilized by the benzene rings of polystyrene derivatives. *Angew. Chem.-Int. Edit.* 2007, *46* (22), 4151-4154.

3. Comotti, M.; Della Pina, C.; Matarrese, R.; Rossi, M.; Siani, A. Oxidation of alcohols and sugars using Au/C catalysts - Part 2. Sugars. *Applied Catalysis a-General* 2005, *291* (1-2), 204-209.

4. Tsunoyama, H.; Sakurai, H.; Tsukuda, T. Size effect on the catalysis of gold clusters dispersed in water for aerobic oxidation of alcohol. *Chemical Physics Letters* 2006, *429* (4-6), 528-532.

5. Burato, C.; Centomo, P.; Pace, G.; Favaro, M.; Prati, L.; Corain, B. Generation of size-controlled palladium(0) and gold(0) nanoclusters inside the nanoporous domains of gel-type functional resins Part 11: Prospects for oxidation catalysis in the liquid phase. *J. Mol. Catal. A-Chem.* 2005, *238* (1-2), 26-34.

6. Storhoff, J. J.; Elghanian, R.; Mucic, R. C.; Mirkin, C. A.; Letsinger, R. L. One-pot colorimetric differentiation of polynucleotides with single base imperfections using gold nanoparticle probes. *J. Am. Chem. Soc.* 1998, *120* (9), 1959-1964.

7. Wang, J. T.; Moore, J.; Laulhe, S.; Nantz, M.; Achilefu, S.; Kang, K. A. Fluorophore-gold nanoparticle complex for sensitive optical biosensing and imaging. *Nanotechnology* 2012, *23* (9).

8. Tessier, P. M.; Velev, O. D.; Kalambur, A. T.; Rabolt, J. F.; Lenhoff, A. M.; Kaler, E. W. Assembly of gold nanostructured films templated by colloidal crystals and use in surface-enhanced Raman spectroscopy. *J. Am. Chem. Soc.* 2000, *122* (39), 9554-9555.

9. Wustholz, K. L.; Henry, A. I.; McMahon, J. M.; Freeman, R. G.; Valley, N.; Piotti, M. E.; Natan, M. J.; Schatz, G. C.; Van Duyne, R. P. Structure-Activity Relationships in

Gold Nanoparticle Dimers and Trimers for Surface-Enhanced Raman Spectroscopy. *J. Am. Chem. Soc.* 2010, *132* (31), 10903-10910.

10. Oldenburg, S. J.; Averitt, R. D.; Westcott, S. L.; Halas, N. J. Nanoengineering of optical resonances. *Chemical Physics Letters* 1998, *288* (2-4), 243-247.

11. Yong, K. T.; Sahoo, Y.; Swihart, M. T.; Prasad, P. N. Synthesis and plasmonic properties of silver and gold nanoshells on polystyrene cores of different size and of gold-silver core-shell nanostructures. *Colloids and Surfaces a-Physicochemical and Engineering Aspects* 2006, *290* (1-3), 89-105.

12. Shi, W. L.; Sahoo, Y.; Swihart, M. T.; Prasad, P. N. Gold nanoshells on polystyrene cores for control of surface plasmon resonance. *Langmuir* 2005, *21* (4), 1610-1617.

13. Pham, T.; Jackson, J. B.; Halas, N. J.; Lee, T. R. Preparation and characterization of gold nanoshells coated with self-assembled monolayers. *Langmuir* 2002, *18* (12), 4915-4920.

14. Cole, J. R.; Halas, N. J. Optimized plasmonic nanoparticle distributions for solar spectrum harvesting. *Applied Physics Letters* 2006, *89* (15).

15. Lv, W.; Phelan, P. E.; Swaminathan, R.; Otanicar, T. P.; Taylor, R. A. Multifunctional Core-Shell Nanoparticle Suspensions for Efficient Absorption. *J. Sol. Energy Eng. Trans.-ASME* 2013, *135* (2).

16. Hale, G. D.; Jackson, J. B.; Shmakova, O. E.; Lee, T. R.; Halas, N. J. Enhancing the active lifetime of luminescent semiconducting polymers via doping with metal nanoshells. *Applied Physics Letters* 2001, *78* (11), 1502-1504.

17. Sershen, S. R.; Westcott, S. L.; Halas, N. J.; West, J. L. Temperature-sensitive polymer-nanoshell composites for photothermally modulated drug delivery. *Journal of Biomedical Materials Research* 2000, *51* (3), 293-298.

18. West, J. L.; Halas, N. J. Applications of nanotechnology to biotechnology - Commentary. *Current Opinion in Biotechnology* 2000, *11* (2), 215-217.

19. Perro, A.; Reculusa, S.; Ravaine, S.; Bourgeat-Lami, E. B.; Duguet, E. Design and synthesis of Janus micro- and nanoparticles. *Journal of Materials Chemistry* 2005, *15* (35-36), 3745-3760.

20. Nisisako, T.; Torii, T.; Takahashi, T.; Takizawa, Y. Synthesis of monodisperse bicolored janus particles with electrical anisotropy using a microfluidic co-flow system. *Advanced Materials* 2006, *18* (9), 1152-+.

21. Glotzer, S. C.; Solomon, M. J. Anisotropy of building blocks and their assembly into complex structures. *Nature Materials* 2007, *6* (8), 557-562.

22. Perro, A.; Reculusa, S.; Ravaine, S.; Bourgeat-Lami, E.; Duguet, E. Design and synthesis of Janus micro- and nanoparticles. *Journal of Materials Chemistry* 2005, *15* (35-36), 3745-3760.

23. Yang, S.-M.; Kim, S.-H.; Lim, J.-M.; Yi, G.-R. Synthesis and assembly of structured colloidal particles. *Journal of Materials Chemistry* 2008, *18* (19), 2177-2190.

24. Tsai, H.-J.; Lee, Y.-L. Facile Method to Fabricate Raspberry-like Particulate Films for Superhydrophobic Surfaces. *Langmuir* 2007, *23* (25), 12687-12692.

25. Puretskiy, N.; Ionov, L. Synthesis of Robust Raspberry-like Particles Using Polymer Brushes. *Langmuir* 2011, *27* (6), 3006-3011.

26. Ho, K. M.; Chan, C. T.; Soukoulis, C. M. EXISTENCE OF A PHOTONIC GAP IN PERIODIC DIELECTRIC STRUCTURES. *Physical Review Letters* 1990, *65* (25), 3152-3155.

27. Tagliazucchi, M.; Blaber, M. G.; Schatz, G. C.; Weiss, E. A.; Szleifert, I. Optical Properties of Responsive Hybrid Au@Polymer Nanoparticles. *ACS Nano* 2012, *6* (9), 8397-8406.

28. Contreras-Caceres, R.; Sanchez-Iglesias, A.; Karg, M.; Pastoriza-Santos, I.; Perez-Juste, J.; Pacifico, J.; Hellweg, T.; Fernandez-Barbero, A.; Liz-Marzan, L. M. Encapsulation and growth of gold nanoparticles in thermoresponsive microgels. *Adv. Mater.* 2008, *20* (9), 1666-+.

29. Karg, M.; Pastoriza-Santos, I.; Perez-Juste, J.; Hellweg, T.; Liz-Marzan, L. M. Nanorod-coated PNIPAm microgels: Thermoresponsive optical properties. *Small* 2007, *3* (7), 1222-1229.

30. Sorrell, C. D.; Carter, M. C. D.; Serpe, M. J. Color Tunable Poly (N-isopropylacrylamide)-co-Acrylic Acid Microgel-Au Hybrid Assemblies. *Adv. Funct. Mater.* 2011, *21* (3), 425-433.

31. Kim, J. H.; Boote, B. W.; Pham, J. A.; Hu, J. Y.; Byun, H. Thermally tunable catalytic and optical properties of gold-hydrogel nanocomposites. *Nanotechnology* 2012, *23* (27).

32. Wu, S.; Dzubiella, J.; Kaiser, J.; Drechsler, M.; Guo, X. H.; Ballauff, M.; Lu, Y. Thermosensitive Au-PNIPA Yolk-Shell Nanoparticles with Tunable Selectivity for Catalysis. *Angew. Chem.-Int. Edit.* 2012, *51* (9), 2229-2233.

33. Tagliazucchi, M.; Azzaroni, O.; Szleifer, I. Responsive Polymers End-Tethered in Solid-State Nanochannels: When Nanoconfinement Really Matters. *J. Am. Chem. Soc.* 2010, *132* (35), 12404-12411.

34. Tagliazucchi, M.; Szleifer, I. Stimuli-responsive polymers grafted to nanopores and other nano-curved surfaces: structure, chemical equilibrium and transport. *Soft Matter* 2012, *8* (28), 7292-7305.

35. Bradley, M.; Garcia-Risueno, B. S. Symmetric and asymmetric adsorption of pH-responsive gold nanoparticles onto microgel particles and dispersion characterisation. *J. Colloid Interface Sci.* 2011, *355* (2), 321-327.

36. Schild, H. G. POLY (N-ISOPROPYLACRYLAMIDE) - EXPERIMENT, THEORY AND APPLICATION. *Progress in Polymer Science* 1992, *17* (2), 163-249.

37. Ramsden, W. Separation of Solids in the Surface-Layers of Solutions and 'Suspensions' (Observations on Surface-Membranes, Bubbles, Emulsions, and Mechanical Coagulation). -- Preliminary Account. *Proceedings of the Royal Society of London* 1903, *72* (ArticleType: research-article / Full publication date: 1903 - 1904 / Copyright © 1903 The Royal Society), 156-164.

38. Pickering, S. U. Emulsions. *Journal of the Chemical Society* 1907, *91*, 2001-2021.

39. Kokal, S. Crude-oil emulsions: A state-of-the-art review. *Spe Production & Facilities* 2005, *20* (1), 5-13.

40. Stiller, S.; Gers-Barlag, H.; Lergenmueller, M.; Pflucker, F.; Schulz, J.; Wittern, K. P.; Daniels, R. Investigation of the stability in emulsions stabilized with different surface modified titanium dioxides. *Colloids and Surfaces a-Physicochemical and Engineering Aspects* 2004, *232* (2-3), 261-267.

41. Frelichowska, J.; Bolzinger, M. A.; Valour, J. P.; Mouaziz, H.; Pelletier, J.; Chevalier, Y. Pickering w/o emulsions: Drug release and topical delivery. *International Journal of Pharmaceutics* 2009, *368* (1-2), 7-15.

42. Liang, Z. J.; Susha, A.; Caruso, F. Gold nanoparticle-based core-shell and hollow spheres and ordered assemblies thereof. *Chem. Mat.* 2003, *15* (16), 3176-3183.

43. Peceros, K. E.; Xu, X. D.; Bulcock, S. R.; Cortie, M. B. Dipole-dipole plasmon interactions in gold-on-polystyrene composites. *Journal of Physical Chemistry B* 2005, *109* (46), 21516-21520.

44. Phonthammachai, N.; White, T. J. One-step synthesis of highly dispersed gold nanocrystals on silica spheres. *Langmuir* 2007, *23* (23), 11421-11424.

45. Ou, J. L.; Chang, C. P.; Sung, Y.; Ou, K. L.; Tseng, C. C.; Ling, H. W.; Ger, M. D. Uniform polystyrene microspheres decorated with noble metal nanoparticles formed without using extra reducing agent. *Colloids and Surfaces a-Physicochemical and Engineering Aspects* 2007, *305* (1-3), 36-41.

46. Ma, H.; Luo, M. X.; Sanyal, S.; Rege, K.; Dai, L. L. The One-Step Pickering Emulsion Polymerization Route for Synthesizing Organic-Inorganic Nanocomposite Particles. *Materials* 2010, *3* (2), 1186-1202.

47. Sanyal, S.; Huang, H.; Rege, K.; Dai, L. L. Thermo-Responsive Core- Shell Composite Nanoparticles Synthesized via One-Step Pickering Emulsion Polymerization for Controlled Drug Delivery. *Nanomedicine & Nanotechnology* 2011, *2* (7), 126.

48. Chern, C. S. Emulsion polymerization mechanisms and kinetics. *Progress in Polymer Science* 2006, *31* (5), 443-486.

49. Tauer, K.; Hernandez, H.; Kozempel, S.; Lazareva, O.; Nazaran, P. Towards a consistent mechanism of emulsion polymerization - new experimental details. *Colloid Polym. Sci.* 2008, *286* (5), 499-515.

50. Yamamoto, T.; Kanda, Y.; Higashitani, K. Molecular-scale observation of formation of nuclei in soap-free polymerization of styrene. *Langmuir* 2004, *20* (11), 4400-4405.

51. Yamamoto, T.; Nakayama, M.; Kanda, Y.; Higashitani, K. Growth mechanism of soap-free polymerization of styrene investigated by AFM. *J. Colloid Interface Sci.* 2006, *297* (1), 112-121.

52. Feeney, P. J.; Napper, D. H.; Gilbert, R. G. COAGULATIVE NUCLEATION AND PARTICLE-SIZE DISTRIBUTIONS IN EMULSION POLYMERIZATION. *Macromolecules* 1984, *17* (12), 2520-2529.

53. Feeney, P. J.; Napper, D. H.; Gilbert, R. G. SURFACTANT-FREE EMULSION POLYMERIZATIONS - PREDICTIONS OF THE COAGULATIVE NUCLEATION THEORY. *Macromolecules* 1987, *20* (11), 2922-2930.

54. Richter, A.; Paschew, G.; Klatt, S.; Lienig, J.; Arndt, K.-F.; Adler, H.-J. Review on Hydrogel-based pH Sensors and Microsensors. *Sensors* 2008, *8* (1), 561-581.

55. Duracher, D.; Sauzedde, F.; Elaissari, A.; Perrin, A.; Pichot, C. Cationic amino-containing N-isopropylacrylamide-styrene copolymer latex particles: 1 - Particle size and morphology vs. polymerization process. *Colloid Polym. Sci.* 1998, *276* (3), 219-231.

56. Sanyal, S.; Slay, L.; Dai, L. L. Tuning the Thermal Transition of Poly(N-isopropylacrylamide) Based Core-Shell Composite Nanoparticles. *Sci. Adv. Mater.* 2013, *5* (4), 309-315.

57. Bernard P. Binks, T. S. H. *Colloidal Particles at Liquid Interfaces*; Cambridge University Press: New York, 2006.

58. Binks, B. P. Particles as surfactants - similarities and differences. *Current Opinion in Colloid & Interface Science* 2002, *7* (1-2), 21-41.

59. Binks, B. P.; Lumsdon, S. O. Influence of particle wettability on the type and stability of surfactant-free emulsions. *Langmuir* 2000, *16* (23), 8622-8631.

60. Tambe, D. E.; Sharma, M. M. THE EFFECT OF COLLOIDAL PARTICLES ON FLUID-FLUID INTERFACIAL PROPERTIES AND EMULSION STABILITY. *Advances in Colloid and Interface Science* 1994, *52*, 1-63.

61. Komura, S.; Hirose, Y.; Nonomura, Y. Adsorption of colloidal particles to curved interfaces. *Journal of Chemical Physics* 2006, *124* (24).

62. Schulman, J. H.; Leja, J. CONTROL OF CONTACT ANGLES AT THE OIL-WATER-SOLID INTERFACES - EMULSIONS STABILIZED BY SOLID PARTICLES (BASO4). *Transactions of the Faraday Society* 1954, *50* (6), 598-605.

63. Yan, N. X.; Gray, M. R.; Masliyah, J. H. On water-in-oil emulsions stabilized by fine solids. *Colloids and Surfaces a-Physicochemical and Engineering Aspects* 2001, *193* (1-3), 97-107.

64. Binks, B. P.; Whitby, C. P. Silica particle-stabilized emulsions of silicone oil and water: Aspects of emulsification. *Langmuir* 2004, *20* (4), 1130-1137.

65. Yang, F.; Liu, S. Y.; Xu, J.; Lan, Q.; Wei, F.; Sun, D. J. Pickering emulsions stabilized solely by layered double hydroxides particles: The effect of salt on emulsion formation and stability. *J. Colloid Interface Sci.* 2006, *302* (1), 159-169.

66. Yang, F.; Niu, Q.; Lan, Q.; Sun, D. J. Effect of dispersion pH on the formation and stability of Pickering emulsions stabilized by layered double hydroxides particles. *J. Colloid Interface Sci.* 2007, *306* (2), 285-295.

67. Binks, B. P.; Philip, J.; Rodrigues, J. A. Inversion of silica-stabilized emulsions induced by particle concentration. *Langmuir* 2005, *21* (8), 3296-3302.

68. SEEDED EMULSION POLYMERISATION http://www.chemical-associates.co.uk/.

69. Gilbert, R. *Emulsion Polymerization (Colloid science Series)*; Academic Press1995.

70. Lovell, P. A. a. E.-A., M.S. *Emulsion Polymerization and Emulsion Polymers*. J Wiley & Sons: 1997.

71. Bunten, M. J. Emulsion Polymerisation and Plastisols. In *Polymer Science and Engineering*; J Wiley & Sons, 1989; Vol. 17.

72. Kim, I. H.; Shin, J. S.; Cheong, I. W.; Kim, J. I.; Kim, J. H. Seeded emulsion polymerization of methyl methacrylate using aqueous polyurethane dispersion: effect of hard segment on grafting efficiency. *Colloids and Surfaces A: Physicochemical and Engineering Aspects* 2002, *207* (1–3), 169-176.

73. Reculusa, S.; Mingotaud, C.; Bourgeat-Lami, E.; Duguet, E.; Ravaine, S. Synthesis of daisy-shaped and multipod-like silica/polystyrene nanocomposites. *Nano Letters* 2004, *4* (9), 1677-1682.

74. Nguyen, D.; Ravaine, S.; Bourgeat-Lami, E.; Duguet, E. About the suitability of the seeded-dispersion polymerization technique for preparing micron-sized silica-polystyrene clusters. *Journal of Materials Chemistry* 2010, *20* (42), 9392-9400.

75. Kumar, A.; Mandal, S.; Mathew, S. P.; Selvakannan, P. R.; Mandale, A. B.; Chaudhari, R. V.; Sastry, M. Benzene- and anthracene-mediated assembly of gold nanoparticles at the liquid-liquid interface. *Langmuir* 2002, *18* (17), 6478-6483.

76. Nakazawa, M.; Somorjai, G. A. ADSORPTION OF SUBSTITUTED BENZENES ON POLYCRYSTALLINE GOLD AND ON ZINC-OXIDE AND IRON-OXIDE OVERLAYERS. *Applied Surface Science* 1993, *68* (4), 517-537.

77. Ohnuma, A.; Cho, E. C.; Camargo, P. H. C.; Au, L.; Ohtani, B.; Xia, Y. N. A Facile Synthesis of Asymmetric Hybrid Colloidal Particles. *J. Am. Chem. Soc.* 2009, *131* (4), 1352-+.

78. Zeng, S. W.; Yong, K. T.; Roy, I.; Dinh, X. Q.; Yu, X.; Luan, F. A Review on Functionalized Gold Nanoparticles for Biosensing Applications. *Plasmonics* 2011, *6* (3), 491-506.

79. Underwood, S.; Mulvaney, P. EFFECT OF THE SOLUTION REFRACTIVE-INDEX ON THE COLOR OF GOLD COLLOIDS. *Langmuir* 1994, *10* (10), 3427-3430.

80. Olah, G. A. Beyond oil and gas: The methanol economy. *Angew. Chem.-Int. Edit.* 2005, *44* (18), 2636-2639.

81. Armaroli, N.; Balzani, V. The future of energy supply: Challenges and opportunities. *Angew. Chem.-Int. Edit.* 2007, *46* (1-2), 52-66.

82. Hashmi, A. S. K.; Hutchings, G. J. Gold catalysis. *Angew. Chem.-Int. Edit.* 2006, *45* (47), 7896-7936.

83. Zhang, Y.; Cui, X. J.; Shi, F.; Deng, Y. Q. Nano-Gold Catalysis in Fine Chemical Synthesis. *Chemical Reviews* 2012, *112* (4), 2467-2505.

84. Okumura, M.; Akita, T.; Haruta, M. Hydrogenation of 1,3-butadiene and of crotonaldehyde over highly dispersed Au catalysts. *Catalysis Today* 2002, *74* (3-4), 265-269.

85. Corma, A.; Garcia, H. Supported gold nanoparticles as catalysts for organic reactions. *Chem. Soc. Rev.* 2008, *37* (9), 2096-2126.

86. Hashmi, A. S. K.; Hutchings, G. J. Gold Catalysis. *Angewandte Chemie International Edition* 2006, *45* (47), 7896-7936.

87. Hashmi, A. S. K. Gold-Catalyzed Organic Reactions. *Chemical Reviews* 2007, *107* (7), 3180-3211.

88. Hashmi, A. S. K.; Salathé, R.; Frey, W. Gold-Catalyzed Cyclization of N-Alkynyl Carbamates. *Synlett* 2007, *2007* (11), 1763-1766.

89. Caporusso, A. M.; Aronica, L. A.; Schiavi, E.; Gianmario, M.; Vitulli, G.; Salvadori, P. Hydrosilylation of 1-hexyne promoted by acetone solvated gold atoms derived catalysts. *Journal of Organometallic Chemistry* 2005, *690* (4), 1063-1066.

90. Corma, A.; González-Arellano, C.; Iglesias, M.; Sánchez, F. Gold Nanoparticles and Gold(III) Complexes as General and Selective Hydrosilylation Catalysts. *Angewandte Chemie International Edition* 2007, *46* (41), 7820-7822.

91. Liu, X.-Y.; Li, C.-H.; Che, C.-M. Phosphine Gold(I)-Catalyzed Hydroamination of Alkenes under Thermal and Microwave-Assisted Conditions. *Organic Letters* 2006, *8* (13), 2707-2710.

92. Zhang, X.; Corma, A. Effective Au(iii)-CuCl2-catalyzed addition of alcohols to alkenes. *Chemical Communications* 2007, (29), 3080-3082.

93. Hashmi, A. S. K.; Schwarz, L.; Rubenbauer, P.; Blanco, M. C. The Condensation of Carbonyl Compounds with Electron-Rich Arenes: Mercury, Thallium, Gold or a Proton? *Advanced Synthesis & Catalysis* 2006, *348* (6), 705-708.

94. Corma, A.; García, H. Lewis Acids: From Conventional Homogeneous to Green Homogeneous and Heterogeneous Catalysis. *Chemical Reviews* 2003, *103* (11), 4307-4366.

95. Hashmi, A. S. K.; Salathé, R.; Frey, W. Gold Catalysis: No Steric Limitations in the Phenol Synthesis. *Chemistry – A European Journal* 2006, *12* (26), 6991-6996.

96. Carrettin, S.; Blanco, M. C.; Corma, A.; Hashmi, A. S. K. Heterogeneous Gold-Catalysed Synthesis of Phenols. *Advanced Synthesis & Catalysis* 2006, *348* (10-11), 1283-1288.

97. Yamamoto, Y. From σ- to π-Electrophilic Lewis Acids. Application to Selective Organic Transformations. *The Journal of Organic Chemistry* 2007, *72* (21), 7817-7831.

98. Asao, N.; Sato, K. AuCl-Catalyzed [4+2] Benzannulation between o-Alkynyl(oxo)benzene and Benzyne. *Organic Letters* 2006, *8* (23), 5361-5363.

99. González-Arellano, C.; Corma, A.; Iglesias, M.; Sánchez, F. Gold (I) and (III) catalyze Suzuki cross-coupling and homocoupling, respectively. *Journal of Catalysis* 2006, *238* (2), 497-501.

100. González-Arellano, C.; Abad, A.; Corma, A.; García, H.; Iglesias, M.; Sánchez, F. Catalysis by Gold(I) and Gold(III): A Parallelism between Homo- and Heterogeneous Catalysts for Copper-Free Sonogashira Cross-Coupling Reactions. *Angewandte Chemie International Edition* 2007, *46* (9), 1536-1538.

101. Anastas, P. T.; Kirchhoff, M. M. Origins, Current Status, and Future Challenges of Green Chemistry†. *Accounts of Chemical Research* 2002, *35* (9), 686-694.

102. Poliakoff, M.; Fitzpatrick, J. M.; Farren, T. R.; Anastas, P. T. Green Chemistry: Science and Politics of Change. *Science* 2002, *297* (5582), 807-810.

103. Haruta, M. Catalysis: Gold rush. *Nature* 2005, *437* (7062), 1098-1099.

104. Mallat, T.; Baiker, A. Oxidation of Alcohols with Molecular Oxygen on Solid Catalysts. *Chemical Reviews* 2004, *104* (6), 3037-3058.

105. Xu, Y.-J.; Landon, P.; Enache, D.; Carley, A.; Roberts, M. W.; Hutchings, G. Selective conversion of cyclohexane to cyclohexanol and cyclohexanone using a gold catalyst under mild conditions. *Catal Lett* 2005, *101* (3-4), 175-179.

106. Zhu, K.; Hu, J.; Richards, R. Aerobic oxidation of cyclohexane by gold nanoparticles immobilized upon mesoporous silica. *Catal Lett* 2005, *100* (3-4), 195-199.

107. Hayashi, T.; Tanaka, K.; Haruta, M. Selective Vapor-Phase Epoxidation of Propylene over Au/TiO2Catalysts in the Presence of Oxygen and Hydrogen. *Journal of Catalysis* 1998, *178* (2), 566-575.

108. Taylor, B.; Lauterbach, J.; Delgass, W. N. Gas-phase epoxidation of propylene over small gold ensembles on TS-1. *Applied Catalysis A: General* 2005, *291* (1–2), 188-198.

109. Sheldon, R. A.; Arends, I. W. C. E.; ten Brink, G.-J.; Dijksman, A. Green, Catalytic Oxidations of Alcohols. *Accounts of Chemical Research* 2002, *35* (9), 774-781.

110. Sheldon, R. A. Catalytic oxidation and fine chemicals. *Catalysis Today* 1987, *1* (3), 351-355.

111. Brink, G.-J. t.; Arends, I. W. C. E.; Sheldon, R. A. Green, Catalytic Oxidation of Alcohols in Water. *Science* 2000, *287* (5458), 1636-1639.

112. Yamaguchi, K.; Mizuno, N. Supported Ruthenium Catalyst for the Heterogeneous Oxidation of Alcohols with Molecular Oxygen. *Angewandte Chemie International Edition* 2002, *41* (23), 4538-4542.

113. Ishida, T.; Haruta, M. Gold catalysts: Towards sustainable chemistry. *Angew. Chem.-Int. Edit.* 2007, *46* (38), 7154-7156.

114. Tsunoyama, H.; Sakurai, H.; Ichikuni, N.; Negishi, Y.; Tsukuda, T. Colloidal gold nanoparticles as catalyst for carbon-carbon bond formation: Application to aerobic homocoupling of phenylboronic acid in water. *Langmuir* 2004, *20* (26), 11293-11296.

115. Shi, F.; Zhang, Q. H.; Ma, Y. B.; He, Y. D.; Deng, Y. Q. From CO oxidation to CO2 activation: An unexpected catalytic activity of polymer-supported nanogold. *J. Am. Chem. Soc.* 2005, *127* (12), 4182-4183.

116. Dupont, J.; Consorti, C. S.; Spencer, J. The Potential of Palladacycles: More Than Just Precatalysts. *Chemical Reviews* 2005, *105* (6), 2527-2572.

117. Astruc, D.; Lu, F.; Aranzaes, J. R. Nanoparticles as Recyclable Catalysts: The Frontier between Homogeneous and Heterogeneous Catalysis. *Angewandte Chemie International Edition* 2005, *44* (48), 7852-7872.

118. Telang, C.; Otanicar, T.; Dai, L.; Phelan, P.; Swaminathan, R.; Zhang, M. Controllable Optical Properties of Polystyrene/PNIPAm-Gold Composite Nanoparticles. *Plasmonics* 2014, 1-9.

119. Lange, H.; Juarez, B. H.; Carl, A.; Richter, M.; Bastus, N. G.; Weller, H.; Thomsen, C.; von Klitzing, R.; Knorr, A. Tunable Plasmon Coupling in Distance-Controlled Gold Nanoparticles. *Langmuir* 2012, *28* (24), 8862-8866.

120. Lv, W.; Phelan, P. E.; Swaminathan, R.; Otanicar, T. P.; Taylor, R. A. Multifunctional Core-Shell Nanoparticle Suspensions for Efficient Absorption. *Journal of Solar Energy Engineering* 2012, *135* (2), 021004-021004.

121. Binks, B. P.; Clint, J. H.; Fletcher, P. D. I.; Lees, T. J. G.; Taylor, P. Growth of gold nanoparticle films driven by the coalescence of particle-stabilized emulsion drops. *Langmuir* 2006, *22* (9), 4100-4103.

122. Larson-Smith, K.; Pozzo, D. C. Pickering Emulsions Stabilized by Nanoparticle Surfactants. *Langmuir* 2012, *28* (32), 11734-11741.

123. Sorrell, C. D.; Serpe, M. J. Reflection Order Selectivity of Color-Tunable Poly(N-isopropylacrylamide) Microgel Based Etalons. *Adv. Mater.* 2011, *23* (35), 4088-+.

124. Peters, K. Intensity-, Interferometric-, and Scattering-Based Optical-Fiber Sensors. In *Encyclopedia of Structural Health Monitoring*; John Wiley & Sons, 2009.

125. Mie, G. Contributions to the optics of turbid media, particularly of colloidal metal solutions. *Ann. Phys.* 1908, *25* (3), 377-445.

126. Chen, H. W.; Ye, X. D.; Zhang, G. Z.; Zhang, Q. J. Dynamics of thermoresponsive PNIPAm-g-PEO copolymer chains in semi-dilute solution. *Polymer* 2006, *47* (25), 8367-8373.

127. Liz-Marzan, L. M.; Giersig, M.; Mulvaney, P. Synthesis of nanosized gold-silica core-shell particles. *Langmuir* 1996, *12* (18), 4329-4335.

128. Wang, Y. F.; Wang, Y.; Breed, D. R.; Manoharan, V. N.; Feng, L.; Hollingsworth, A. D.; Weck, M.; Pine, D. J. Colloids with valence and specific directional bonding. *Nature* 2012, *491* (7422), 51-U61.

129. Kim, J.-W.; Larsen, R. J.; Weitz, D. A. Synthesis of Nonspherical Colloidal Particles with Anisotropic Properties. *J. Am. Chem. Soc.* 2006, *128* (44), 14374-14377.

130. Liu, Y.; Quan, X.; Choi, H. Synthesis and characteristics of snowman-like fluorescent PMMA microbeads. *Colloid Polym. Sci.* 2012, *290* (16), 1703-1706.

131. Chaturvedi, N.; Juluri, B. K.; Hao, Q.; Huang, T. J.; Velegol, D. Simple fabrication of snowman-like colloids. *J. Colloid Interface Sci.* 2012, *371* (1), 28-33.

132. Dendukuri, D.; Doyle, P. S. The Synthesis and Assembly of Polymeric Microparticles Using Microfluidics. *Adv. Mater.* 2009, *21* (41), 4071-4086.

133. Wang, F.-w.; Liu, H.-r.; Zhao, L.-l.; Zhang, X.-y. Facile fabrication of polymer-inorganic hybrid particles with various morphologies by combination of hydrolytic

condensation process with radiation seeded emulsion polymerization. *Colloid Polym. Sci.* 2014, *292* (5), 1171-1179.

134. Haruta, M.; Kobayashi, T.; Sano, H.; Yamada, N. NOVEL GOLD CATALYSTS FOR THE OXIDATION OF CARBON-MONOXIDE AT A TEMPERATURE FAR BELOW 0-DEGREES-C. *Chemistry Letters* 1987, (2), 405-408.

135. Hutchings, G. J. VAPOR-PHASE HYDROCHLORINATION OF ACETYLENE - CORRELATION OF CATALYTIC ACTIVITY OF SUPPORTED METAL CHLORIDE CATALYSTS. *Journal of Catalysis* 1985, *96* (1), 292-295.

136. Shi, S.; Zhang, L.; Wang, T.; Wang, Q.; Gao, Y.; Wang, N. Poly(N-isopropylacrylamide)-Au hybrid microgels: synthesis, characterization, thermally tunable optical and catalytic properties. *Soft Matter* 2013, *9* (46), 10966-10970.

137. Harrison, S.; Cruickshank, C. A. A review of strategies for the control of high temperature stagnation in solar collectors and systems. *Energy Procedia* 2012, *30* (0), 793-804.

138. Köhl, M.; Heck, M.; Brunold, S.; Frei, U.; Carlsson, B.; Möller, K. Advanced procedure for the assessment of the lifetime of solar absorber coatings. *Solar Energy Materials and Solar Cells* 2004, *84* (1–4), 275-289.

139. Sarit K. Das, S. U. C., Wenhua Yu, T. Pradeep. *Nanofluids: Science and Technology*; John Wiley & Sons2007.

140. Ma, H.; Dai, L. L. Structure of Multi-Component Colloidal Lattices at Oil-Water Interfaces. *Langmuir* 2009, *25* (19), 11210-11215.

141. Aveyard, R.; Binks, B. P.; Clint, J. H.; Fletcher, P. D. I.; Horozov, T. S.; Neumann, B.; Paunov, V. N.; Annesley, J.; Botchway, S. W.; Nees, D.; Parker, A. W.; Ward, A. D.; Burgess, A. N. Measurement of long-range repulsive forces between charged particles at an oil-water interface. *Physical Review Letters* 2002, *88* (24).

142. Horozov, T. S.; Aveyard, R.; Clint, J. H.; Binks, B. P. Order-disorder transition in monolayers of modified monodisperse silica particles at the octane-water interface. *Langmuir* 2003, *19* (7), 2822-2829.

143. Pieranski, P. TWO-DIMENSIONAL INTERFACIAL COLLOIDAL CRYSTALS. *Physical Review Letters* 1980, *45* (7), 569-572.

144. Lu, Z. D.; Goebl, J.; Ge, J. P.; Yin, Y. D. Self-assembly and tunable plasmonic property of gold nanoparticles on mercapto-silica microspheres. *Journal of Materials Chemistry* 2009, *19* (26), 4597-4602.

145. Quinten, M.; Kreibig, U. OPTICAL-PROPERTIES OF AGGREGATES OF SMALL METAL PARTICLES. *Surface Science* 1986, *172* (3), 557-577.

146. Ohnuma, A.; Cho, E. C.; Jiang, M.; Ohtani, B.; Xia, Y. N. Metal-Polymer Hybrid Colloidal Particles with an Eccentric Structure. *Langmuir* 2009, *25* (24), 13880-13887.

147. Sperling, R. A.; Parak, W. J. Surface modification, functionalization and bioconjugation of colloidal inorganic nanoparticles. *Philosophical Transactions of the Royal Society a-Mathematical Physical and Engineering Sciences* 2010, *368* (1915), 1333-1383.

148. Li, Y. X.; Lu, G. X.; Li, S. B. Photocatalytic transformation of rhodamine B and its effect on hydrogen evolution over Pt/TiO2 in the presence of electron donors. *Journal of Photochemistry and Photobiology a-Chemistry* 2002, *152* (1-3), 219-228.

149. Jiang, Z. J.; Liu, C. Y.; Sun, L. W. Catalytic properties of silver nanoparticles supported on silica spheres. *Journal of Physical Chemistry B* 2005, *109* (5), 1730-1735.

150. Jana, N. R.; Sau, T. K.; Pal, T. Growing small silver particle as redox catalyst. *Journal of Physical Chemistry B* 1999, *103* (1), 115-121.

151. Besson, M.; Gallezot, P. Deactivation of metal catalysts in liquid phase organic reactions. *Catalysis Today* 2003, *81* (4), 547-559.

152. Papp, A.; Miklos, K.; Forgo, M.; Molnar, A. Heck coupling by Pd deposited onto organic-inorganic hybrid supports. *Journal of Molecular Catalysis a-Chemical* 2005, *229* (1-2), 107-116.

153. Carregal-Romero, S.; Buurma, N. J.; Perez-Juste, J.; Liz-Marzan, L. M.; Herves, P. Catalysis by Au@PNIPAm Nanocomposites: Effect of the Cross-Linking Density. *Chem. Mat.* 2010, *22* (10), 3051-3059.

154. Contreras-Caceres, R.; Pacifico, J.; Pastoriza-Santos, I.; Perez-Juste, J.; Fernandez-Barbero, A.; Liz-Marzan, L. M. Au@PNIPAm Thermosensitive Nanostructures: Control over Shell Cross-linking, Overall Dimensions, and Core Growth. *Adv. Funct. Mater.* 2009, *19* (19), 3070-3076.

155. Karg, M.; Jaber, S.; Hellweg, T.; Mulvaney, P. Surface Plasmon Spectroscopy of Gold-Poly-N-isopropylacrylamide Core-Shell Particles. *Langmuir* 2011, *27* (2), 820-827.

156. Yang, L. P.; Liu, Z. Y. Study on light intensity in the process of photocatalytic degradation of indoor gaseous formaldehyde for saving energy. *Energy Conv. Manag.* 2007, *48* (3), 882-889.

157. Horie, Y.; David, D. A.; Taya, M.; Tone, S. Effects of light intensity and titanium dioxide concentration on photocatalytic sterilization rates of microbial cells. *Ind. Eng. Chem. Res.* 1996, *35* (11), 3920-3926.

158. Aslan, K.; Lakowicz, J. R.; Geddes, C. D. Plasmon light scattering in biology and medicine: new sensing approaches, visions and perspectives. *Curr. Opin. Chem. Biol.* 2005, *9* (5), 538-544.

159. Garner, B. W.; Cai, T.; Ghosh, S.; Hu, Z. B.; Neogi, A. Refractive Index Change Due to Volume-Phase Transition in Polyacrylamide Gel Nanospheres for Optoelectronics and Bio-photanics. *Applied Physics Express* 2009, *2* (5).

160. Schmidt, S.; Motschmann, H.; Hellweg, T.; von Klitzing, R. Thermoresponsive surfaces by spin-coating of PNIPAm-co-PAA microgels: A combined AFM and ellipsometry study. *Polymer* 2008, *49* (3), 749-756.

161. Aslan, K.; Lakowicz, J. R.; Geddes, C. D. Nanogold plasmon resonance-based glucose sensing. 2. Wavelength-ratiometric resonance light scattering. *Anal. Chem.* 2005, *77* (7), 2007-2014.

162. Ma, X. Y.; Lu, J. Q.; Brock, R. S.; Jacobs, K. M.; Yang, P.; Hu, X. H. Determination of complex refractive index of polystyrene microspheres from 370 to 1610 nm. *Physics in Medicine and Biology* 2003, *48* (24), 4165-4172.

163. Zhang, M. M.; Ngo, T. H.; Rabiah, N. I.; Otanicar, T. P.; Phelan, P. E.; Swaminathan, R.; Dai, L. L. Core-Shell and Asymmetric Polystyrene-Gold Composite Particles via One-Step Pickering Emulsion Polymerization. *Langmuir* 2014, *30* (1), 75-82.

164. Zhang, M. M.; Rabiah, N. I.; Ngo, T. H.; Otanicar, T. P.; Phelan, P. E.; Swaminathan, R.; Dai, L. L. Thermo-responsiveness and tunable optical properties of asymmetric polystyrene/PNIPAm-gold composite particles. *J. Colloid Interface Sci.* 2014, *425*, 12-19.

165. Binks, B. P.; Lumsdon, S. O. Pickering Emulsions Stabilized by Monodisperse Latex Particles: Effects of Particle Size. *Langmuir* 2001, *17* (15), 4540-4547.

166. Mayer, K. M.; Hafner, J. H. Localized Surface Plasmon Resonance Sensors. *Chemical Reviews* 2011, *111* (6), 3828-3857.

167. Gunawan, A.; Li, H.; Lin, C.-H.; Buttry, D. A.; Mujica, V.; Taylor, R. A.; Prasher, R. S.; Phelan, P. E. The amplifying effect of natural convection on power generation of thermogalvanic cells. *International Journal of Heat and Mass Transfer* 2014, *78*, 423-434.

168. Gunawan, A.; Lin, C.-H.; Buttry, D. A.; Mujica, V.; Taylor, R. A.; Prasher, R. S.; Phelan, P. E. Liquid Thermoelectrics: Review of Recent And Limited New Data of Thermogalvanic Cell Experiments. *Nanoscale and Microscale Thermophysical Engineering* 2013, *17* (4), 304-323.

169. Çengel, Y. A. *Heat and Mass Transfer: A Practical Approach*. (third ed.)McGraw-Hill Companies Inc, New York: New York, 2007.

170. Bejan, A.; Tien, C. L. Laminar Natural Convection Heat Transfer in a Horizontal Cavity with Different End Temperatures. *Journal of Heat Transfer* 1978, *100* (4), 641-647.

171. Bejan, A. *Convection Heat Transfer, Hoboken (third ed.)*. John Willey & Sons: New Jersey, 2004.

172. Busse, F. H. Non-linear properties of thermal convection. *Rep. Prog. Phys* 1978, *41*, 1929–1967.